Università degli Studi di Milano – Bicocca

Facoltà di Scienze Matematiche, Fisiche e Naturali

Dipartimento di Scienze Geologiche e Geotecnologie

Doctor of Philosophy
in
Earth Sciences

Borehole flowmeter and hydrogeophysics surveys: new possibilities for characterizing hydrogeological heterogeneities

Stefano Basiricò

Supervisor
Prof. Giovanni Battista Crosta

Academic year 2010/2011

Contents

List of Figures

Acknowledgements

Desidero ringraziare le tante persone che in vario modo mi hanno aiutato in questi tre anni di dottorato.

Il prof. Giovanni Crosta mi ha dato sia la spinta iniziale sia l'opportunità di fare delle esperienze professionali uniche.

Con Alberto Villa ho condiviso mille idee e mille spunti. Grazie Alberto sei stato un collega e un amico unico in tante occasioni.

Paolo Frattini mi ha sempre dato l'appoggio per credere in me stesso e migliorarmi.

Gli amici della stanza 2027 meriterebbero un capitolo a parte: grazie Antonio Pola Villasenor *el Cobra*, grazie Marco *il Biondino*, grazie *biondina* Sere, grazie *Time-Lapse Meteoman* Richard, grazie Ahmal. Siete delle gran belle persone.

Tutto il Dipartimento di Scienze Geologiche si è sempre interessato a quello che facevo e come stava andando, in tutti i sensi: grazie Federico, Nicoletta, Valentina, Rosanna, Elena, Angela, Cinzia, Anna.

Grazie al prof. Alberto Godio e a Diego Franco del Politecnico di Torino per la disponibilità del sito di Serravalle Scrivia e di Trecate e per gli indispensabili approfondimenti geofisici.

Un grazie ad Alessandro Paladini, Claudio Piantadosi, Roberto Colombo e Daniele Fusi con cui ho diviso tanto lavoro di terreno.

Grazie a Fredy Pena Reyes per le revisioni.

Grazie a Francesco Serra per l'esperienza libanese.

Ringrazio mia mamma, mia sorella e i miei nipoti Francesco, Federico e Ludovica: non lo immaginate l'aiuto che mi avete dato.

Grazie ad Andrea per esserci sempre.

Questo lavoro lo dedico a Valentina, la persona più bella che abbia mai conosciuto. Ti amo Vale, con te ho scoperto cosa conta veramente nella vita.

Abstract

The research subject of this PhD thesis consists in the development and application of techniques for analyzing well-log, well-test, and tracer data to infer the distribution of hydrologic properties in heterogeneous geologic settings, including fractured rock and complex aquifer systems.

This thesis is organized in an introductory section presenting the state of the art about heterogeneous geologic media characterization and a focus on flowmeter log analysis.

The second chapter regards applications of an integrated surveying approach where an hydrogeophysical characterization was used for a complex aquifer in calcareous and gypsiferous formation. The most important topic is the joint use of the Electromagnetic Borehole Flowmeter (EBF) in single hole mode and the Ground Penetrating Radar in single and cross borehole configuration.

The third chapter is a completion of the studies performed and described in chapter two, with an extensive study involving a conventional hydrogeological characterization (pumping test, core analysis) with flowmeter log in cross hole mode and its application to design and interpretation two tracer tests. The aim is to provide an approach to optimize a set of hydrogeological and geophysical survey techniques.

In chapter four another application of the flowmeter log is presented. This application has been designed to monitor infiltration in the vadose zone of a sandy-gravelly soil and use results as calibration data for the geophysical investigation (ERT and Georadar Borehole survey).

This thesis involved coordination of laboratory and field work; collaboration with geophysicists, geochemists and geologists in interdisciplinary studies.

Main applications of this work include advanced hydrogeological characterization, groundwater and vadose-zone contaminant remediation as well as optimal utilization of water resources.

Chapter 1

Heterogeneous geologic media studies and flowmeter log analysis

Geological heterogeneity is recognized as a major control on reservoir production and a constrain on many aspects of quantitative hydrogeology. Hydrogeologists and reservoir geologists need to characterize groundwater flow through many different types of geological media for different purposes.

For example, close the source of contamination, local heterogeneities in hydraulic and geochemical characteristics strongly influence the development of a solute/contaminant plume. Preferential pathways of solute spreading occur along horizons of high hydraulic conductivity (K), while along regions of small K solute tends to lag behind in. To accurately model the movement and spreading of the plume near the solute source (on a scale of a few tens of meters) a detailed measurements of the local heterogeneity are needed. In a stratified aquifer near Mobile (Alabama) Molz et al. (1986) showed that even at a scale of 32 meters, tracer movement and spreading were governed largely by the vertical distribution of hydraulic conductivity.

The type of geological heterogeneity that needs to be taken into account depends on the scale of the problem under consideration (Schulze-Makuch and Cherkauer, 1998; Beliveau, 2002; Neuman, 2003). Nevertheless must be kept in mind that significant heterogeneity is present everywhere, on a scale down to centimeters (Allen-King et al., 1998), and even in aquifers originally treated as homogeneous equivalent porous media.

In unlithified sediments, geological heterogeneity that controls flow is represented by variations in lithofacies, whereas in hard, crystalline bedrock, it is also represented by fractures. The hydrogeology of unlithified sediments and of fractured rocks has received much attention by hydrogeologists interested in the question of heterogeneity (Fraser and Davies, 1998; Huggenberg and Aigner, 1999).

Two classes of models describe flow in heterogeneous media: continuous and discrete methods.

Continuum is based on the following assumption: flow is considered on a volumetrically averaged basis at a macroscopic scale in what is assumed to be equivalent to an ideal porous medium. Application of the principle of mass conservation to the averaged volumes allows the derivation of the governing partial differential equation of the flow.

The minimal volume over which the governing equations of flow apply is generally referred to

as a *representative elementary volume* (*REV*) (**Bear, 1972**). This method is called ***equivalent porous medium method*.**

Eaton (2006) argues that the dimensions of REV are defined according to the purpose of the investigation, but it must be of a size range within which measurable characteristics are statistically significant and remain more or less constant. Therefore, in a heterogeneous continuum, the REV size must be smaller than the major variations in hydraulic conductivity for this approach to be applicable to quantitative hydrogeology.

From a flow modeling perspective, the size of REV can be defined as a volume across which hydraulic head changes are not significant (Anderson and Woessner, 1992), which is in effect the size of the model grid cells. Therefore REV size must be able to capture the geological heterogeneity for a given modeling application.

The continuum approach could be appropriate to explain flow in highly heterogeneous settings such as strongly fractured rocks. In this case flow through each individual fracture is not considered but overall flow through the fracture network is assumed to be reproduced well by an equivalent porous medium (Hsieh, 1998) (Figure 1)

When hydraulic properties due to flow through pore space and fractures are considered simultaneously in superimposition, this constitutes a ***double porosity model*** (Pirson, 1953).

Some of the fluid flows in the matrix, while the rest flows in the fracture system. The matrix flow is of Darcy type.

The most important and difficult thing to model is the exchange of fluid between the matrix and the fracture system. Generally, this exchange is assumed to be in an quasi-steady state and depends on the differences between the matrix fluid pressure and the fracture system fluid pressure. This assumption effectively ignores the pattern of flow in an individual matrix block. Fluid exchange actually takes place at the surface of the blocks, while the rate of exchange depends basically on the fluid pressure and on the geometry of the matrix blocks.

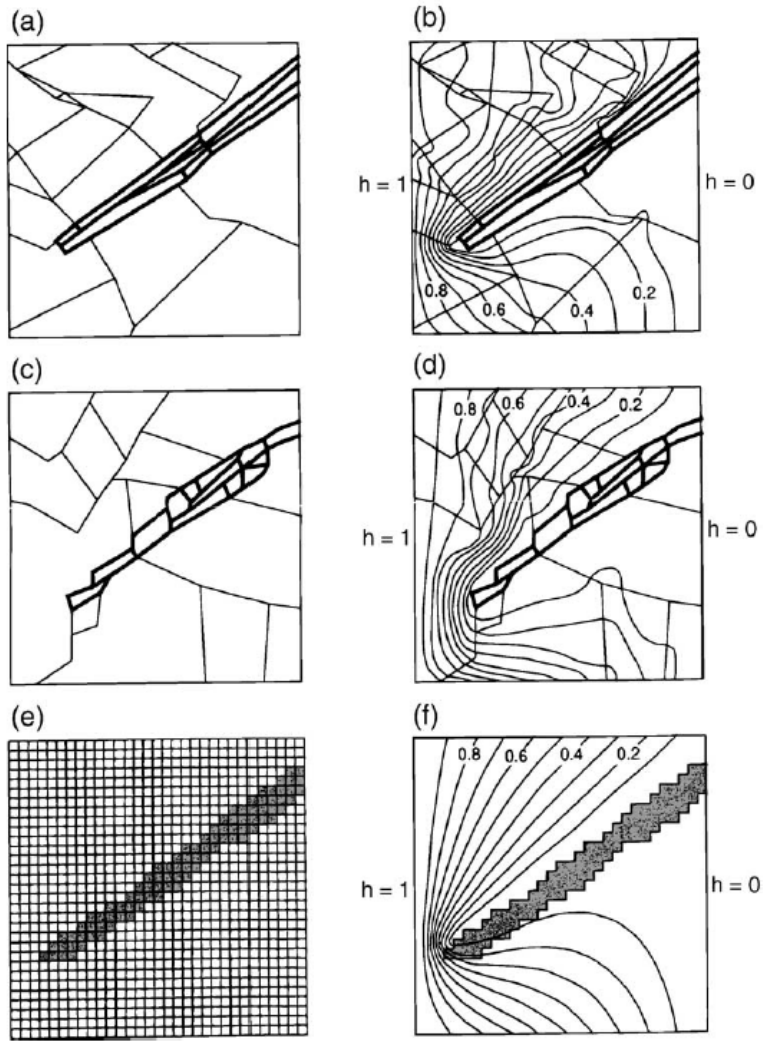

Figure 1:fractured geological heterogeneity and its representation in numerical flow models: (a) real fracture network; (b) distribution of head in real network; (c) discrete fracture (DF) model; (d) distribution of head in DF model; (e) continuum model; (f) distribution of head in continuum model (from Hsieh, 1998).

Discrete fracture and other methods. The discrete fracture approach considers the structure of the model domain to be a network of transmissive fracture (Hsieh, 1998).

The discrete fracture approach takes into account flow through each fracture characterized by a location, orientation, size and transmissivity. Often, fractures are represented in three dimensions by intersecting circular or elliptic disks (Dershowitz and Einstein, 1998)

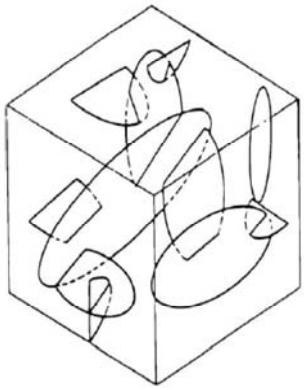

Figure 2: representation of three-dimensional fracture geometry as intersecting disks in space (Dershowitz and Einstein, 1998).

The major difficulty with this approach is that it is extremely computationally intensive and it is generally practical only at a very small scale site.

Simpler approaches limit the analysis to two dimensions analysis (Min et al., 2004) or represent the three-dimensional network of disks with a network of channels but neither of these techniques is in widespread use for computational reasons.

From Figure 1 it is clear that both continuum and discrete fracture approaches can reproduce the basic elements of the heterogeneous flow field but cannot reproduce all the details.

Another approach is represented by the percolation theory (Berkowitz and Balberg, 1993) in which statistics about connections between elements that represent pores or fractures provide information about the hydraulic conductivity of larger systems. This connectivity is associated with a critical threshold, the *percolation limit*, above which a system will conduct flow. Few hydrogeologists (e.g. Koudina et al, 1998) applied percolation theory to understanding flow through heterogeneous rocks.

According to heterogeneity approaches described above, the simulation of flow through heterogeneous geologic media requires a formulation to structure the model domain. The ***geostatistical formulation*** assumes a groundwater domain with continuously variable properties, in which the spatial distribution of these properties is uncertain. Therefore if a discrete fracture network conceptualization is used, it is considered impossible to collect enough field data to completely characterize the locations, orientations, extents and transmissivities of the discrete fractures (*Eaton, 2006*). So, fracture geometric properties and parameters of the flow model are considered to be random variables whose probability density functions are estimated from field data (*Hsieh, 1998*).

As above mentioned, natural geologic formations are heterogeneous, and few transmissivity values do not provide sufficient information to contaminant transport or more simply to locate the screened intervals of monitoring wells. Furthermore contaminant transport analysis based on aquifer properties averaged over the vertical dimension are frequently inadequate (Molz et al., 1990). An appropriate site characterization or the assumption of homogeneity conditions can moreover lead to incorrect design of remediation projects or data analysis.

Flowmeter log: a state of the art

Because of the recognized need to improve predictions of flow and transport of pollutants, especially in heterogeneous and fractured aquifers, from the '80 the interest in borehole flowmeters log for environmental applications increased (eg. the determination of K logs).
Vertical flowmeter logging measures substantially, vertical movement of fluid in a borehole.
The three main types of vertical flowmeters are differentiated by the method used to measure flow and the range of flow that they can measure. These three types of flowmeters are:

- heat-pulse, that uses the velocity of a heated packet of water that moves with the flow;
- electromagnetic, that is based on Faraday's Law of Induction;
- spinner, that uses an impeller that revolves in response to fluid flow.

Hess (1982, 1986), Morin et al. (1988) and Hess and Paillet (1989) reviewed heat-pulse technology, while Hufschmied (1983), Molz et al. (1990) and Rehfeldt et al. (1989) have shown major interest in application of spinner flowmeters.
These authors emphasized that the main handicap to widespread use of borehole flowmeter log for environmental purpose was the lack of commercially available meters of sufficient precision and sensitivity. Major problems included inability to sense low flows and, especially for spinner flowmeters, calibration of the rotation-flow relationship.
The electromagnetic (EM) borehole flowmeter was developed in 1989 by the Tennessee Valley Authority (TVA). This flowmeter immediately has appeared very promising for characterizing three-dimensional hydraulic conductivity field (Young and Waldrop, 1989).
The Electromagnetic Borehole Flowmeter consists of an electromagnet and two electrodes that are cast in a durable epoxy (Figure 3 and Figure 4). The epoxy is molded in a cylindrical shape to minimize turbulence associated with channeling water past the electrodes and electromagnet. Having no moving parts, the flowmeter operates according to Faraday's Law

of Induction, which states that the voltage, ε, induced across a conductor moving at right angle through a magnetic field, B, is directly proportional to the velocity, V, of the conductor:

$$\varepsilon = BlV \qquad \text{Eq. 1}$$

With l the distance between the electrodes in the magnetic flow meter.

Flowing water is the conductor, the electromagnet generates a magnetic field, and the electrodes are used to measure the induced voltage. Electronics connected to the electrodes transmit a voltage that is directly proportional to the velocity of the water.

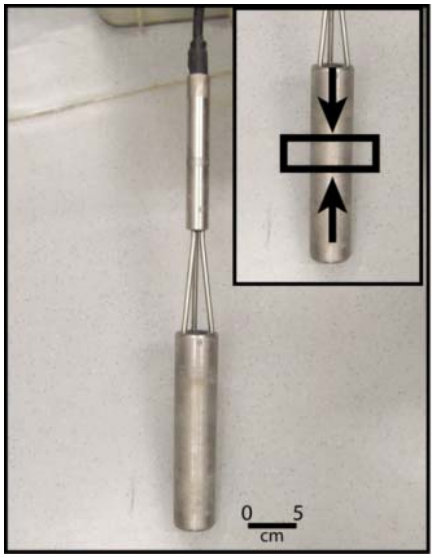

Figure 3: electromagnetic borehole flowmeter produced by Quantum Engineering corp. Black arrow shows the possible direction of the flow measured by two electrodes.

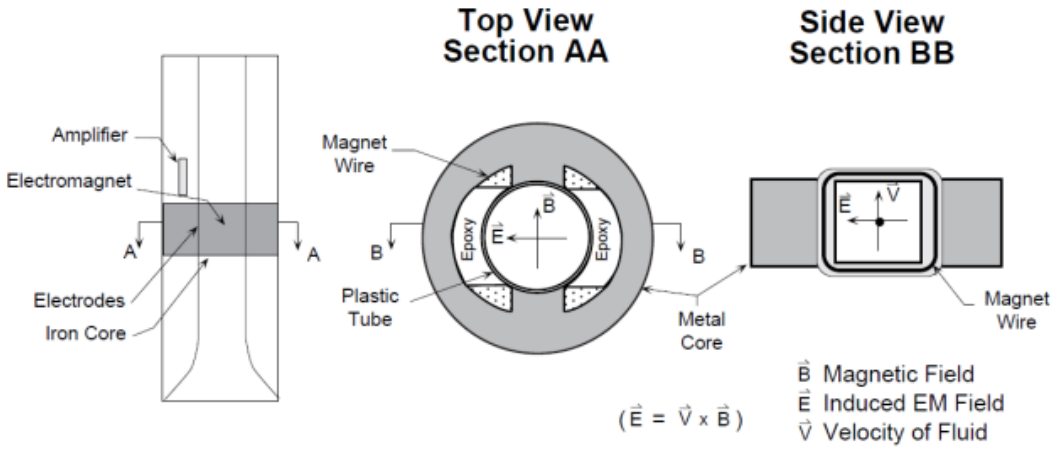

Figure 4: Schematic diagram of the TVA electromagnetic borehole flowmeter (EPA/600/R-98/058).

Two probes are available - one with a half-inch inside throat diameter and another with a one-inch throat diameter. The performance specifications of both probes are presented in Table 1.

	1.27 cm (1/2 inch) id Probe	2.54 cm (1 inch) id Probe
Minimum Flow	0.010 L/min	0.04 L/min
Minimum Velocity	0.131 cm/sec	0.131 cm/sec
Maximum Flow	10 L/min	40 L/min
Maximum Velocity	131 cm/sec	131 cm/sec

Table 1: Performance Specifications of the EBF Probes

To prevent bypass flow around the recording section of the flowmeter, a collar or inflatable packer can be used to seal the area around the exterior of the flowmeter for large diameter wells. However, whenever it is not possible to block all bypass flow around the flowmeter, then blocking a constant percentage of bypass flow will provide data adequate for computing the vertical distribution of hydraulic conductivity. Such a condition is typical when testing in wire-wrapped screens.

Ambient flow is usually recorded throughout the screened interval of the well first. This is typically initiated with the flowmeter at the bottom of the screen where flow rates should be zero. The probe is then raised one increment. After any flow disturbance caused by the probe movement has subsided, the vertical flow at that station is recorded. This process is repeated throughout the entire screened or uncased region. These ambient flows reveal the presence of vertical pressure gradients, positive or negative, between strata, and provide a baseline for analyzing induced flow into the well during pumping. The test can also be initiated in the solid casing above the screen where the ambient flow rate should also be zero and proceed downward as described above.

Once the ambient flow pattern has been recorded, the induced flow test is initiated by pumping either from or into the well at a constant rate. The water surface is monitored to determine when equilibrium conditions have been achieved. The probe is then systematically moved vertically with flow rates recorded at predetermined intervals throughout the well screen or uncased region. Data at each depth are displayed on a digital readout and stored in a data file of a portable computer.

Paillet et al. (1987), indicate that a critical need for new methods to determine local in-situ fracture permeability using the access provided by exploratory boreholes exists. At time of the work the most effective method for measuring in situ permeability consisted in local pumping tests, after isolation of borehole sections by means of downhole packers. This is a very time

consuming method, and it requires complicated equipment. Paillet et al. stated that "the measurement of fracture permeability in the vicinity of boreholes would be improved considerably if a sensitive flowmeter was available to measure the flows into or out of boreholes under an imposed flow field". Satisfactory results in these studies depended on the existence of vertical hydraulic head gradients resulting from recharge or hydraulic connections between two or more independent fracture-permeability systems. An induced flow system might be imposed, e.g. during a pumping test, and then the flowmeter is used to identify flow rates into and out of individual fractures. The authors investigated the distribution of fracture permeability in granitic rocks by measuring the distribution of vertical flow in boreholes during periods of steady pumping at two sites: one of moderately fractured and another of intensely fractured rocks. An heat pulse flowmeter was used for accurate measurement of the vertical flow as low as 0.2 liter per minute. Results indicated, by the detection of inflow and outflow zone the importance of assessing the effective permeability of fractures in situ.

Reilly et al. (1989) studied a hypothetical ground water system numerically in order to demonstrate that significant amounts of flow can occur within long-screen wells installed in homogeneous aquifers. The authors applied a vertical hydraulic gradient to the regional model. A local system that consisted of a three dimensional section of the regional model was simulated in order to analyze and quantify the wellbore flow (Figure 5). The most important result of the study by Reilly et al. (1989) is the clear prediction that a flow rate detectable with borehole flowmeters occurs in aquifer with very small typical vertical head differences. The authors conclude that, under this "common" conditions, samples from monitoring wells with long screen might be almost useless for quantifying the concentration of contaminants. Their warning seems to have been largely ignored.

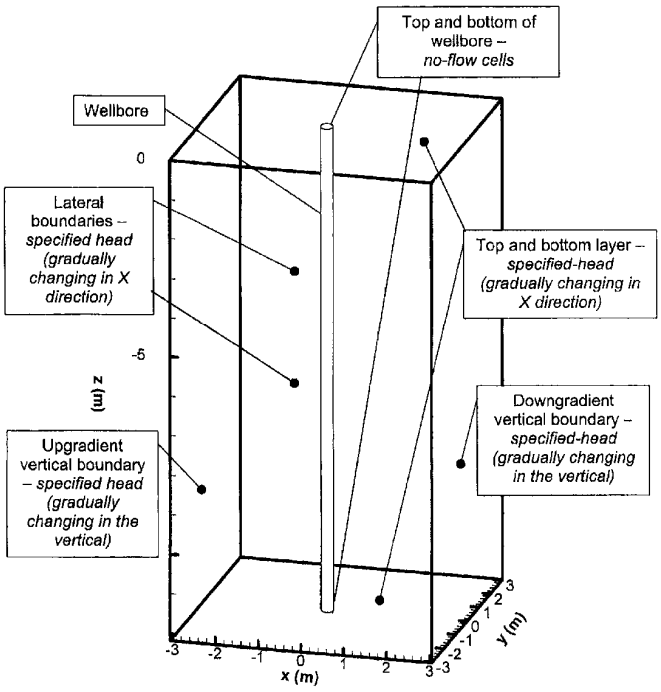

Figure 5: boundary conditions of the Reilly et al. model,(1989).

Young and Pearson (1991) introduced one of the first systematic field methodology involving flowmeter log. It includes performing short-duration single well pump or injection tests in screened wells followed by a flowmeter log in trolling mode. On the cumulative discharges measured at different depths in the well, profiles of hydraulic conductivity are determined. They present the results from 37 wells at a research site (Columbus Air Force Base, Mississippi). Although the aquifer was very heterogeneous (with transmissivities varying over four orders of magnitude), collected data were used to map the three-dimensional hydraulic structure of the aquifer. Conclusions based on the flowmeter data were validated by results from several tracer tests conducted with different pumping and injection schemes.

Keys (1990), in a complete review of conventional borehole geophysical methods, supports the thesis that these methods are useful at defining the general lithology of rock mass encountered by boreholes but they are not very useful at identifying individual fractures. Caliper logs indicate those intervals where fracturing has weakened the borehole wall rock so that the borehole is locally enlarged. Natural gamma logs indicate where fractures may be associated with lithologic contacts or where radioisotopes may be deposited as fracture infillings. Electrical resistivity and acoustic logs indicate where rock properties have been altered adjacent to fractures. All of these techniques, sample rock properties over too large volumes to be directly affected by fracture permeability, but each of them provides useful

indications on the effects of fracture on the bulk properties of rocks.

According to Molz and Young (1993), the borehole flowmeter offers the most direct technique available for developing a log of hydraulic conductivity in the horizontal direction. They introduced the calculation of K distribution, for a granular aquifer, or a flowpath distribution, for a fracture flow, based on flowmeter data. Applications of both spinner and electromagnetic flowmeters to granular and fractured-rock aquifers are described, and results indicate that the electromagnetic meter is capable of supplying a new level of detail concerning the K distribution. The authors introduce the concept that borehole flowmeter measurements can be viewed as a natural generalization of a standard fully penetrating pumping test, where just the steady pumping rate was measured, whereas in a flowmeter test the vertical flow rate distribution within the borehole or well screen is recorded.

Molz and Young declare that few models for the interpretation of vertical flow in wells have been developed: the Cooper-Jacob (1946) equation, based on relating drawdown to pumping rate in a well screened and fully penetrating confined aquifer, and the study by Javandel and Witherspoon (1969). In both methods it is assumed that flow in the aquifer is horizontal (Figure 6).

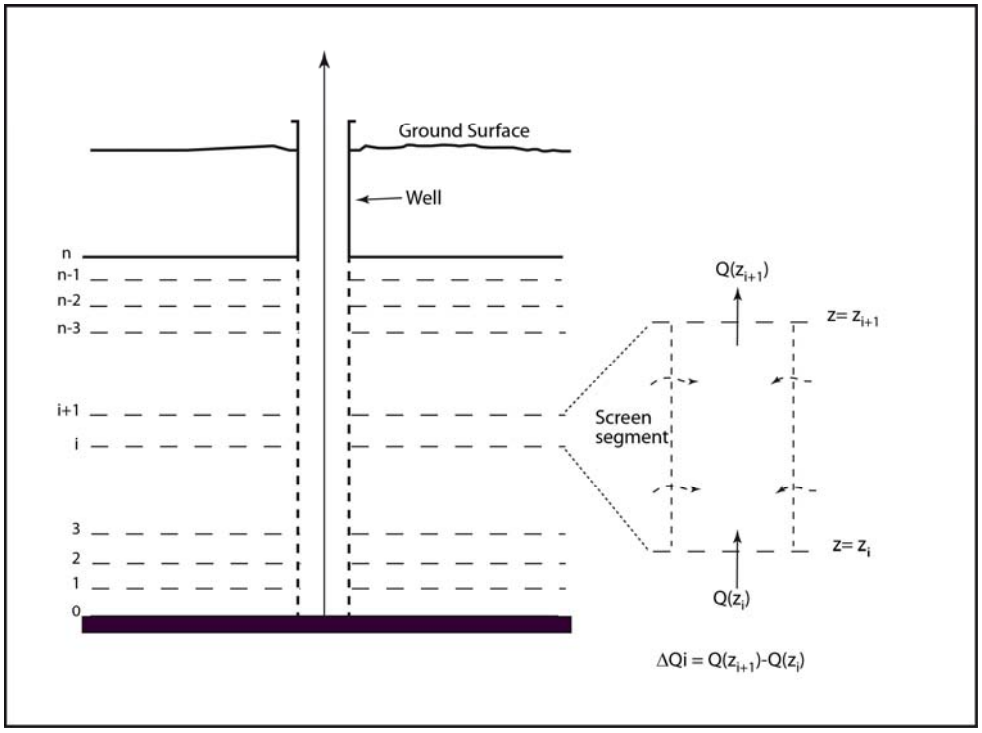

Figure 6: layered geometry within which flow measurement are collected and analyzed (adapted and modified from Molz, 1993)

In the Cooper-Jacob method (1946), the horizontal flow in each layer is assumed as if it were

coming from an aquifer of infinite horizontal extent and thickness Δ_{zi}. Then for each layer, *i*, one can write:

$$\Delta H_i(r,t) = \frac{(\Delta Q_i - \Delta q_i)}{2\pi K_i \Delta z_i} \ln\left[\frac{1.5}{r_w}\sqrt{\frac{K_i \Delta z_i t}{S_i}}\right] \quad \textbf{Eq. 2}$$

Where ΔH_i = drawdown in *i*th layer, ΔQ_i = flow from ith layer into the well under stressed conditions, Δq_i = ambient flow from i-th layer, K_i = horizontal hydraulic conductivity of the i-th layer, Δz_i = i-th layer thickness, r = effective well radius, t = time since pumping started, and S_i = storage coefficient for the i-th layer.

If it is possible to assume that head losses associated with flow within the well are negligible, and that the hydraulic diffusivity of each layer, $K_i \Delta z_i / S_i$ remains constant and equal to the hydraulic diffusivity of the aquifer T/S, where T is the transmissivity and S is the Storage coefficient, so Eq. 2 can be solved for K_i yielding

$$K_i = \frac{(\Delta Q_i - \Delta q_i)}{2\pi \Delta H_i \Delta z_i} \ln\left[\frac{1.5}{r_w}\sqrt{\frac{Tt}{S}}\right] \quad \textbf{Eq. 3}$$

T/S can be obtained from standard pumping tests, while ΔH_i can be obtained from multilevel head measurements.

Further details about head losses can be found in Rehfeldt et al. (1989).

Molz et al. (1989), mentioning the work of Javandel and Witherspoon (1969), suggested an alternative data analysis method. In idealized, layered aquifers, flow at wellbore radius r_w rapidly becomes horizontal. Under such conditions, the flow into the well from a given layer, for example due to pumping, is proportional to the transmissivity of that layer (Δz_i)

$$\Delta Q_i - \Delta q_i = \alpha K_i \Delta z_i = \alpha T_i \quad \textbf{Eq. 4}$$

with α = costant, Eq. 4 occurs when the dimensionless time $t_D \geq 100$

$$t_D = \frac{\overline{K}t}{\left(S_s r_w^{\,2}\right)} \quad \textbf{Eq. 5}$$

with $\overline{K}$ the average horizontal hydraulic conductivity:

$$\overline{K} = \frac{\sum K_i \Delta z_i}{b} \qquad \textbf{Eq. 6}$$

and b is the aquifer thickness, S_s is the aquifer specific storage, t is time since pumping started and r_w is wellbore radius.

The sum over the aquifer thickness of the Eq. 4 is

$$\sum (\Delta Q_i - \Delta q_i) = QP(PumpingFlowRate) = \alpha \sum K_i \Delta z_i \Rightarrow QP = \alpha \sum K_i \Delta z_i \frac{b}{b} = \alpha \overline{K} b \Rightarrow \qquad \textbf{Eq. 7}$$

$$\alpha = \frac{QP}{\overline{K} b}$$

Substiting for α in Eq. 4

$$\Delta Q_i - \Delta q_i = \frac{QP}{\overline{K} b} K_i \Delta z_i \qquad \textbf{Eq. 8}$$

and solving for $K_i/\overline{K}$ gives:

$$\frac{K_i}{\overline{K}} = \frac{(\Delta Q_i - \Delta q_i) b}{QP \Delta z_i} \qquad \textbf{Eq. 9}$$

To obtain Eq. 9 it is assumed that $(\Delta Q_i - \Delta q_i)$ and Q_P do not change with time (pseudosteady-state). This will occur when $r_w^2 S / 4Tt < 0.01$ (similarly to Cooper and Jacob solution) where S and T are aquifer storage coefficient and transmissivity, respectively.

Thus, from the flowmeter basic data it is quite easy to derive a plot of $K_i/K_{averaged}$ versus elevation. Therefore if one has the value of $K_{averaged}$ (eg. from a pumping test), one can easily obtain dimensional values for K_i by multiplying the ratio $K_i/K_{averaged}$ by the pumping test results.

In predicting fluid transport through fractures, the heterogeneity of the distribution of hydraulic conductivity in the fractured rock mass would require an unrealistic large number of boreholes to yield a representative sample of the fracture population. Furthermore the distribution of fractures identified from borehole studies may not indicate how individual fractures and fracture set are integrated into large scale flow system (Long et al., 1982).

Paillet (1993) presents new insights into inter-well flow connectivity in fractured rock aquifers.

The author introduces a systematic approach to fracture characterization designed to define the distribution of fractures along boreholes, and defines the nature of fracture flow paths across borehole arrays. This scale effect is one of the most challenging aspects of fracture studies using borehole methods. Estimation of the local hydraulic apertures of fractures is important, but this information is not sufficient to describe larger scale flow paths through fractured rock. Paillet (1993) used high resolution flow logging of boreholes during pumping to identify those fractures associated with flow into or out of observation and pumped boreholes. This information is then integrated over several different scales of borehole separation to infer the hydraulic properties of natural and induced flows in the vicinity of the study site. Such information is much more directly applicable to contaminant dispersal studies in fractured rock aquifers than simple descriptions of the frequency and orientation of fractures encountered by a few exploratory boreholes (Paillet, 1993).

The author define "cross-borehole flow testing" the measurement of the flows in both pumped and observation boreholes in an aquifer test. The aim of the test is to understand how the individual fractures identified in the boreholes are connected into larger-scale flow paths in the rock mass between boreholes (Figure 7).

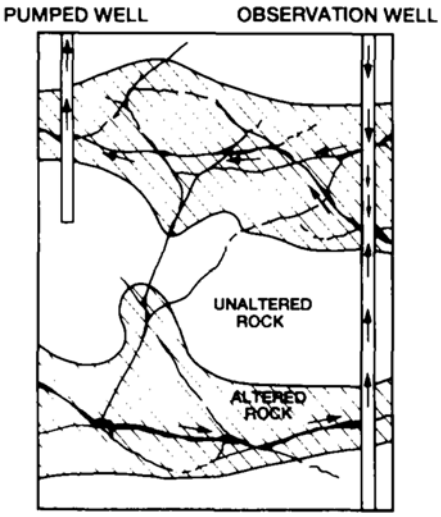

Figure 7: schematic illustration of fracture characterization, with two fracture zones intersected by the pumped and observation boreholes (Paillet, 1993)

Paillet introduced the "transient flow" concept as the change of the flow field between pumped and observation boreholes over time, starting from flow under ambient condition before pumping and evolving into a quasi-steady flow across the borehole array after the pump has been turned on for several hours (Figure 8).

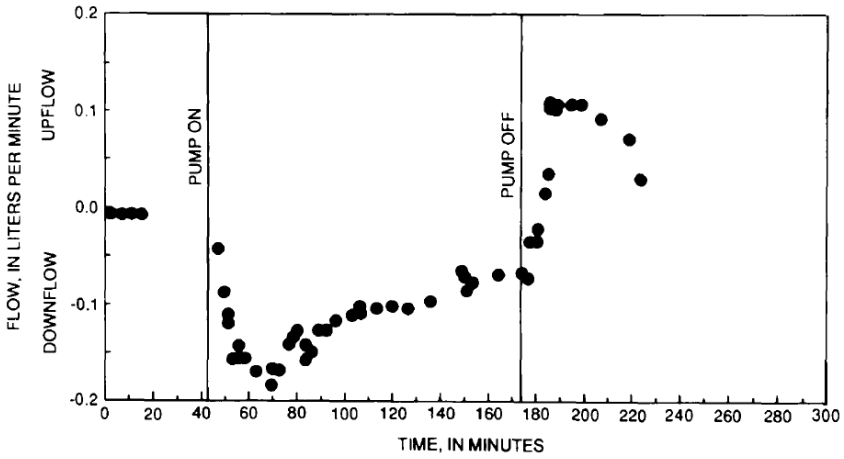

Figure 8: an example of transient vertical flow in an observation borehole connected to the pumped well (Paillet, 1993).

An analytical model for vertical groundwater flow in an observation well due to pumping in an adjacent well was suggested by Lapcevic et al. (1993). They assumed that both wells intersect the same discrete fractures and all flow in the observation well is due to well bore storage. This model is the first step in the development of more complicated models which will account for both wellbore storage and the contribution from other fractures. Single fractures are assumed as analogous to a confined aquifer, which is homogeneous, isotropic and of infinite extent.

Kabala (1994) analyzed the theory, assumptions, limitations and the relative errors of the flowmeter test methodology, proposing the "double flowmeter" test which eliminates those errors and provides measurements of the downhole distributions of the horizontal hydraulic conductivity, and specific storativity, and to analyze if it is possible to account for wellbore storage in the flowmeter test. Kabala argues that flowmeter methodology provides only an order of magnitude estimate of the hydraulic conductivity distribution mainly because the assumption of water flowing horizontally in each layer after a quasi-steady state is not always justified. Kabala suggests to perform the flowmeter test twice for each layer at two different times so that the borehole drawdowns at these two times differ appreciably from each other. This allows to solve Eq. 3 not interactively. The author applies this approach to a synthetic example and performs a first-order sensitivity analysis. Double flowmeter test has not been widely used in practical work mainly for technical reasons.

Young (1995) reviews different borehole flowmeter analysis methods and evaluates their applicability in fluvial deposits. He turns his attention to the so-called "K skin effect", a

reduced or increased permeability zone, due for example to backfill partially blocking the connection between one or more aquifer layers and the well screen. In presence of low-K skin effect, Young suggests to avoid use of Eq. 3 based on Cooper-Jacob (1946) method. Use of Molz's (1989) relation is certainly the best option. The trends and the magnitude of the K values are consistent with results from geologic investigations, tracer tests and multilevel pumping tests.

Hanson and Nishikawa (1996) combined flowmeter data and time-drawdown data collected from a long screened production well and nearby monitoring wells to estimate the vertical distribution of hydraulic conductivity in a complex multilayer coastal aquifer system. These data are processed analytically to estimate the bulk K value of the entire system and the K values of specific layers penetrated by monitoring wells. The authors emphasize the resolution limitation of the impeller flowmeter used in their experiment. Furthermore, neither time-drawdown or flowmeter data alone provide all the information needed for better aquifer test analysis.

A field experiment comparing water quality constituents, specific conductance, geophysical measurements (borehole induction logging, natural gamma) and aquifer test by Church and Granato (1996) suggests that the well screen acts as a conduit for vertical flow because it connects zones of different head and transmissivity, even in a relatively homogeneous, unconfined, sand and gravel aquifer where such zones are almost indistinguishable. Flow in the wellbore redistributes water and solutes in the aquifer adjacent to the well, increasing the risk of bias in water quality samples, failure of plume detection, and cross-contamination of the aquifer. The authors debate on the works of Giddings (1987) that instead proposes long screen wells as monitoring wells because they are more sensitive to the presence of contaminants for their better hydrologic connection with the aquifer.

Boman et al. (1997) describe applications of Electromagnetic Borehole Flowmeter in fluvial sediments. Data analysis of many tests in gravel packed wells suggests that flowmeter produces misleading data for a variety of reasons in such situations. Among other things, an annulus of high permeability around a well screen allows flow to bypass the meter, and the phenomenon is amplified by high pumping rates. Figure 9 illustrates the possibility of flow by-passing the meter in gravel packed wells. Thus, the authors argue about the deeper parts of a test well that would be isolated hydraulically and have less drawdown than the more shallow parts. The net effect of both phenomena would be to transfer apparent flow sensed by the meter to the top of the well where all external flow is forced to enter the screen near the

pump. If such data are collected and analyzed, a false, or at least magnified zone of high hydraulic conductivity will appear near the top of well screen. The authors conclude that flowmeter tests must be applied carefully and that further studies are needed to better understand the hydraulics of the flowmeter-well interaction. None of these problems, however, prevent effective use of Electronic Borehole Flowmeter, because the hydraulic conductivity information is far superior to that derived from standard pumping tests that assume aquifers homogeneous in the vertical direction.

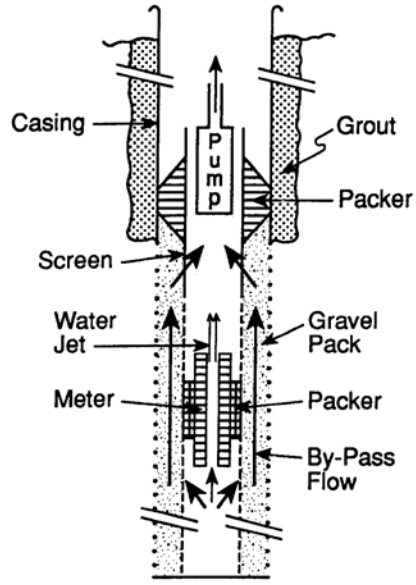

Figure 9: illustration of the discharge distribution around a borehole flowmeter in a gravel –packed well. Undetected flow may by-pass the flowmeter in the permeable gravel pack. Vertical flow in the gravel pack may also occur independent of the meter (Boman et al, 1996)

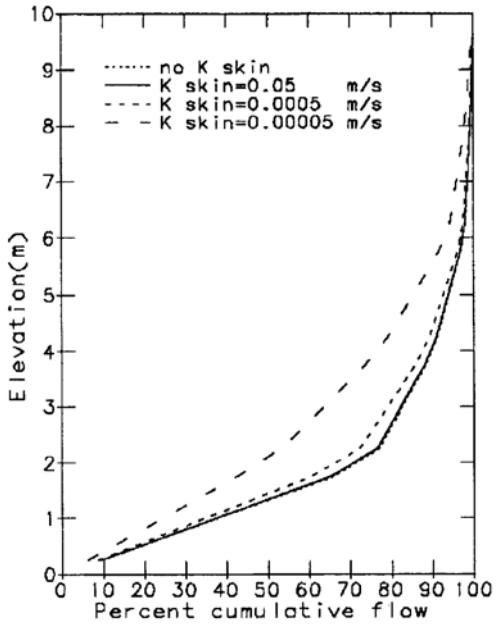

Figure 10: numerically simulated profiles of vertical flow in a pumping well for the case of no skin, negative skin (K=0.05 m/s), and positive skin (K=0.005 m/s and K=0.00005 m/s) effects (from Young, 1998).

Young (1998) examines the impacts of positive skin effects on borehole flowmeter tests in a granular aquifer. Positive skin is a zone of reduced K values near a well. Possible causes are drilling operations can cause an intrusion of drilling fluid in well annulus. Positive skin effects include head losses and changes in flow pathways in proximity of a pumping well. Positive skin effect can cause errors in the analysis of pumping test data (Figure 10).

Paillet (1998) proposes a numerical model of flow in the vicinity of a borehole to analyze flowmeter data obtained with high resolution heat-pulse flowmeters. Among other purposes, the model is designed to allow for an arbitrary number (N) of entry/exit points connected to

M<N far field aquifers (see Figure 11).

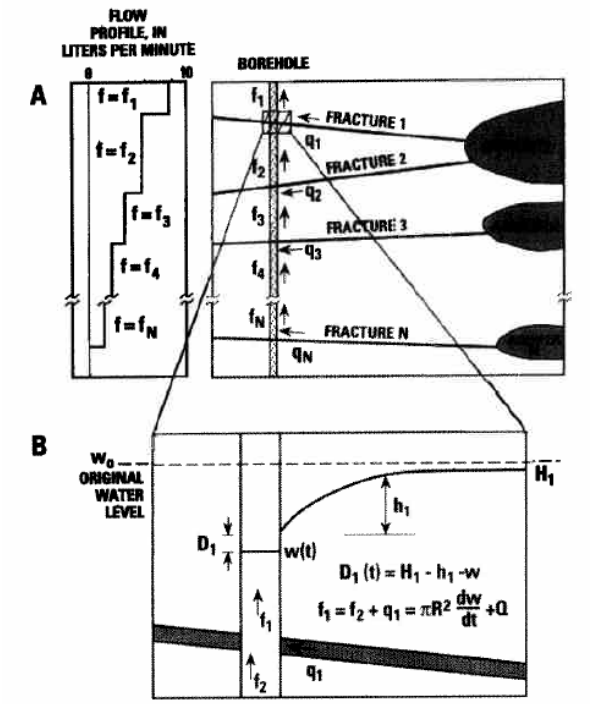

Figure 11: schematic illustration of fracture flow model: (a) N permeable fracture zones connecting the observation borehole to M far-field aquifers; (b) water balance in the uppermost fractures zone showing the relationship between measure flow, rate of inflow from the K=1 fracture, pumping rate Q and changes in water level in the borehole (Paillet, 1998).

Dinwiddie et al. (1999) based on Foley (1997) show by numerical simulation, that by-pass flow during flowmeter tests in gravel packed wells is directly proportional to flow rate used in tests in stressed conditions (Figure 12). By-pass flow is further enhanced by head loss through the probe and by increasing the gravel pack permeability. The authors performed their tests with an Electromagnetic flowmeter with 1.25 cm inner diameter.

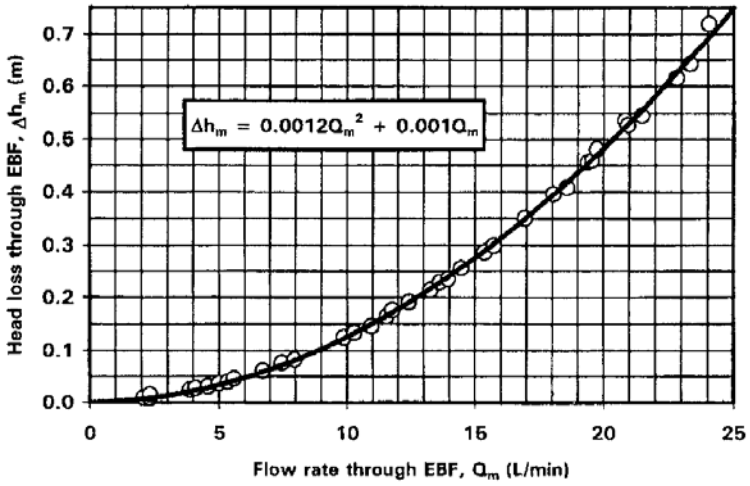

Figure 12: empirical parabolic curve-fit, wich relates head loss though the EBF to flow rate (Foley, 1997)

As illustrated in Figure 13, the head loss associated with the presence of the EBF in a wellbore divides an homogeneous aquifer into two distinct regions. EBF head loss isolates the portion of the aquifer below the flowmeter elevation from the drawdown measured at the surface. This isolation increases as the meter is raised because flow through the EBF increase and therefore the head loss increases (see Figure 12).

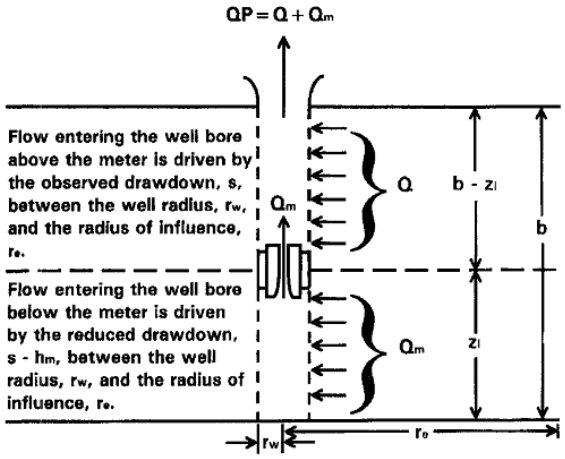

Figure 13: illustration of the two aquifer regions resulting from the presence of an EBF with its associated head losses. As a necessary approximation, the vertical length of the meter apparatus is assumed to be zero. (Dinwiddie, 1999)

Arnold and Molz (2000) repeated Dinwiddie et al. (1999) simulation trying to minimize the head loss. The authors tested four options to do it: (1) using an EBF without a packer at different flow rate; (2) using an EBF with a larger inner diameter (1 inch) with and without packer; (3) performing a mathematical correction of the head losses, and (4) using EBF at lower flowrate. Results of these applications were: (1) negligible head losses without a packer using flow rate until 30 l/min; (2) significant head losses reduction (until 1/16) using the 1 inch flowmeter respect the 0.5 inch, (3) during a flowmeter test with a packer, a flow rate under 10 l/min makes insignificant the head losses.

Paillet and Reese (2000) describe the integration of flow logs and aquifer tests in the development of a hydrostratigraphic model for a superficial aquifer system. Borehole flowmeter tests provided qualitative permeability profiles in most of 26 boreholes indicating the depth of transmissivity units.

Hutchins and Acree (2000) discuss the misleading data that are often generated using samples collected from conventional monitoring wells. They conclude that "the well acts as a "short circuit" along the well bore with the resulting ambient flow often of sufficient magnitude to compromise the integrity of any samples collected from the well.

Genereux and Guardiario (2001) arguing about flowmeter measurements reliability, support the idea that the two potentially significant concerns in a highly permeable rock unit are: (1) redistribution of flow into the borehole in response to head loss across the flowmeter and (2) reproducibility of the measurements, mainly the reproducibility with which the inflatable packer can be seated at a measurement point. About the reproducibility of packer seating a very conservative approach is to discard any measurement showing a net inflow lower than the measurement point immediately below in the same borehole

Elci et al. (2001) developed a detailed three-dimensional model of flow and transport in the vicinity of a fully penetrating monitoring well. The model was used to simulate a measured ambient flow distribution around a test well in a heterogeneous aquifer. Tracer transport simulations then illustrated how a contaminant located initially in a lower portion of the aquifer was continuously transported into the upper portion and diluted throughout the entire well by in-flowing water.

Even after full purging or micropurging, samples from such a well will yield misleading and ambiguous data concerning solute concentrations, location of a contaminant source, and plume geometry. For all these reasons the author suggest not to use long screened monitoring wells unless an appropriate multilevel sampling device that prevents vertical flow.

As concern the cross borehole flowmeter tests Williams and Paillet (2002) introduced an alternative approach to the conventional aquifer test for fractured rock aquifer application. The basis of this approach is the observation of the propagation of short (typically 15 or 20 min) pulses of drawdown (for example performed with pumping or injection) across the observation borehole array. The complete method is based on the identification of permeable fractures in each borehole by single well flowmeter test, followed by a series of specific pulse tests that can be used to define connections between the individual fractures detected in each borehole. The shapes of the transient flow profiles are compared to type curves computed for several different types of fracture connections (Figure 14). The fitting of the data to the type curve yields an estimate of fracture transmissivity and storage coefficient.

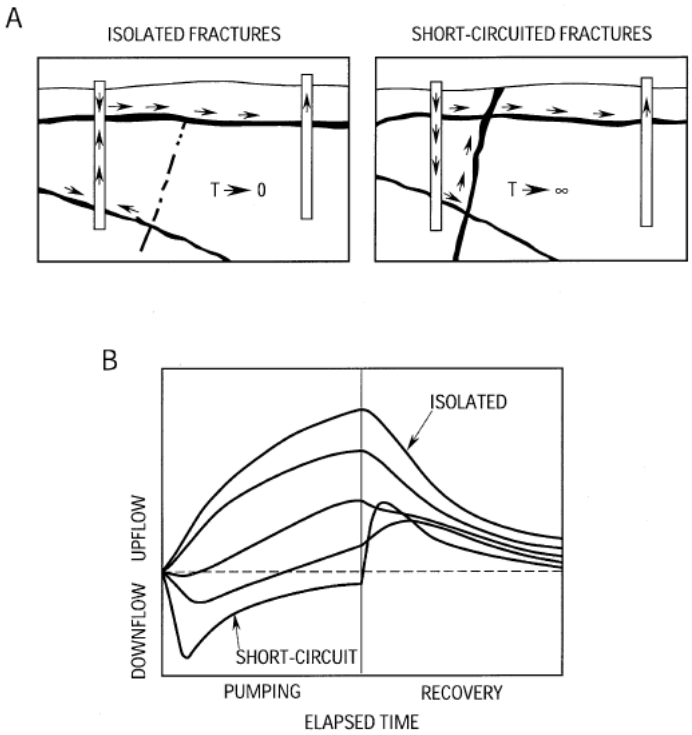

Figure 14: Type curves computed for a situation where (A) a single fracture connects pumped and observation borehole intersects a deeper fracture of approximately the same transmissivity and (B) type curves vary in direction and magnitude of flow according to the transmissivity of a third fracture in the surrounding formation (William and Paillet, 2002).

Zlotnik and Zurbuchen, 2003 intended to (1) determine the analytical solutions to correct the head loss caused by EBF and (2) to apply these solutions to real data.

In the case of an *ideal EBF* without head losses, Eq. 9 is valid. In the case of a *non-ideal EBF* with head losses, this equation needs a correction.

They rewrite Eq. 9 as:

$$\left(\frac{K_i}{K}\right)_{ideal} = \left(\frac{K_i}{K}\right)_{non-ideal} + \delta$$

Eq. 10

where δ is a "correction factor" (Zlotnik et al., 2003) and *K* is the bulk permeability.

The authors indicate that the drawdown, *s'*, due to the difference between the drawdown for a non-ideal flowmeter and an ideal flowmeter, can be attributed to an "equivalent recirculation well", where the lower section (below the flowmeter) injects water to the aquifer, while the upper portion extract water from the aquifer with an equivalent flow rate.

Paillet (2004) analyzes in particular the correction for the suppression of the effects of diameter variations and rugose borehole on trolled flow logs. Variations in borehole diameter has as its main consequence to allow for various amounts of by-pass around the flowmeter. The author suggests to use a particular "under fit diverter", especially for the heat-pulse flowmeter, to force at least some of the flow into the probe measurements section. Furthermore a correction flow factor needed to be computed to correct the increased wellbore diameter. To determine correction factor, flow measurements were made as close to the diameter change as possible. Comparison of flow above and below the diameter change, indicate the factor to account for the much greater by-pass flow.

Le Borgne et al. (2006a) present a characterization of flow paths connectivity at the Ploemeur fractured crystalline aquifer (Brittany-France) resulting from cross-borehole flowmeter tests and argue about scale effects in hydraulic properties. They synthetize hydraulic properties estimates obtained from field technique having distinct scales of investigation: single borehole flowmeter experiment, cross borehole flowmeter experiments and long term pumping test. The conclusion is that borehole scale variability of transmissivity estimates vanishes at larger scale and that the transmissivity converges towards the high values of the transmissivity distribution. The authors explain this effect (for the test site) by the organization of the flow field in the subsurface and particularly the good connectivity of the permeable zones all over the site.

Le Borgne et al. (2006b) propose a framework for cross-borehole flowmeter test interpretation that is based on a "two-scale conceptual model": discrete fractures at the borehole scale and zones of interconnected fractures at the aquifer scale. The first problem consists of estimating the hydraulic head variations that drive the transient borehole flow observed in the cross borehole flowmeter experiments. The second inverse problem is related to estimating the geometry and hydraulic properties of large scale flowpaths in the region between pumping and observation wells that are compatible with the head variations deduced from the first problem.

Le Borgne et al. (2007) compare flowmeter and single packer tests to show that few of the fractures interpreted as open from other geophysical logs (e.g. ERT, Fluid Electric Conductivity, optical and acoustic image logs) are significantly transmissive. To determine fracture zone connectivity, the authors propose a methodology based on the variation with packer depth of the ratio of the drawdown in the observation well and the drawdown in the pumping well. These results are also compared to the analysis of cross-borehole flowmeter

tests. Both methods provide consistent results with a similar level of information on connectivity.

Barahona-Palomo et al. (2011), analyze hydraulic conductivity data obtained by Kozeny-Carman empirical formulation (based on particle-size distribution) and borehole impeller-type flow tests. They found that correlation between the two sets of estimates are practically absent (R^2=0.0095). Hydraulic conductivity values are similar in terms of mean value and differ in terms of variogram ranges and sample variances. The authors argue that the two types of estimates can be associated with different measurement scales. Furthermore the relationship between measured vertical fluxes and the micro-structure of the system is still not clear and should be further analyzed in real site applications (*Barahona-Palomo et al., 2011*).

The relationship between fluid temperature and flow logs in a fractured karst aquifer are discussed in Chatelier et al. (2011). For the authors both techniques complement each other since flow log measures local flow velocities in well whereas water column temperature profile (under different hydrodynamics conditions) could delineate inflow depths and sources feeding. The vertical distribution of temperatures is, in fact, perturbed when a borehole intercepts local flow conduits or fractures (Keys, 1990). An important conclusion of the study by Chatelier et al. is that it is advisable to monitor both water temperature and flow in a well. This avoids or reduces the uncertainty in the interpretation of temperature measurements alone. Furthermore temperature logging is not expensive and relatively rapid to conduct.

Chapter 2

Hydrogeophysical characterization of a complex aquifer in calcareous and gypsiferous formations

Paper in preparation

A. Godio, Politecnico di Torino

S. Basiricò, G. B. Crosta, P. Frattini, A. Villa,

Università degli Studi di Milano Bicocca – Milano

Abstract

We performed a coupled hydrogeological and geophysical investigation to characterize a part of an aquifer hosted in calcareous- gypsiferous formation at shallow depth. The work is in the framework of a cleanup project from groundwater contamination of chlorinated solvents. The hydro-geophysical characterization was aimed to detect the most conductive levels within the gypsum-calcareous formation in a depth range between 10 and 20 m from the surface, observe the hydraulic connection of the main productive levels and estimate the hydrodynamic properties of the aquifer.

We surveyed the main productive level by borehole radar to assess the lateral continuity of the porous and permeable zones between closely-spaced boreholes. Flowmeter tests identified the zones of inflow-outflow in the boreholes and allowed us to estimate the hydraulic parameters. The hydrogeophysical characterization detected with good accuracy the spatial heterogeneity of the aquifer, supporting a more reliable design of the remediation activities.

Key-words: Hydrogeophysics, Flowmeter testing, Borehole radar

1 Introduction

In an aquifer, characterized by a complex sequence of gypsum-marl and calcareous layers, the spatial heterogeneity is a major controlling factor for a remediation project. The design of the cleanup project by injection of an opportune reagent requires an accurate prediction of the geometrical conditions of the aquifer, to detect the main productive levels and to estimate the hydrodynamic parameters. The combined use of geophysical methods and hydraulic tests can be useful in assessing the hydrogeological response of the system under dynamic

conditions (eg. recharge of groundwater, effect of injection of fluid at high pressure).

The joint use of borehole and surface geophysical investigation is a cost-effective approach that permits to integrate the hydrogeological characterization by providing additional and spatially reliable information on the continuity of permeable or less permeable layers or more in general on the geometry of the aquifer. The most useful parameters are the electrical bulk conductivity and/or dielectrical permittivity as their sensitivity to the soil/rocks texture and fluid content. Moreover the use of geophysics in time lapse fashion offers an effective tool for monitoring the dynamic processes within the aquifer, as the effect of pumping or recharge of the aquifer, for mapping 2D/3D evolution of water infiltration from the surface and for estimating the hydraulic parameters of the aquifer. Aquifers in fissured rock can be characterized by the joint use of georadar and electrical resistivity tomography. Time-lapse difference-attenuation radar tomography was conducted during saline tracer experiments in a fractured aquifer by Day-Lewis et al.) 2004. The presence of electrically conductive saline tracer effectively illuminates permeable fractures or pathways for geophysical imaging. Cross-hole radar monitoring in time lapse fashion is often adopted to monitor dynamic processes in aquifer or the effect of biostimulation processes (e.g. Lane et al. 2004, Kuras et al. 2004, Slater et al. 2000, Wilkinson et al. 2009). High-resolution time-lapse ground-penetrating radar (GPR) has been adopted for imaging the rainfall drainage within limestone (Truss et al., 2007). Moreover, it has been widely demonstrated that the response of ground penetrating radar is mainly affected by the soil water content (Huisman et al. 2003) spatial and temporal changes.

We performed hydrogeological and geophysical investigations to characterize a part of an aquifer hosted in calcareous-gypsum formations at shallow depth (10-40 m) subjected to a remediation project of a diffused contamination by chlorinated solvents in soil and dissolved in groundwater.

The hydro-geophysical characterization involved several approaches: pumping tests, tracer experiments and electromagnetic borehole flow-meter in single well mode. The methods aimed to estimate the lateral continuity of the most permeable layers and to estimate the water content of the main productive layers. We used the GPR in cross-hole and single hole configuration for a fast estimate of the main productive levels in a gypsum and calcareous formation, the absence of radar signature or response being due to the signal attenuation caused by the high electrical conductivity of marl and clay levels.

We performed flowmeter surveys to detect flow patterns inside the boreholes, fractures or geologic units with very high hydraulic conductivity and understand potential

interconnections between permeable layers. Flowmeter logs (Hess, 1986, Paillet, 1999, for heatpulse flowmeter, Moltz and Young, 1993, for electromagnetic flowmeter) can improve the conceptual models, providing information for the design and interpretation of other hydraulic tests and input data required by mathematical models.

2. Materials and methods

2.1 Geological settings

The study site is located in a plain area at the foot of a hilly zone geologically belonging to the Apennin ligurian nappes formed within the –Piedmont-Ligurian ocean basin (Figure 15).

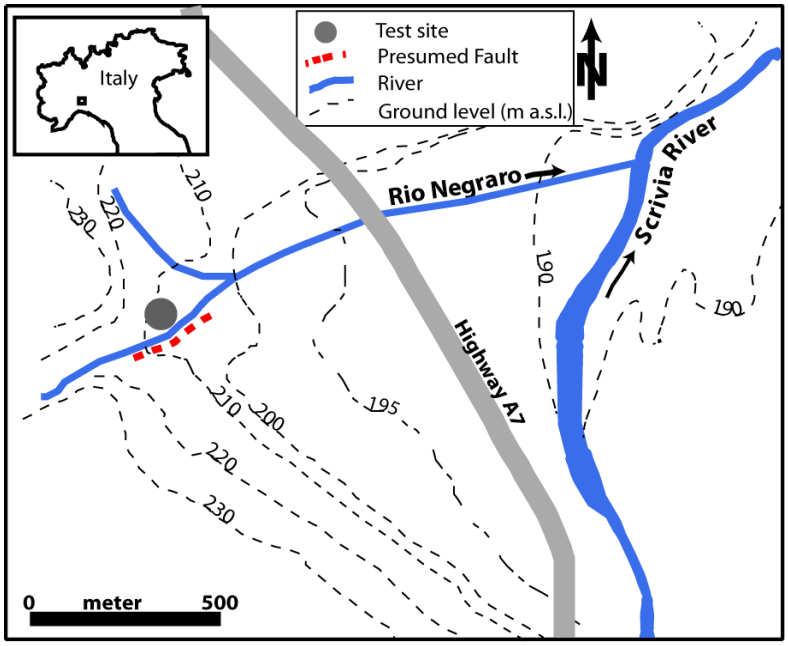

Figure 15: location and main features of the test site area

The local geological setting has been characterized through the description of more than 20 boreholes that have been drilled since 2005. The depth of the drilling ranges from 6.5 m up to a maximum of 63.5 m from ground level.

Gravelly sandy to loamy fluvial deposits and anthropic soils extend from the surface to a depth of about 5-8 meters (Figure 16). Below this layer lies a Tertiary bedrock, whose stratigraphic sequence is formed, from the bottom to the top, by silty marls (S. Agata Fossili Marls–Tortonian) overlaid by a complex geological unit (cd. Gessoso-Solfifera Formation, Messinian), 40 meter thick, composed of a succession of sandy loam, clayey loam and sand with levels of weathered limestone and gypsum. Gypsum layers are characterized by small

crystals locally substituted by large selenite crystals. At the regional scale bedrock layers present a regular bedding dipping to NW at 25° to 35°.

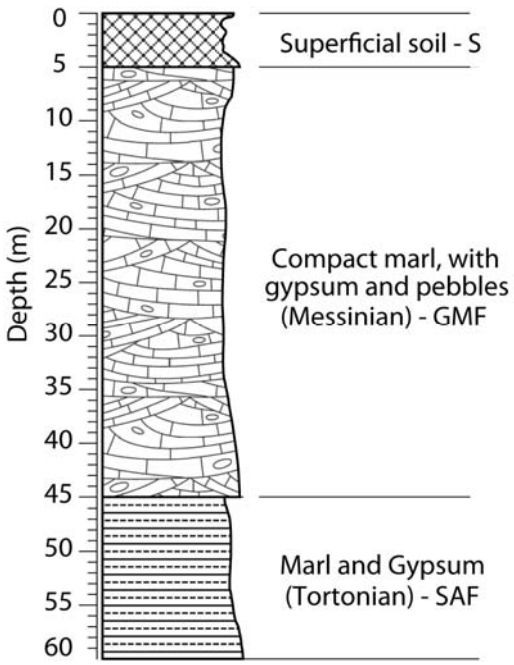

Figure 16: stratigraphic column for the test site zone. The wells used for hydrogeophisic test involving superficial soils and Messinian Formation

Water inflows have been observed while drilling through the thin layers of the Messinian Gypsum formation, at different depth (e.g., 9 inflows along 35 m of borehole S7 in Fig. 3), from 5 to 45 m below the ground surface (Arpa Piemonte, 2006). In general, the formations present a widely variable permeability, due both to the sedimentary sequence and fracturing.

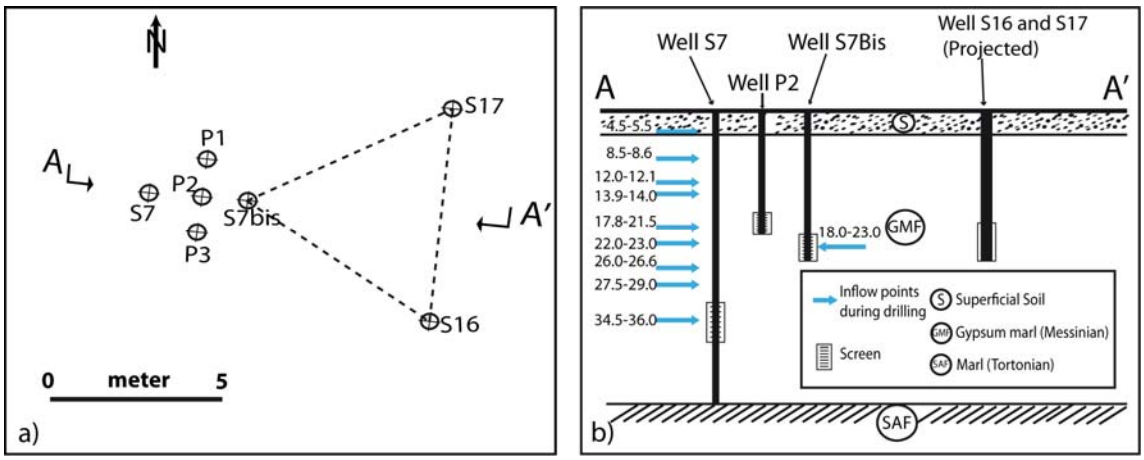

Figure 17: a) geometric disposition of the wells present in study area. Wells S7 and S7bis were drilled in 2007, S16 and S17 in 2009 and P1, P2 and P3 in 2010. Well Px were useful (see fig. 5), but not were used for hydrogeophysics test for this study. b) evidence of inflows of water observed in S7 and S7bis during drilling operation.

Geology and hydrogeology of the area is also complicated by the presence of a fault oriented approximately SW-NE, in proximity of Rio Negraro, and causing the uplift of the Tortonian marls and the possible occurrence of associated fractures.

2.1.1 Borehole characterization

We performed geophysical and hydrogeological within three boreholes drilled between 2007 (S7bis) and 2009 (S16 and S17) by rotary drilling (Table 2) with core recovery. All boreholes are equipped with an open standpipe screened along a depth interval which includes the most important water inflows observed during drilling.

Borehole Name	Wellbore diameter	Drilling diameter	Drilling Depth (b.g.s.).	Screen Depth (b.g.s.)
S16	76.2 mm	176 mm	23.0 m	16 m to 23 m
S17	76.2 mm	176 mm	23.0 m	16 m to 23 m
S7bis	101.6 mm	152 mm	23.0 m	18 m to 23 m

Table 2: technical characteristic of borehole

Cores have been visually inspected along the screened zone to detect different layers. Samples have been collected from these layers to describe the grain-size distribution of the fine fraction (diameter < 1mm), by using a laser granulometer. With the exception of a few slightly coarser samples, the analyzed sediments are almost completely composed of silt.
Many discontinuities and open fractures probably related to the dissolution of gypsum levels and lenses have been observed (Figure 18).

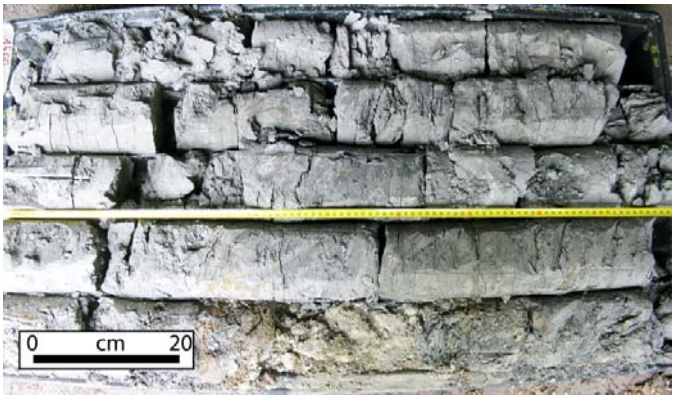

Figure 18: photograph of core taken from borehole S17 between 15 and 20 m BGS.

2.2 Hydrogeological setting

The shallower aquifer is hosted in alluvial deposits in the depth range between the ground

surface and about 10 m. The second aquifer in gypsum-calcareous formations is located between 10 m and 60 m in depth; the groundwater circulation is mainly controlled by the network of fractures. The relationship between the two aquifers has been established by drilling wellbore P2 (see Figure 19) on September 2010. Groundwater level fluctuations up to two meters above the static level were observed in well S7bis (equipped with a pressure transducer) due the pressure of the drilling fluids. These data could be consistent with a series of very steep fractures which connect the two aquifers.

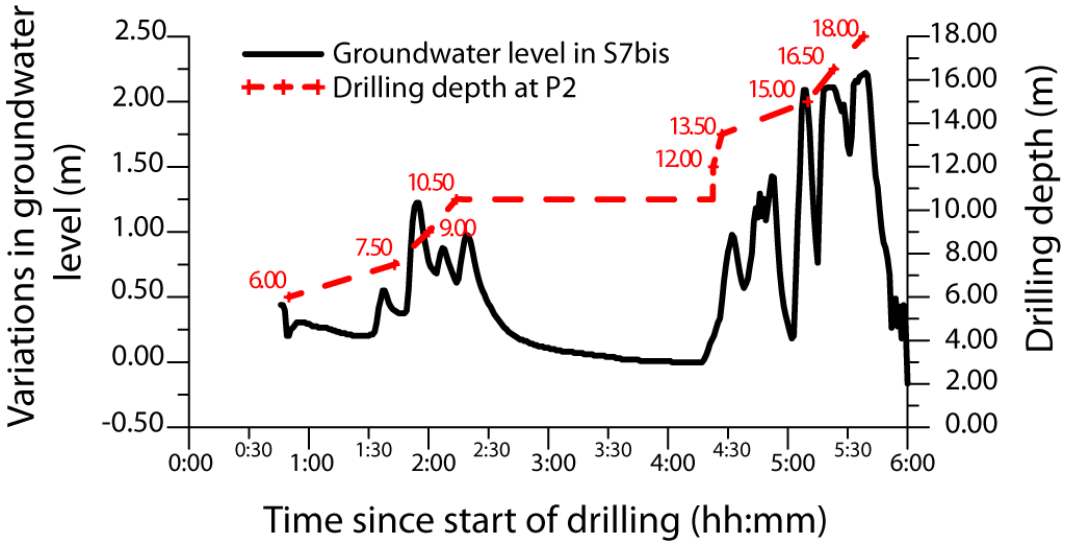

Figure 19: groundwater level in wellbore S7bis when drilling the wellbore P2. Each peak is relative at different drilling fluid pressure used. A recession is observed during a 2 hours stop of drilling operation.

Furthermore, groundwater level in the second depth aquifer is very sensitive to rainfall. We have recorded instantaneous changes both in piezometric level and in water specific electric conductivity. Figure 20 shows monitoring data relative to a short time period with distributed rainfall (about 470 mm in 3 months).

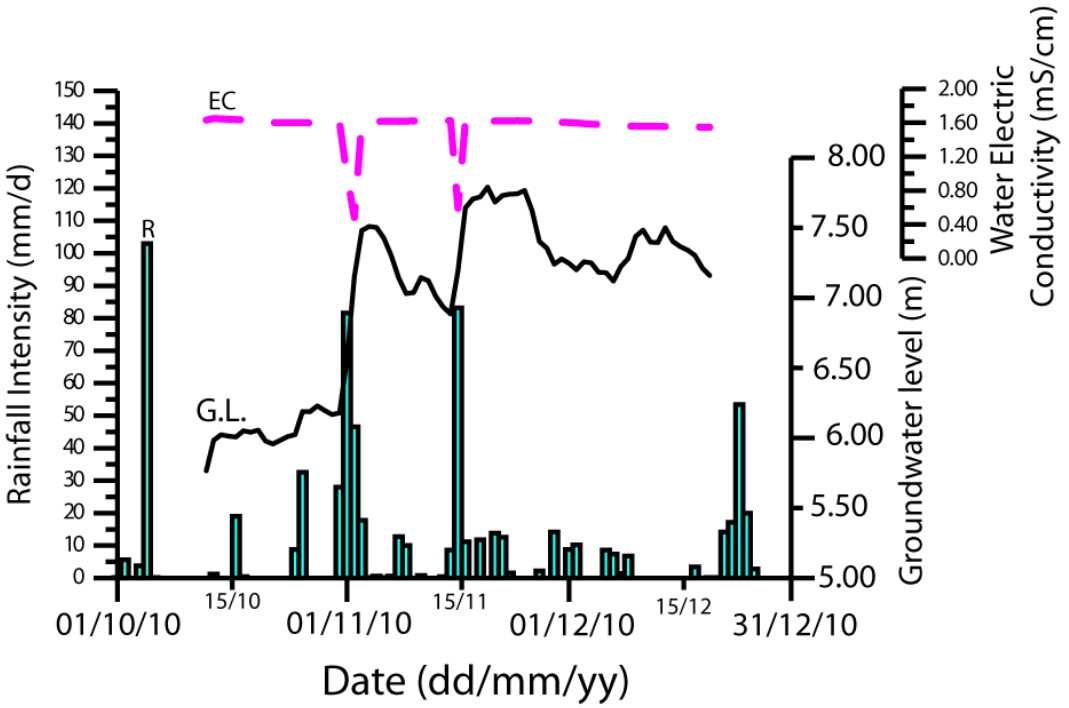

Figure 20: rainfall daily intensity (R), groundwater level (G.L.) and specific electric conductivity (EC) observed in wellbore S16 between October 13rd and December 20th , 2010.

Borehole characterization was also integrated by conventional pumping test. During the pumping test, boreholes S7bis was used as pumping well and borehole S16 and S17 as monitoring wells. The test was carried out using a flow rate of Q_p equal to 15 $l*min^{-1}$. The measured drawdown was 2.85 m in the pumping well and 0.96 m and 1.03 m in boreholes S16 and S17 respectively.

We analyzed the data from pumping test using Theis' fitting method for confined aquifer. We obtained the transmissivity value of 1.2 10^{-4} m^2*s^{-1} and the Storativity is $1*10^{-4}$.

2.3 Georadar survey

We performed the georadar survey by in-hole and cross-hole configurations. The in-hole survey involved the use of a IDS Ris K-100 georadar system operating at the main frequency of 150 MHz and 300 MHz. The antenna was moved along the boreholes with a constant offset of 2 cm from the bottom to the top of the well. The data were collected in single reflection mode in common off-set modality within 8 boreholes of the monitoring network. Main goals of this first step were: i) to detect or to confirm the existence of the main productive horizon in the second aquifer, characterized by a complex network of fractures in the calcareous and gypsum; ii) to assess the performance of the georadar in this environment in terms of data

quality and radial penetrating distance.

In cross-hole configuration, two acquisition schemes are usually adopted: the multi-offset gathering (MOG, tomography geometry) and zero-offset profiling (ZOP, cross-hole geometry) (Binley et al., 2001). MOG offers multi-dimensional imaging through high-resolution tomography, but data acquisition is relatively slow due to the huge amount of the measurements. Tomographic schemes typically rely on some kind of ray approximation of the EM waves. Straight-ray algorithms give reliable results if the velocity variations in the medium are moderate. If strong velocity variations are expected, algorithms that take bending of the rays into account will produce more reliable results. ZOP data do not require tomographic inversion, and the electromagnetic-wave velocity is calculated for a known antenna separation, assuming that the first-arriving energy travels along a direct path from the transmitter to the receiver. This assumption, however, can give rise to erroneous velocity estimates if the traveltime of the refracted waves is lower than the direct wave traveltimes (Huisman et al., 2003, Rucker and Ferré, 2003 and Rucker and Ferré, 2004).

By assuming a straight ray-path, a first arrival time is used to calculate velocity (v) as $v = d/t$, where d is the offset distance between transmitter and receiver and t is the traveltime. By further assuming that frequency-dependent dielectric loss is relatively small, the electrical permittivity is obtained from the velocity values. The time lapse cross-hole survey permits to estimate the wave velocity changes that are governed by the variations of the water content. The main sources of uncertainties are related to:

- mislocations and errors in the source-receiver positioning at different time steps, because usually the antennas are manually moved by the operator along the borehole;
- the traveltime estimation;
- error in simulation of raypaths and the inversion procedure (MOG data only);
- bias introduced by the model used to convert the traveltimes into water content changes.

In ZOP investigation the first source can be neglected with respect to the importance of the other sources, while in tomographic inversion the mislocation in source-transmitter positioning could strongly affect the final results, because of the ill-poseness and ill-conditioning of the cross-hole tomography.

The cross-hole radar survey was focused on the small-scale test site (4 boreholes). We initially collected 3 different panels between the boreholes S7b, S16 and S17 (see Figure 21); the three

boreholes are about 5 meter spaced for a depth of 23 m. We acquired further data along the section between the borehole S7b and a new borehole, called S7. The two boreholes are 2.5 m apart. We used the Sensor and Software georadar, equipped with a couple of separated antennas at the main frequency of 100 MHz.. The data acquisition involved the positioning of the antennas at the same level within each couple of boreholes. The antennas were kept at the same elevation and moved along the boreholes at spacing of 12.5 cm. The main objective was to check the reliability of the georadar survey in cross-hole arrangement for the water content estimate of the main productive horizons.

We processed the data processing according to the following steps: i) trace editing and removal of noisily data ii) correction for the zero-shifting by analyzing the data calibration iii) application of the Automatic Gain Control amplification to enhance the response of targets. In ZOP data set the traveltimes, where detectable, were picked up to estimate the wave velocity and the electrical permittivity.

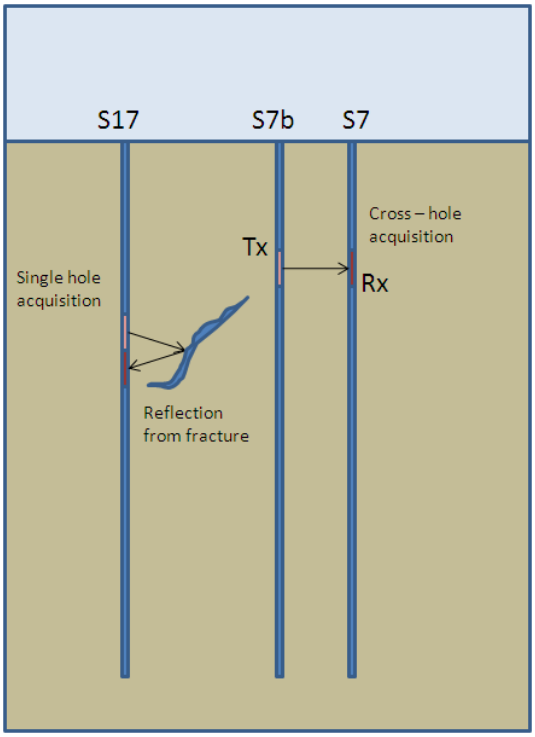

Figure 21: georadar data acquisition in single hole and cross-hole configuration in the test site.

2.4 Flowmeter survey

We adopted an electromagnetic borehole flowmeter (EBF) (by Quantum Engineering Corp) with an inner diameter of 2.54 cm able to measure flow rates in the range from 0.04 $l*min^{-1}$ to 40 $l*min^{-1}$.

The open annulus (filled with gravel pack)- see table 1 - between the well screen and the well

bore acted as a possible disturbing factor during flowmeter logging. This zone provided an open conduit for water to flow outside the probe. We sealed the annulus between the probe and the screen a packer inflated by an hand pump..

We checked the accuracy and precision of the probe, in laboratory by testing it in a 3" PVC column (the same diameter of the test site wellbore); the tests were performed at three different flow-rates. Results are shown in Figure 22.

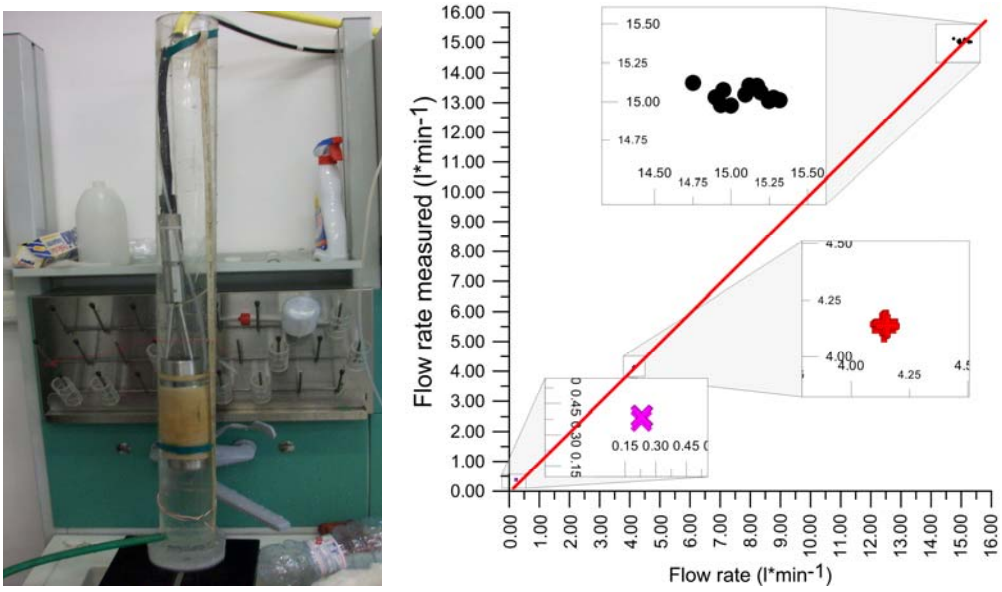

a) b)

Figure 22: a) 3" PVC column for laboratory test; b) check of accuracy and precision of the EM Flowmeter, three different flow-rates were used: 0.18 l min-1; 4.12 l min-1; 15 l min-1;

In the field, we calibrated the system before the surveys by setting the zero flow value in the unscreened casing.

We logged along the screened part with 0.25 m spacing. We waited a sufficient time to stabilize the flow value; this reduced the disturbance to the borehole flow condition due to the probe movement and to packer inflation.

We performed the flowmeter logs both under ambient and stressed conditions for each borehole. Flow measurements under pumping conditions were made when a pseudo-stationary condition was reached. Piezometric level was monitored during the whole test.

The depth of the beginning of the test not always matched the depth of the drill because of the sediment deposited on down hole.

We estimated the permeability coefficient (K) using the Molz et al (1989) method: the hydraulic conductivity of an interval of the aquifer along the borehole is a function of the

interval groundwater contribution to the well discharge. The fundamentals of the Molz's theory are the stationary (or pseudo-stationary) conditions of the flow, the horizontal flow to the well and the perfect stratification of the aquifer in the proximity of the well. The Molz's relation is:

$$\frac{K_i}{\overline{K}} = \frac{(\Delta Q_i - \Delta q_i)b}{QP\Delta z_i} \qquad [1]$$

where $\overline{K}$ is the bulk hydraulic conductivity and the K_i is the hydraulic conductivity of i-th layer, ($\Delta Q_i - \Delta q_i$) is the difference between stressed and ambient flow rate, QP = pumping (or injection) flow rate, b = thickness of the aquifer and Δz_i = thickness of the *ith– layer* (corresponding to 1/frequency of sampling).

2.5 Multiparameter log

Specific Electric conductivity (at 25°C) and temperature logs were performed with a 0.25 m step by a multiparameter probe (model Hanna Instruments HI 9828), able to measure the conductivity in a range of 0 to 400 mS cm^{-1} with precision of ±1 uS cm^{-1}; the temperature in the range -5.00 °C to +55.00 °C with precision of 0.1°C.

3. Results and discussion

3.1 Well testing

Well Bore S16

Ambient flow data for wellbore S16 (Figure 23) indicate a no flow zone between the bottom hole and 18.25 m below ground surface (bgs) and an upward vertical flow above 18.25 m bgs until 16.00 m bgs, reaching a maximum of about 2.5 l*min^{-1}. Hence groundwater enters the wellbore between 18.25 and 17.50 m bgs and flows upward to the outflow zone at 16.25 m bgs where an outflow zone exists. Not variations in ambient vertical flow between 17.50 m and 16.25 m bgs were observed.

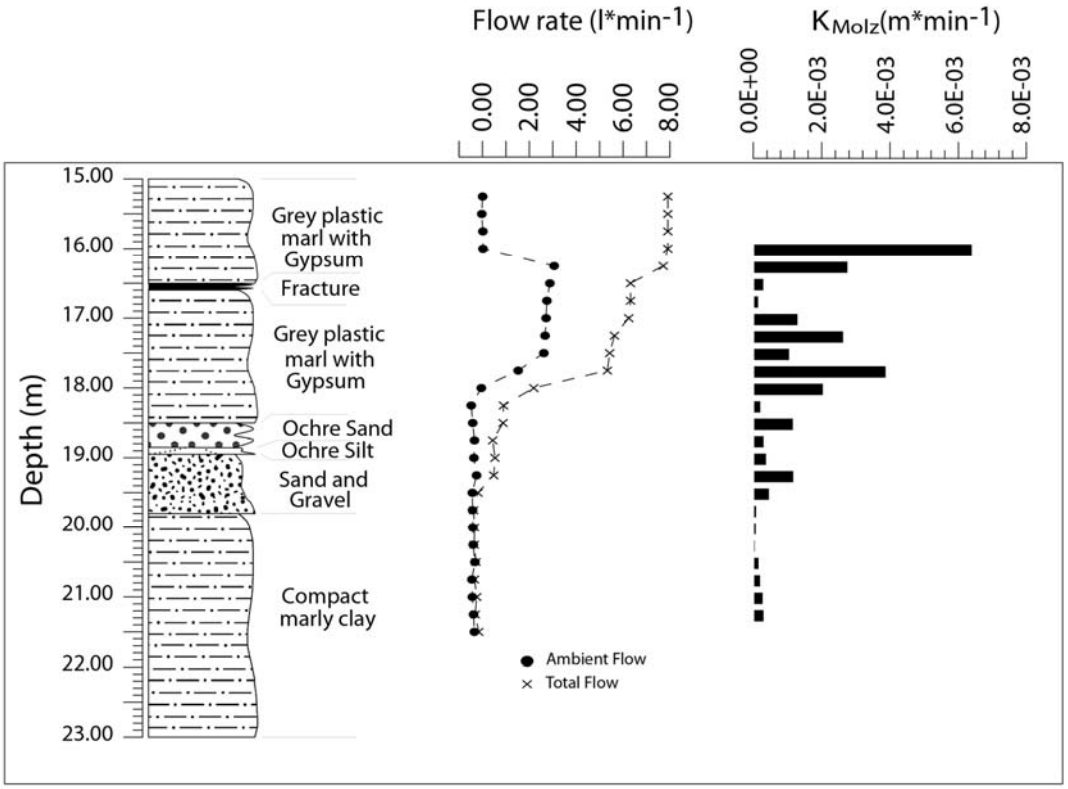

Figure 23: core stratigraphic, entity of ambiental and pumping flow, hydraulic conductivity by Molz's relation for the borehole S16.

We repeated a flowmeter log in stressed conditions at the same depth of the log in ambient conditions using a pump flow rate of 7.7 l*min^{-1}.

Essentially the positions of the more transmissive layers were confirmed, and it was observed a gradual increment of flow between 19.50 m and 19.25 m, probably due at another hydraulically active level in correspondence of sand and sand and gravel formations.

Permeability estimates according to Molz, shows the highest K value at 16.00 m (K=6 10^{-3} m*min^{-1}), in correspondence of the outflow zone, while the level at 18.00 m shown the lowest permeability (K= 4 10^{-6} m*min^{-1}).

The analysis of the differential ambient flow, gives the quantitative horizontal flow contribution for different layers.

In Figure 24, the most of the flow is localized in the two principal transmissive layer intercepted by borehole S16 (the first between 17.25 and 18.25 m and the second in a thin layer around 16.00 m).

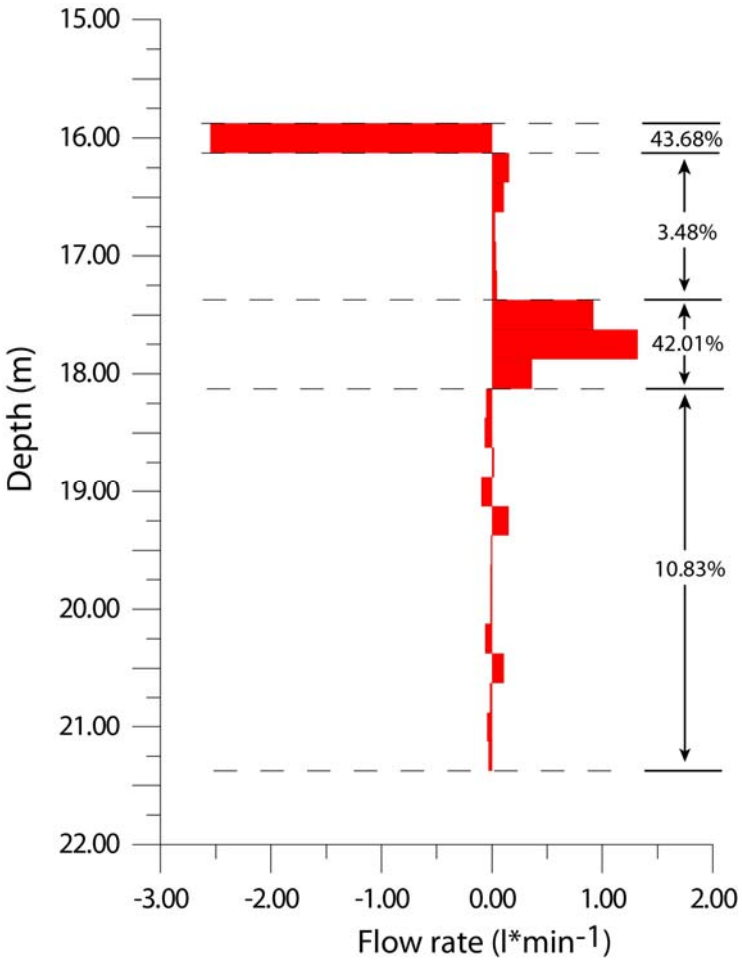

Figure 24: differential ambient flow for borehole S16.

Temperature/Electric Conductivity of the water column (Figure 25)

Fluid temperature along the wellbore has a constant profile at 12.9°C. The EC (electrical conductivity) behavior shows instead some singularities: it has rather constant trend with values around 1200 µS*cm^{-1} between 16.00 and 18.00 m in depth (in a part of the well with

upward flow), while at depth between 18.0 and 19.5 m, where the ambient flow is null.

We observe an increasing in EC values up to 1340 µS*cm^{-1}; EC shows a more complex profile below the depth of 19.5 m where EC increases until 1380 µS*cm^{-1}. We explained the behavior accounting it as a positive anomaly respect to the EC gradient observable in the no-flow zone, eg. below the inflow point at depth of 18.0 m.

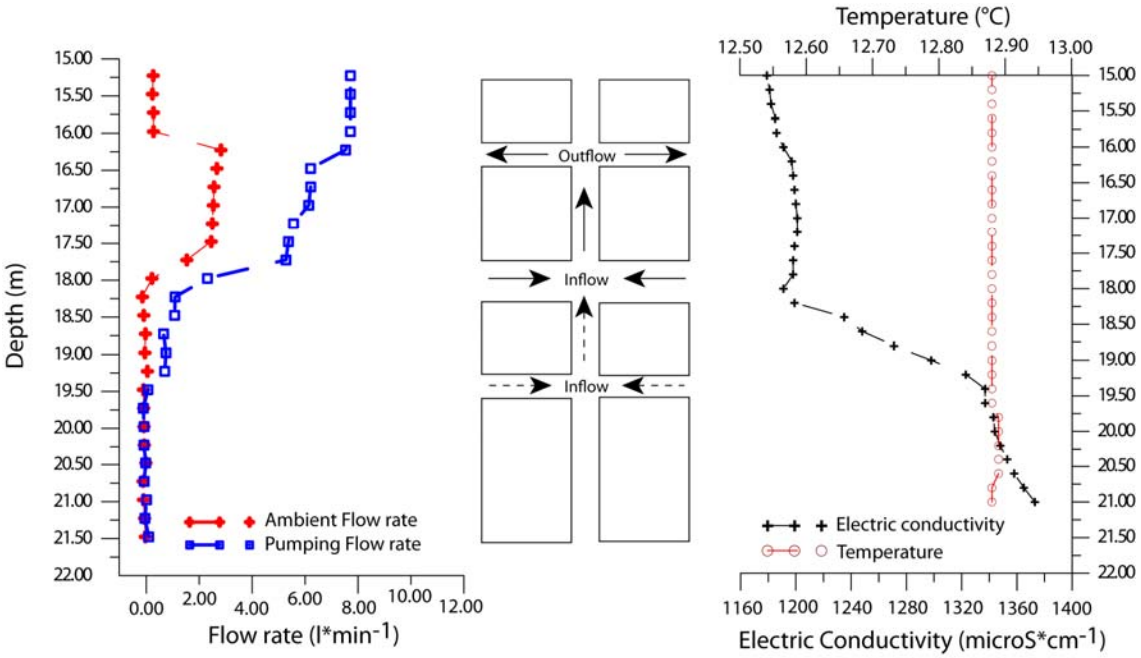

Figure 25: flow log, interpretation of inflow/outflow zones and EC/Temperature log for the borehole S16.

Well Bore S17

Figure 11 shows the vertical ambient flow characterized by no-flow zone from the bottom of the well to 20.5 m bgs, a zone with a sharp increase of downward flow between 20.5m and 19.0 m bgs, a zone with constant downward flow between 19.00 and 17.50 m, with a maximum flow around -2.00 l*min^{-1} and a zone between 17.25 and 16.00 m where the flows decrease to zero value.

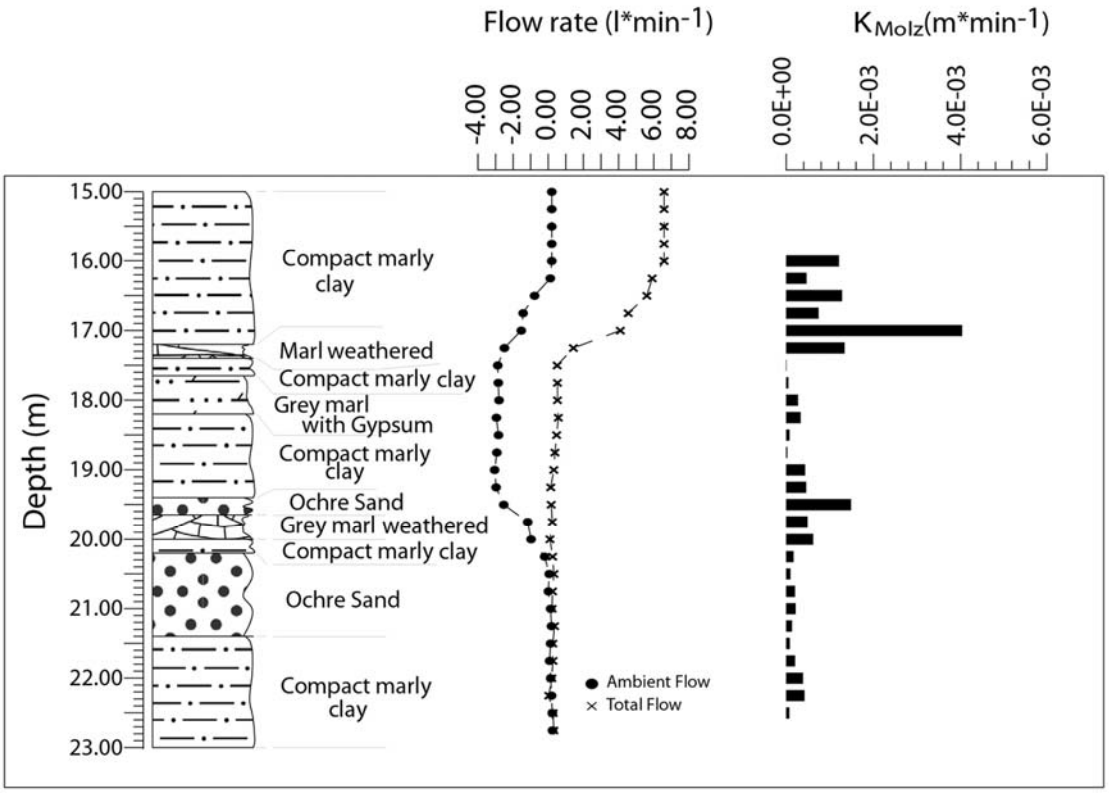

Figure 26: core stratigraphic, entity of ambiental and pumping flow, hydraulic conductivity by Molz's relation for the borehole S17.

From a qualitative point of view this trend was interpreted with the existence of two layers at different hydraulic head: one between 20.25 m and 19.00 m bgs and another one in the upper portion of the aquifer between 16.25 and 17.00 m. In this borehole, in contrast at borehole S16, the upper level has the greater hydraulic head, so the hydraulic gradient is oriented downward.

The flowmeter log in pumping conditions,performed with a pumping rate of 7 $l*min^{-1}$, confirmed the presence of the layers detected in ambient flow conditions; furthermore we calculated the permeability values with Molz's relation. The layer at 17.00 m bgs shows a permeability K=4.0 10^{-3} $m*min^{-1}$, while the layer at 19.50 m bgs has a permeability K=1.5 10^{-3} $m*min^{-1}$.

Differential Ambient Flow Analysis (Fig. 12) shows very clearly the inflow zone between 16.00 m and 17.25 m, while the outflow zone is between 19.00 and 20.25 m.

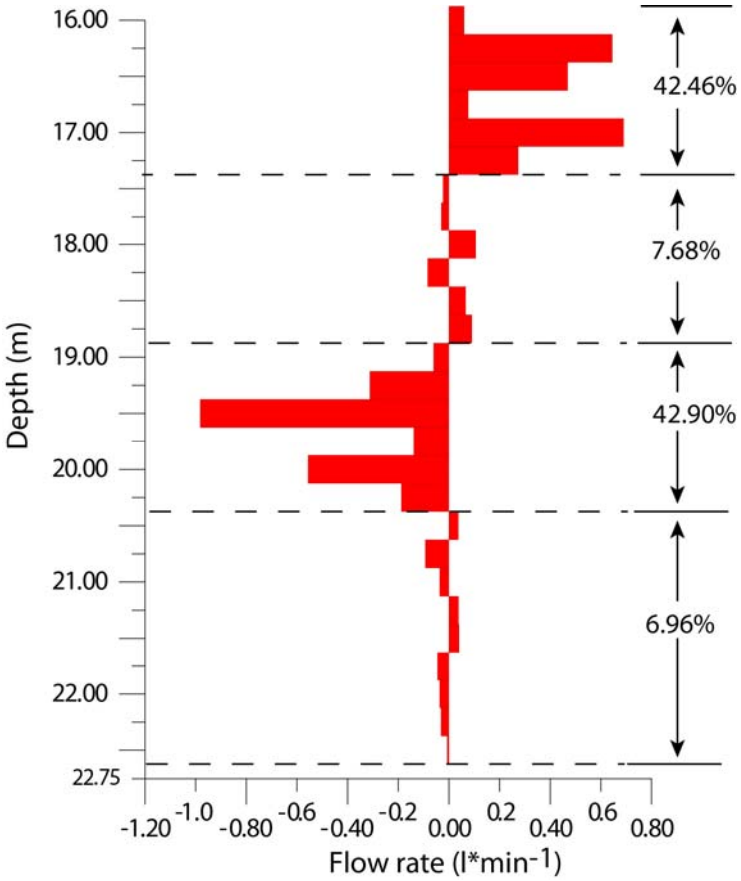

Figure 27: differential ambient flow for borehole S17.

Temperature/Electric Conductivity of the water column

Temperature log shows no relevant variations, with a constant temperature around 12.9 °C (Fig.13).

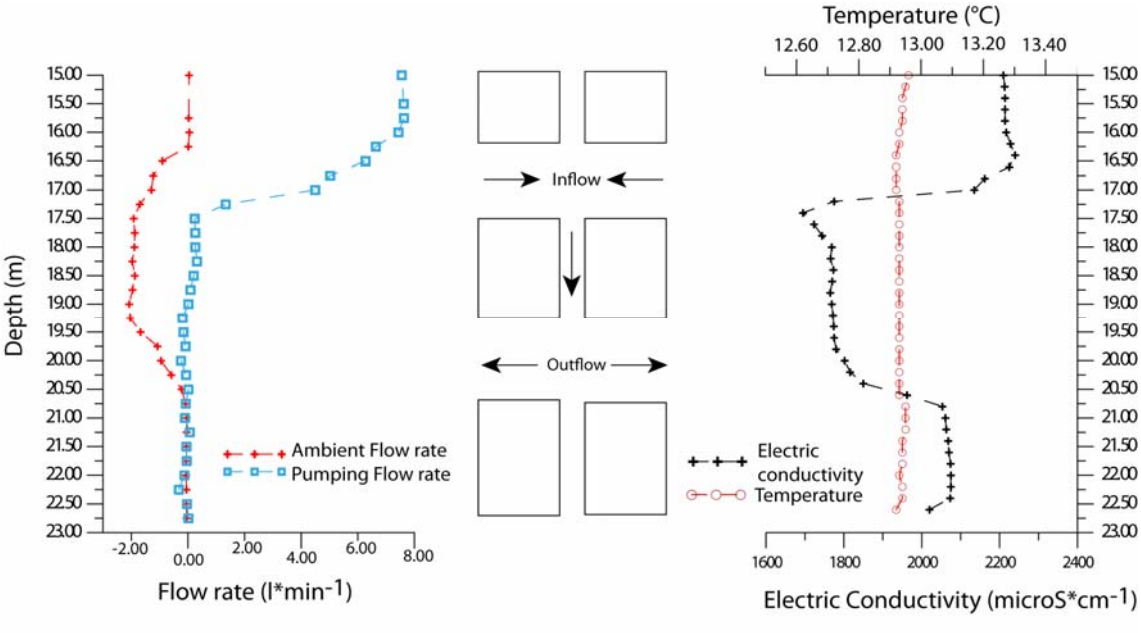

Figure 28: flow log, interpretation of inflow/outflow zones and EC/Temperature log for the borehole S17.

EC profile is more complex than profile in S17. The mean values are higher than those measured in S16. In details, from the bottom of the well to 21.00 m bgs (in a no flow sector), the electric conductivity is constant at 2070 µS*cm^{-1}. Between 21.00 m and 20.00 EC decrease to around 1800 µS*cm^{-1}, then it stay constant until 17.50 m. Between 17.50 m to 16.00 m we observe another positive gradient that increases EC to about 2200 µS*cm^{-1}.

This trend is interpreted with the hypothesis that at inflow point (between 16.00 and 17.25 m bgs) we have the entry of water less conductive that exits in outflow zone between 19.50 m and 21.00 m bgs.

Wellbore S7bis

Ambient flow is oriented upward between 18.00 and 19.00 m bgs and is negligible between 19.00 m and downhole (Figure 29).

We detect a clear inflow point around 19.00 m bgs and an outflow point at 18.00 m. During the flowmeter test in stressed conditions, we noted a zone between 19.00 and 20.25 m bgs that contributed modestly to the vertical flow. Ambient flows are significantly lower than in borehole S16 and S17. Differential ambient flow are synthesized in the bar graph of figure 15.

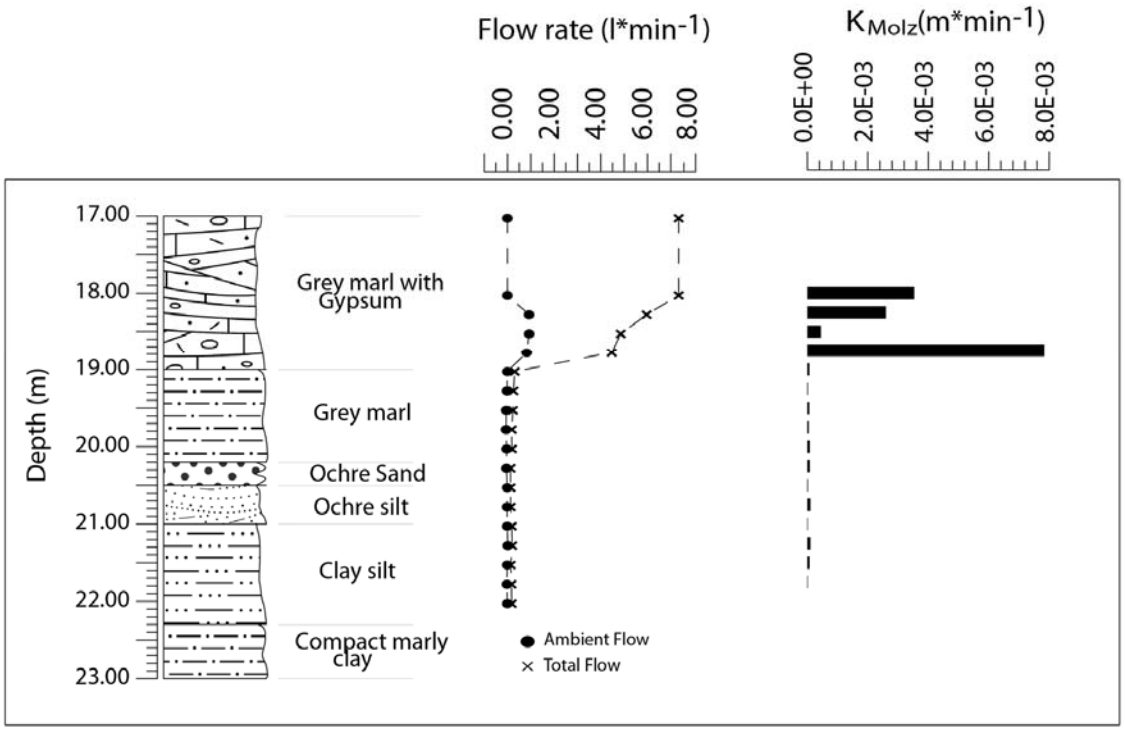

Figure 29: core stratigraphic, entity of ambiental and pumping flow, hydraulic conductivity by Molz's relation for the borehole S7bis.

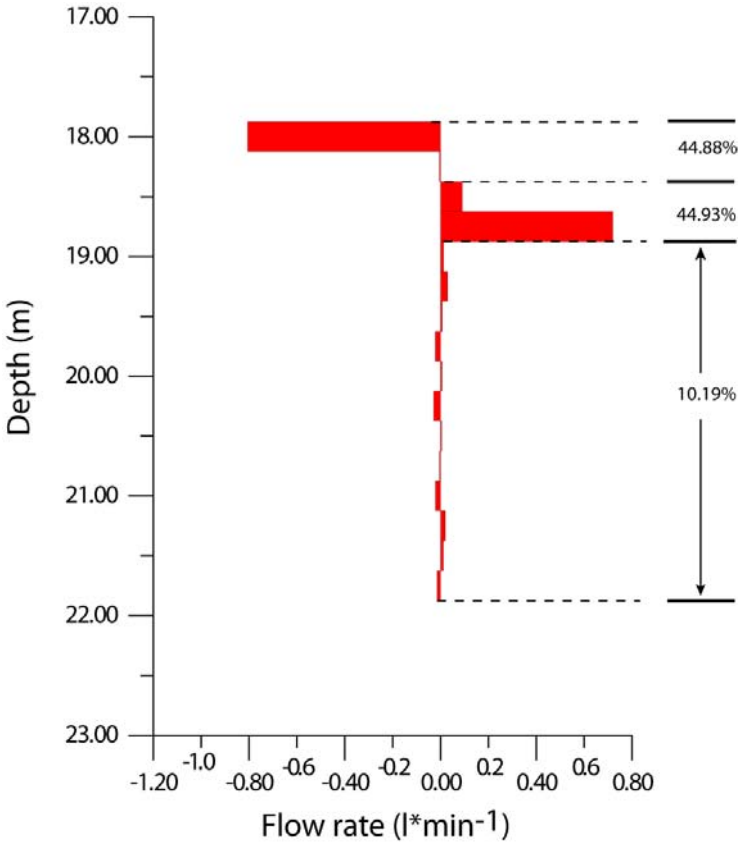

Figure 30: differential Ambient Flow in borehole S7bis.

Temperature/Electric Conductivity of the water column.

Temperature values measured along water column are approximately constant and very similar to those measured in borehole S16 and S17, with a value of 12.9 °C (Figure 31).

EC values instead are in general much lower than those measured in the other boreholes, with values around 1055 and 1063 $\mu S*cm^{-1}$.

EC is roughly constant from the bottom of the well to 19.00 m, whereas between 19.00 and 18.00 m bgs we observe a gradient with a slight decrease upward. The inflow point, located just 19.00 m bgs, could be an entry point of water with a lower EC, causing the observed dilution.

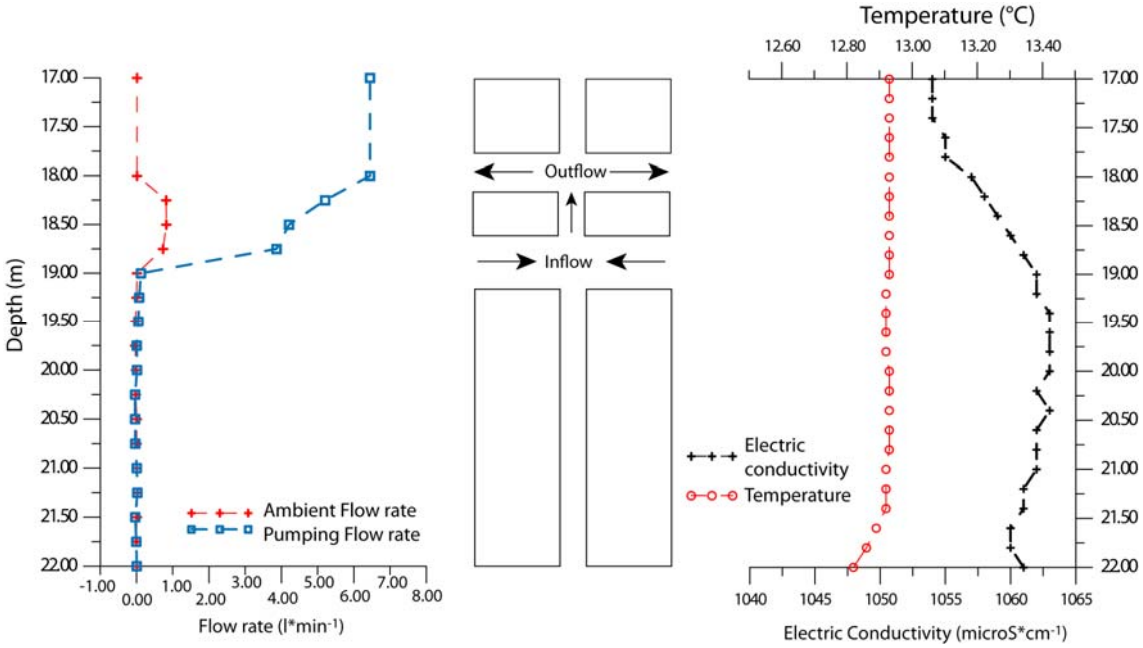

Figure 31: flow log, interpretation of inflow/outflow zones and EC/Temperature log for the borehole S7bis.

3.2 Georadar results

3.2.1 Single-hole survey

The results of the in-hole survey are plotted in Figure 32, where the vertical axis is referred to the depth of the centre of the antenna with respect to the ground surface, whereas the x-axis is the signal traveltime. As we adopted standard not-shielded and non directive antennas (simple vertical dipole), the amplitude of the reflected amplitude at different traveltimes was averaged on a volume that involves a solid angle of 360 degrees. In such a context the response is sensitive to the electromagnetic properties in all the directions.

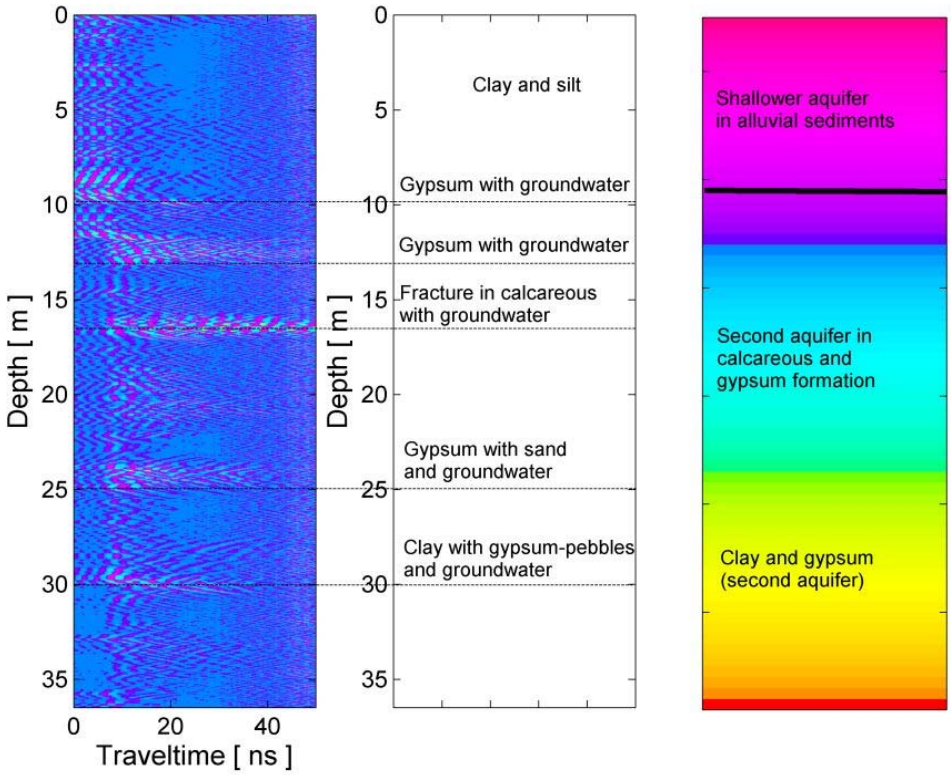

Figure 32: single-hole radargrams collected at the main frequency of 300 MHz in borehole S7bis

Nevertheless, the results pointed out the sensitivity of the method at delineating the main stratigraphic interfaces. In the acquisition at the nominal frequency of 300 MHz, we observe in radargram of Figure 32, the following main features:

- the sandy and gravel levels are pointed out by intense scattering of the radar response, due to the interference of the waveform with pebbles and coarse gravel material;
- silty-sandy materials are usually associated with low scattering because of the reduced size of the grain particles with respect to the main wavelength of the radar waveform; wavelength is in the order of about 0.5 m at these frequencies;
- the signal strength is strongly attenuated when radiation involves electrical conductive layers, such as clay and silt; the signal is strongly attenuated at depths between 10-11 m and 16 m where electrical conductivity of clay and marl-materials is about 0.1 S/m; bulk conductivity has been estimated by electrical resistivity logs in boreholes S17 and S16;
- the more productive zone in the second aquifer, located at the depth of 13-14 m and

16-17 m are well depicted in the radargram; they are characterized by intense scattering of the coarse material, that hosts the main level where water is circulating.

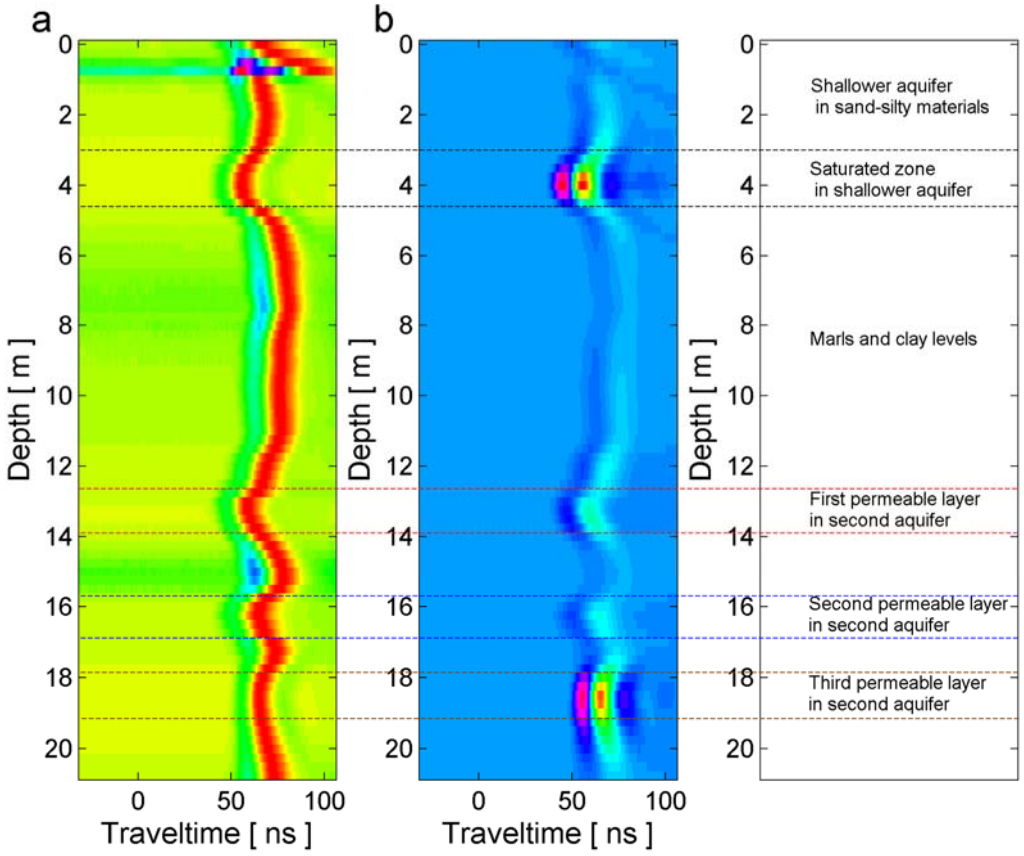

Figure 33: ZOP data between borehole S7 and S7 bis (2.5 m apart); a) normalized amplitude; b) data without any normalization.

3.2.2 Cross-hole survey

In the cross-hole ZOP profile, we observe as the panel acquired between the boreholes S16 and S17 only shows a good data quality, whereas the signal strength for the other two panels is strongly attenuated because of the high electrical conductivity along those sections.

The results of the ZOP between the boreholes S16-S17 section point out:

- the presence of diffuse high frequency noise in the upper part of the section, partially compromising the chance of detecting the response of the level between 13-14 m potentially hosting the groundwater;
- the signal quality improved from the depth of 14 meter to the bottom of the boreholes (23 m); two interesting zones where the radar signal was transmitted with high amplitude were recognized at the depth of 16-17 m and 19-20 m.

The interpretation of the ZOP profile was performed according to the picking of the traveltime of the directed waves that propagated from the transmitter to the receiver, located at the same elevation in the two boreholes (panel S16-S17). We observe that at the top and bottom of each productive level no critical refraction occurred because of the inversion of velocity between the porous more permeable layers and the top or bottom layers, made of saturated clay with higher electrical conductivity. In such condition, the electromagnetic field strength mainly propagates within the high resistivity layer, while it is strongly attenuated at the boundary with the low resistive material, as observed in the single-hole survey. Therefore, we neglect the effect of the critical refraction of the radar signal.

The traveltime values of the direct waves in zone of the permeable layers were converted in water content by means of the Topp's equation (Topp et al. 1980). In the upper zone, a value of 0.5 m^3/m^3 is computed, while the second (deeper)-zone is characterized by an average water content of 0.35-0.38. It can be noted that the application of the Topp's formula permits the computation of the water content averaged on a volume comprised between the two boreholes and including the overall thickness of each porous/permeable level. Moreover, the approach considers the total porosity of the two levels without the possibility to distinguish between the interconnected or the effective porosity. The Topp's formula tends to overestimate the water content for values greater than 0.3 m^3/m^3.

Figure 33 refers to the radar image of the ZOP radar data collected between the boreholes S7 and S7 bis; the two boreholes are 2.5 m apart. The data were collected with step of 0.25 m in the depth range between 21 m and the ground level. In Figure 33, radar traces are normalized with respect to the maximum amplitude of each trace, while normalization has not performed in Figure 33b. Therefore the first image points out the continuity of the first arrival of the signal at the receiver antenna, and the second image preserves the "energy" content of the signal itself. In such a way we note how the clay and marl levels filter out the most energy; the signal amplitudes are greater attenuated with respect to the more permeable layers.

3.3 Validity and limits of borehole georadar

The main results of georadar interpretation consist in the detection of three horizons which are potentially more porous and less permeable. A rough estimate of the porosity was performed by converting the traveltime in water content using the Topp's formula, that is a semi-empirical relationships. The layer permeability could be observed indirectly from the analysis of the radar signal attenuation. The signal was strongly attenuated in levels rich in clay and marl materials. We compared the radar results with the stratigraphical evidences for

boreholes S7, S16 and S17 and we found a good agreement. Particularly, the results of borehole S7 demonstrate the reliability of the single hole georadar acquisition in detecting the saturated levels. Usually, the productive levels or fractures can be detected because of the huge amount of energy that is scattered back by the fracture itself or by the coarse material which often characterizes the more permeable horizons. The preliminary assumption on the productive levels is validated by the cross-hole radar data, that demonstrated the relevance of three main horizons located in the second aquifer.

We observe a relevant attenuation of the radar signal in cross-hole mode in correspondence of the same levels previously detected by single-hole measurements, confirming that the behavior is caused by the presence of clay/marl levels. We consider the skin depth as a tool for estimating the radial distance of the radar survey. The skin depth is a conventional way to check the performance of electromagnetic wave propagating in a lossy (electrically conductive) medium, and it is inversely proportional to the frequency of the electromagnetic field and to the soil electrical conductivity. At 100 MHz and for an electrical resistivity of 10 ohm m (conductivity of 0.1 S/m), the skin depth is about 0.2 m; this means that the radial distance of the penetrating signal is just few times the borehole diameter.

3.4 Integration between geophysics and hydrogeology

The geophysical survey according to the radar cross-hole and borehole results has been useful for a characterization of the productive layers and for an estimate of the porosity of the main productive layer. Particularly we obtain a good match between the depth of the main levels as estimated by single hole georadar and the flow rate, estimated by the well tests. Moreover single hole survey permit to estimate with good accuracy the thickness of the main layer where the flow rate analysis pointed out the intense water circulation.

The integration of the single-hole data with cross-hole data is useful for a preliminary estimate of the porosity according to empirical rules such as the Topp formula (see a previous paragraph).

The values estimated from cross-hole are in good agreement with the overall porosity estimated by laboratory analysis of the sandy-gravel material collected at the depth of 13.5 m and 16.5 m, corresponding to the main productive levels of the aquifer hosted in calcareous and gypsum material. The high porosity pointed out by georadar survey and the absence of fine material are consistent with the high permeability values corresponding to those level.

4. Final remarks

The presence of a complex aquifer hosted in the calcareous-gypsum formation with the coexistence of three main productive levels in the upper part of the system has been observed; the groundwater flow is mainly concentrated at the depth between 12-20 m in three different levels which are separated by low permeability formations characterized by compact clay and marl. The thickness of the productive level is in the order of 1 up to 2 meters. On the contrary of the original assumptions, the groundwater flow is mainly hosted in that porous level more than in fractures in calcareous or gypsum.

The geophysical characterization using electromagnetic methods (georadar) permitted to detect with good resolution the main geometry of the aquifer at the scale of interest (few meters). Moreover the GPR cross-hole survey permitted to estimate the overall porosity value within two of the three main productive layers.

Because of the very high bulk conductivity of the geological formation (clay and marls), we observed a strong attenuation of georadar signal both in the in-hole data acquisition and in cross-hole modality (ZOP profiles). The attenuation limits the performance of georadar at few meters of radial distance from the antennas and make not suitable the integration of data by surveying the test site from the surface. This discouraged us in using the georadar for time lapse monitoring of the dynamic response of the system when the injection of the reagent will take place and have involved the time lapse monitoring by means of electrical resistivity tomography.

The single-hole flowmeter survey has allowed us to make the following remarks:

1. we identify the main productive levels intercepted by each borehole, pointing out a relevant ambient vertical flow, that is indicative of very different hydraulic head between layers;
2. we estimate the variable hydraulic conductivity are calculated and distinguish absolutely non-productive areas are distinguished;
3. we also check as the inflow and outflow zones are poorly correlated with the stratigraphy and detect both levels at secondary permeability (corresponding to rapid changes in the pattern of flows) and levels at primary permeability (when the flow gradually changes);
4. we note that the position of the inflow/outflow points is not the same in the three wells studied; a complex flow pattern, not reconstructed from simple stratigraphic

correlation is recognized;

5. we also note a good correlation between the fluid electric conductivity log and flow pattern: in the inflow-outflow zones there are rapid changes of the EC; the temperature does not seem to react in the same way;
6. we don't point out a clear relationships between geology and points of inflow-outflow.

This complex scenario requires to perform flowmeter and tracer test in cross-hole configuration that has been undertaken.

Chapter 3

Integration between flowmeter log and tracer tests for aquifer characterization

3.1 Abstract

This section describes the methodology and results of a study designed to characterize the geology and hydrogeology of the uppermost tertiary bedrock aquifer underlying a contaminated site. The main aim is to provide an approach to optimize a set of hydrogeological and geophysical survey techniques.

The initial objective of the study was to locate the pathways of groundwater flow and contaminant migration in a complex geological setup in a part of an aquifer hosted in calcareous-gypsifeous formation and to characterize the hydraulic properties of these pathways.

For these reasons, the study was divided into five major components: (1) conventional hydrogeological technique (2) single hole flowmeter test, (3) cross hole flowmeter test, (4) geophysical logging using cross-hole ground penetrating radar and (5) tracer testing.

Conventional hydrogeological techniques (analysis of core samples, pumping tests, collection of static water-level measurements) were used in a preliminary investigation of the site to determine stratigraphy, fracture presence and to estimate the bulk hydraulic conductivity.

Single-hole flowmeter testing was used to detect the presence of heterogeneities and to provide a vertical distribution of the hydraulic conductivity (shown in chapter 2 of this thesis).

Cross hole flowmeter testing was used to detect connections between the discontinuities intercepted by boreholes.

GPR was used to obtain a water content by Topp's relation and compare it with permeability obtained by Molz's relation with flowmeter measurements.

Tracer testing was used to determine - with the highest reliability - the pathways, the effective porosity and rate of ground-water flow through selected flow pathways.

However point (2) and (4) were analyzed and discussed in chapter 2

The complexity of these questions ranges from whether transport connectivity can be confirmed between injection and withdrawal points, to whether quantitative data can be extrapolated from a tracer test.

3.2 Conventional hydrogeological technique

The geological and technical framework (well location and construction) of the test site has been presented in previous section (Chapter 2, par. 2.1.1).

3.2.1 Pumping test

Table 3 summarizes hydraulic properties obtained from pumping tests performed in different months and different configuration of pumping – observation wells.

Date (dd/mm/yyyy)	Pumping well – Observation well	Pumping rate (l/s)	Transmissivity (m^2/s)	Storativity
20/01/2010	S17 – S17	7.50	5.10E-05	3.00E-02
21/01/2010	S16 – S16	10.32	1.00E-04	2.40E-01
01/02/2010	S07bis - S16	15.00	1.20E-04	1.00E-04
01/02/2010	S07bis - S17	15.00	9.68E-05	9.60E-05
21/05/2010	S07bis – S07bis	17.52	3.50E-05	7.70E-02

Table 3: Short term pumping tests hydraulic properties estimates

The pumping test data have been analyzed using Theis' fitting method for confined aquifer (Theis, 1935) that, however, does not fully match the whole time evolution of drawdown for this data set, in particular for long term drawdown variations. Nevertheless, it provides rough estimates of transmissivity and storage coefficient.

The transmissivity ranges from about $3.5*10^{-5}$ to $1.2*10^{-4}$ m^2 s^{-1} while the storage coefficient estimates from about $9.6*10^{-5}$ to $2.4*10^{-1}$.

These average hydraulic conductivity values were then used to convert the relative hydraulic conductivity measurements, obtained from flowmeter data by Molz's relation, into absolute hydraulic conductivity values for each well (Molz and Young, 1993).

3.2.2 Core analysis

The core boxes and the grain size distributions for the samples extracted from boreholes S16, S17 and S7bis are shown in Figure 35

The core recovery is very poor (<30%) for borehole S7bis while it is good (>90%) for boreholes S16 and S17.

Because of the screened interval positions, the investigated section of the cores is just between 15 and 20 m BGS (boreholes S16 and S17) and between 18 and 23 m BGS (borehole S7bis). Samples were taken from the cores in points (red circle in Figure 35), where lithologies changed. For simplicity, just two or three grain size distribution curves are represented for each borehole.

Grain size analyses were carried out by a laser granulometer (model *Malvern* Mastersizer 2000E).

For borehole S16 (Figure 35a), at 17.50 m the grain size distribution shown a silty sediment (silt=89%) with traces of sand and clay (curve1), while between 18.50 m and 20.00 m there is a layer of sandy sediment (sand=51%) with silt (47%) (curve2) and a passage at silt with sand (curve3). Furthermore an evident fracture located at 16.50 m is present.

Figure 34: fracture with evidences of gypsum dissolution at 16.50 m BGS from the extracted S16 core.

For the core S17 (Figure 35b) there is an homogeneous level of silt (curve 1) and a decimetric level of sandy sediment at 19.50 m (curve 2).

For the core S7bis (Figure 35c) a silt and sand level is evident (curve 2) between silty sediments (curves 1 and 3).

Furthermore within the silt matrix there are many evidence of gypsum-rich lenses.

It should be emphasized that this synthetic core description would to be an evidence of the geologic heterogeneity present at this study site.

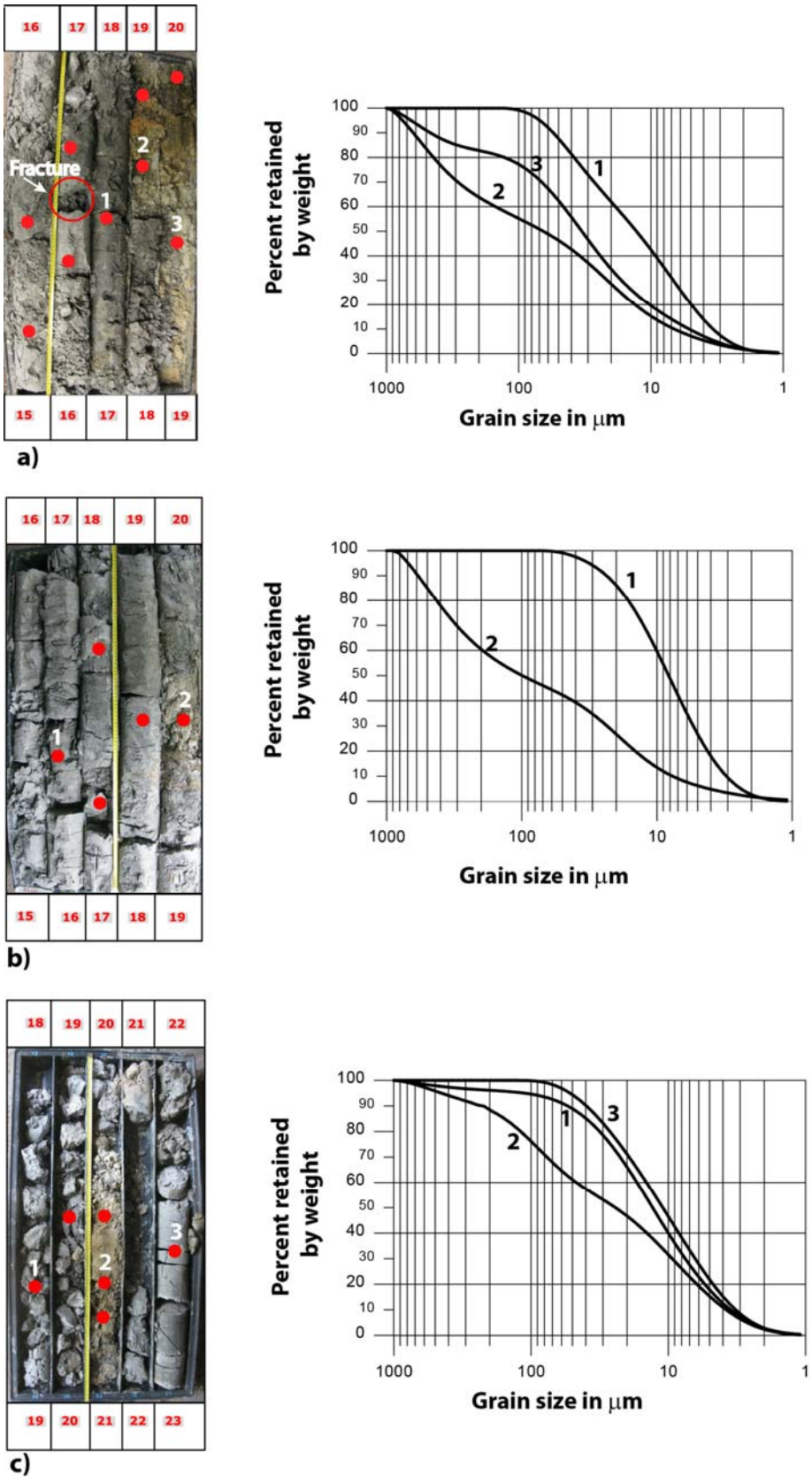

Figure 35: core pictures and grain size distribution for cores extracted from boreholes S16 (a), S17 (b) and S7bis (c); red circles represent points where samples are taken for the grain size analysis.

3.2.3 Static water-level

The piezometric level has been measured during the study at different dates (Figure 36). Unfortunately, no automatic pressure transducers where available, so the piezometric level trend was monitored by manual measurements.

These values were used, by the SURFER software, to draw the maps of groundwater depth (Figure 38). Depth to groundwater levels were interpolated by kriging for February, March, May, September and November of 2010. Furthermore for September it was recorded a measure when a hydraulic stabilization occurred during a water injection in wellbore P2.

Because the boreholes are located in a very small plain area (about 6x6 meters, see Figure 17a), with no changes in ground level height, the depth to groundwater is an indicator for the local head.

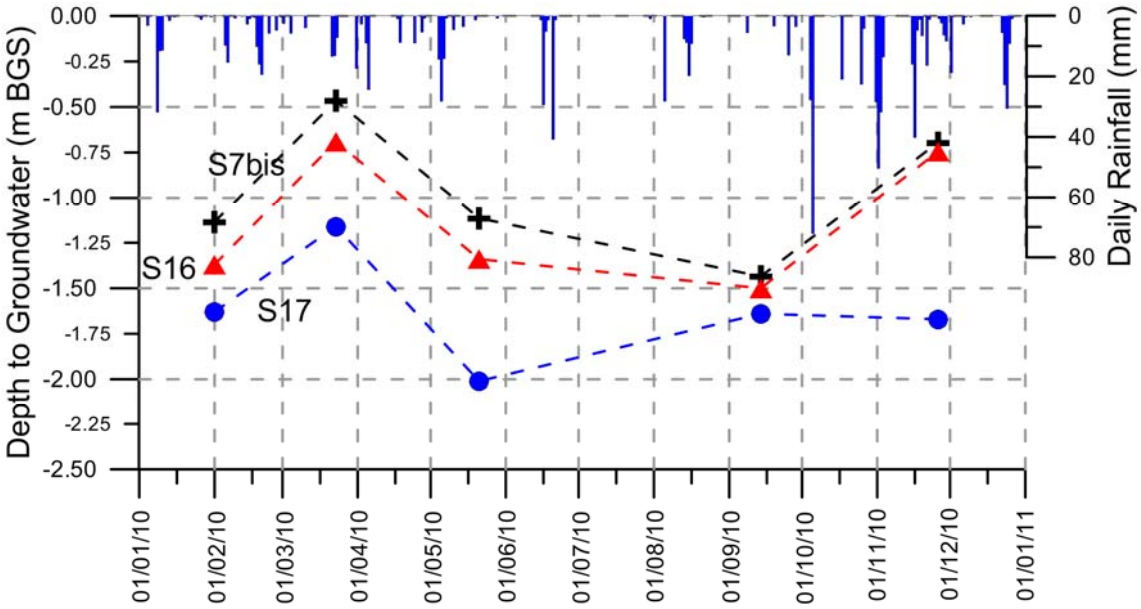

Figure 36: Change in depth to groundwater over time for borehole S16 (red triangle), S17 (blue circle), S7bis (black cross). Daily rainfall in the bar plot on the top (Novi Ligure rain gauge). The piezometric level measurements are so few that no comparison to rainfall can be made.

Figure 36 shows that borehole S17 has an hydraulic head lower than the S16 and S7bis. The overall change in depth over the period was 0.97 m for borehole S7bis, 0.81 m and 0.85 for boreholes S16 and S17 respectively.

As it is evident in Figure 36, from this small amount of data that covers only one year no relationship to local rainfall can be assumed.

In Figure 37 it is possible to observe the relationship between groundwater depth in boreholes

S16 and S17 compared to S7bis, which is characterized by the higher hydraulic head.

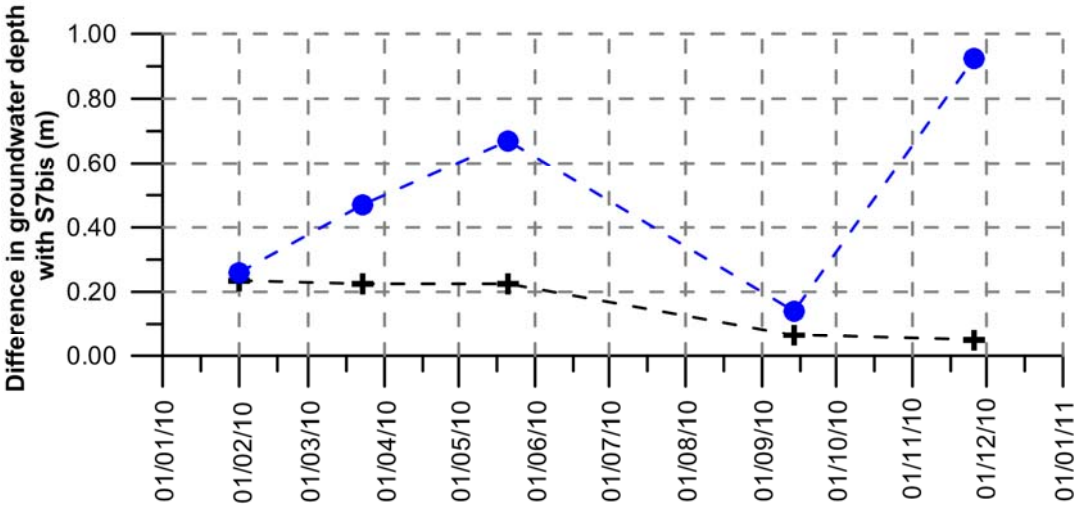

Figure 37. difference in groundwater depth for boreholes S16 (black cross) and S17 (blu circle) with respect to borehole S7bis.

Hydraulic head in borehole S16 follows a trend that is very similar to the trend in S7bis with small deviation (around 0.20 m or lower). On the contrary, the hydraulic head trend in borehole S17 differs from that in borehole S7bis (and therefore in borehole S16).

As shown in Figure 38, the maximum hydraulic gradient is generally oriented from East to West (from Borehole S7bis to S17) with a seasonal variations.

The highest gradient was recorded on May, and on February the lowest. It appears that borehole S17 receives ground water both from borehole S7bis (in major quantity) and from borehole S16.

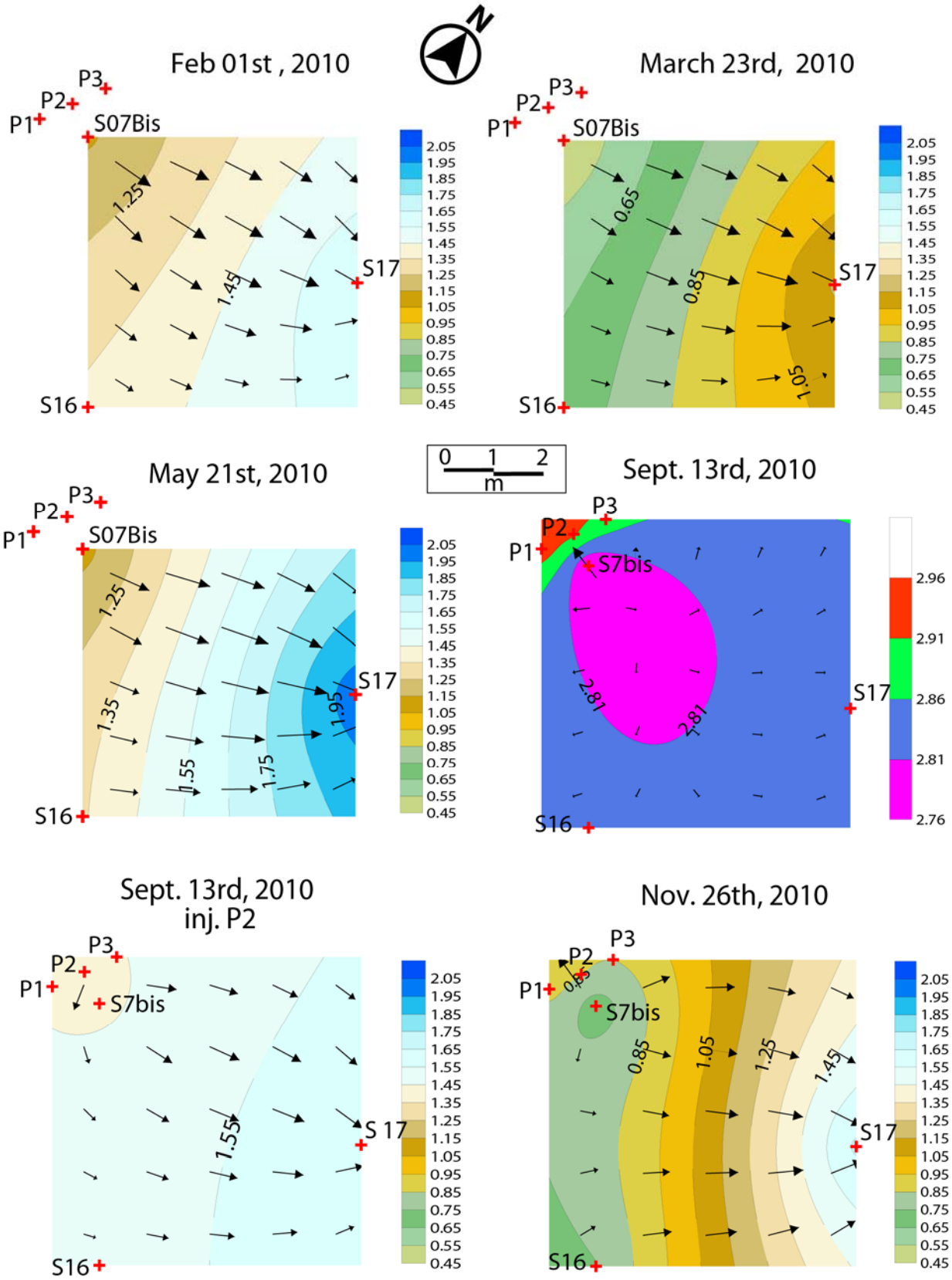

Figure 38: maps of ground water depth. Groundwater level measurements are interpolated by kriging for some dates of 2010 (measure in meters from Ground level). P1, P2 and P3 were drilled on September 13rd, 2010

3.3 Advanced borehole survey methods

3.3.1 Cross - hole flowmeter test. Methodology.

As discussed by Williams and Paillet (2002), although conventional multi-well aquifer tests can effectively define fracture connections in bedrock aquifers, there are two major problems in conducting such test at contaminated sites: (1) there is almost no initial information about which fracture zones need to be monitored in the observation wells and (2) hydraulic stressing produces quantities of contaminated water for disposal or treatment and may mobilize contaminants in the aquifer.

So, in situations where there are many possible water-producing fractures intersecting a borehole, it is important to identify which fractures conduct flow and which sets of fractures may be isolated from each other in the surrounding rock mass. Such information is especially important in planning cross-borehole tracer tests, where there are literally hundreds of possible combinations of fractures forming flow paths between borehole pairs (Paillet, 1998).

In the recent past some authors (Paillet, 1998; Williams and Paillet, 2002) proposed cross borehole flowmeter tests as a reliable methodology to characterize the connectivity of fractures between boreholes.

Cross borehole flowmeter tests simply consist of measuring vertical flow in a borehole when an adjacent borehole is pumped or is subject to water injection.

Le Borgne et al (2006) present a characterization of flow paths connectivity in a crystalline aquifer from cross-borehole flowmeter tests. The authors integrating single and cross borehole flowmeter experiments, to derive hydraulic properties at distinct scales of investigation.

As we have seen in the previous section (chapter 2), flowmeter logging under ambient conditions was performed at each borehole using the electromagnetic flowmeter. After this a second borehole flow profile was obtained while pumping at different flow rates.

According to this procedure, inflow and outflow points for each borehole were identified by the observation of the ambient and stressed profile.

After the inflow points were identified, a pump in a close borehole was turned on (resulting in a pumping or an injection of water) and the flow profiles in an adjacent well was analyzed and compared with the profile at ambient conditions.

Such cross borehole tests were conducted for all pairs of observation wells (see Table 6).

Cross borehole experiments were performed after a stabilization of the hydraulic head in both

wells. Generally, as observed during pumping test, the delay time for the drawdown cone of depression to reach the observation borehole was within few minutes.

Such data obtained were very useful to define the hydraulic connections among borehole S16, S17, S7bis, P1, P2 and P3.

The general criterion to interprete the cross hole flowmeter test is that an increase in an upward flow while pumping in an adjacent well is consistent with a prevalent connection with the upper layer of the logged well. Conversely, a decrease in an ambient upward flow will be consistent with a connection through a lower layer.

In the case of downward flow, an increase of the flow is consistent with a connection through the lower layer, while a decrease is consistent with a connection through the upper layer.

Obviously, in the case of no connections, the ambient flow in observation well is equal at the flow in stressed conditions.

In order to illustrate the use of the interpretation method for cross-borehole flowmeter tests, Figure 39 considers some simple connectivity patterns.

In particular, *Figure 39a, b, c*, *d* and *e*, refer to an upward flow in the monitoring well and Figure 39 *f, g, h, i, j* refer to a downward flow.

Outline of possible interpretations in cross hole flowmeter log analysis involving two fractures or permeable layers intersected by monitoring well

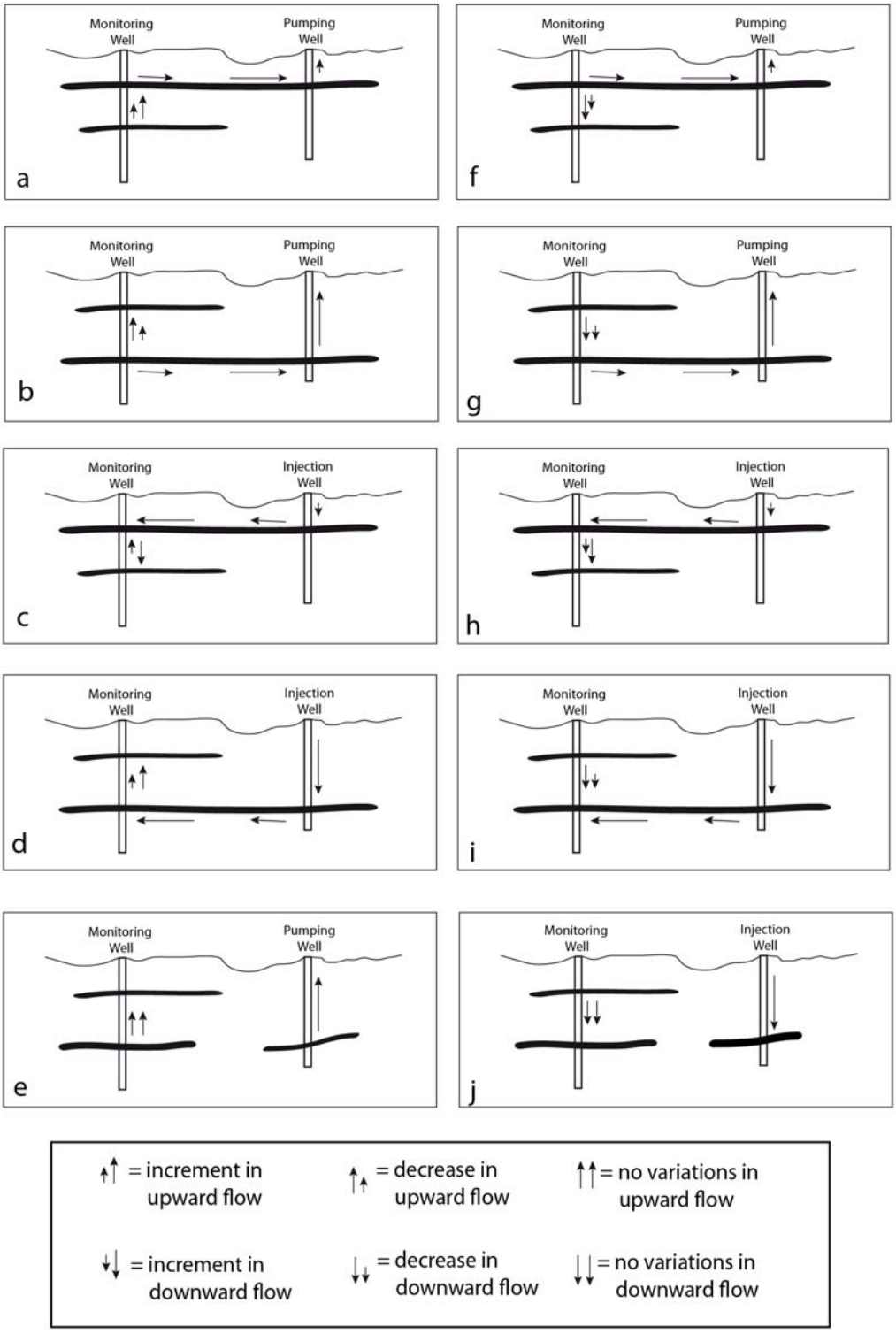

Figure 39: illustration of some simple connectivity configurations. For the different cases it was analyzed the expected evolution of the vertical flow in the observation well.

3.3.1.1 Cross-hole flowmeter test. Results

The flowmeter test performed between wellbore S16 and S7bis (Figure 40) showed a clear evidence of connection. The increase in upflow is consistent with a connection through the upper layer, with a draft of water from S7bis.

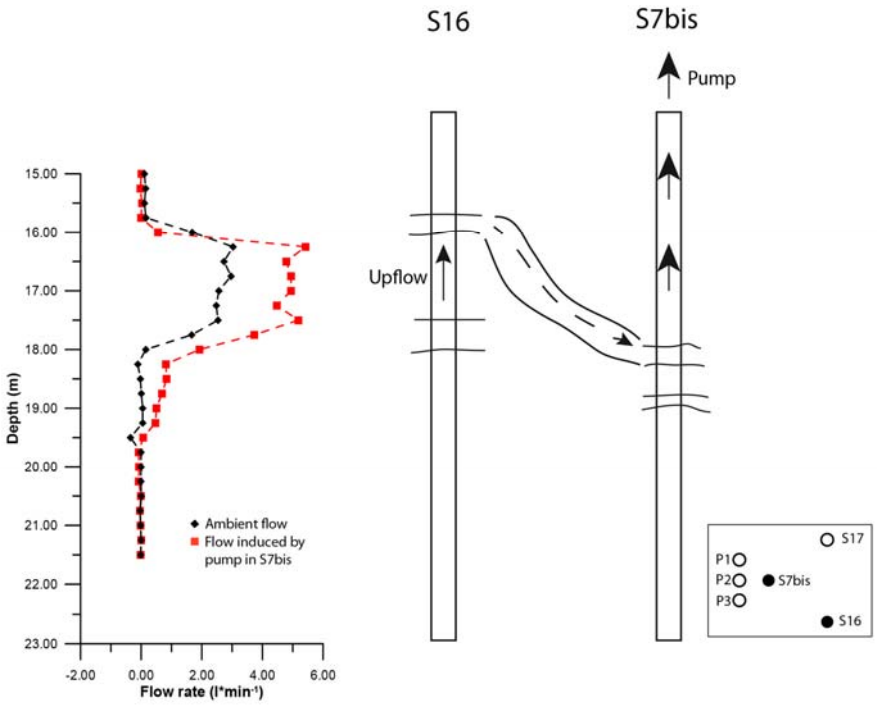

Figure 40: results from cross-hole flowmeter log performed between wellbores S16 and S7bis. Pumping flow rate in wellbore S7bis is 7 $l*min^{-1}$.

The cross flowmeter test between S16 and P2 showed a vertical flow that was reversed during injection in P2. This is consistent with a connection by the upper level in S16. The injection was performed to avoid the extraction of contaminated water.

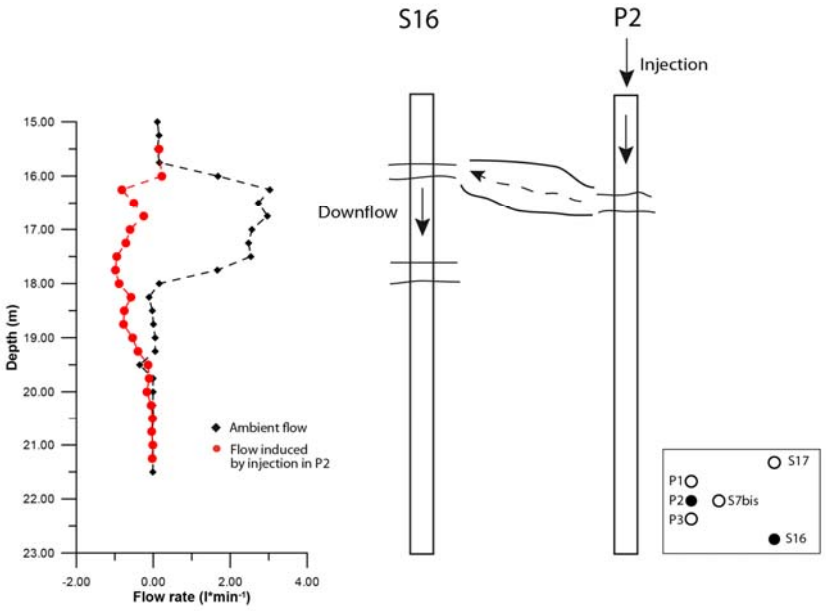

Figure 41: results from cross-hole flowmeter log performed between wellbores S16 and P2. Injection flow rate is 15 l*min^{-1}.

As concern borehole S17, it is clear an absence of connection with borehole S16 (Figure 42), while between S17 and S7bis (Figure 43), the decrease in downward flow rate is indicative of a possible connection with a withdrawal of water from the upper layer.

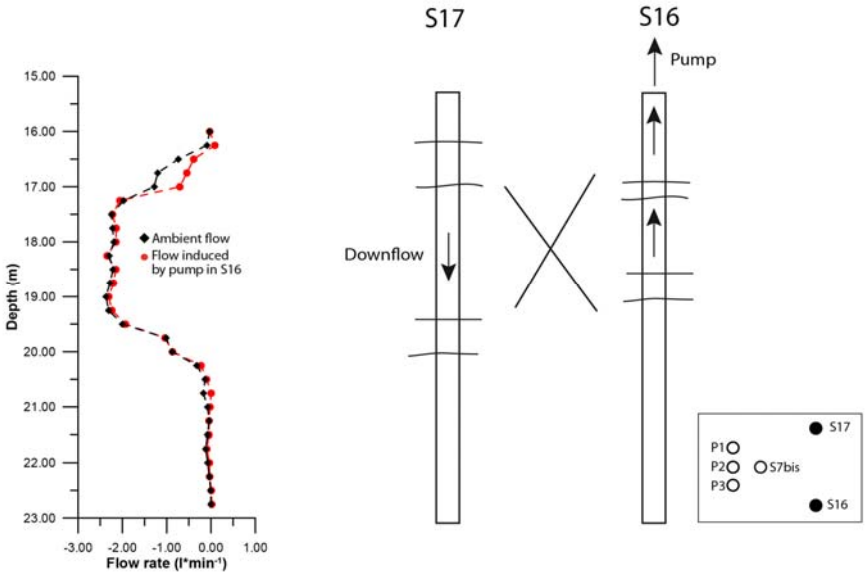

Figure 42: relation between wellbores S17 and S16. Pumping flow rate in wellbore S16 is 7 l*min^{-1}.

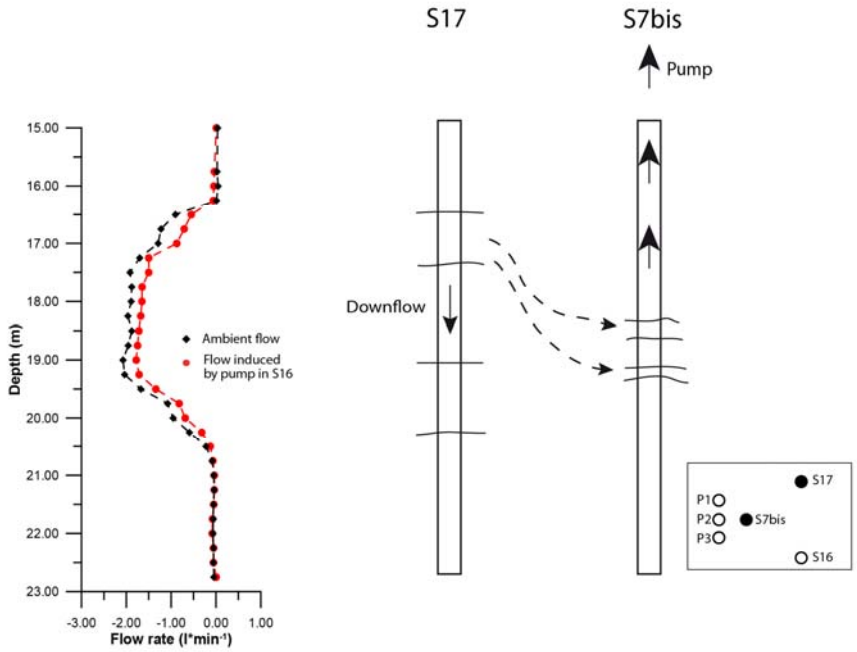

Figure 43: relations between wellbores S17 and S7bis. Pumping flow rate in wellbore S7bis is 7 l*min^{-1}.

When injecting in borehole P2, the decrease in downward flow in S17 is indicative of a connection through the lowest transmissive layer (Figure 44).

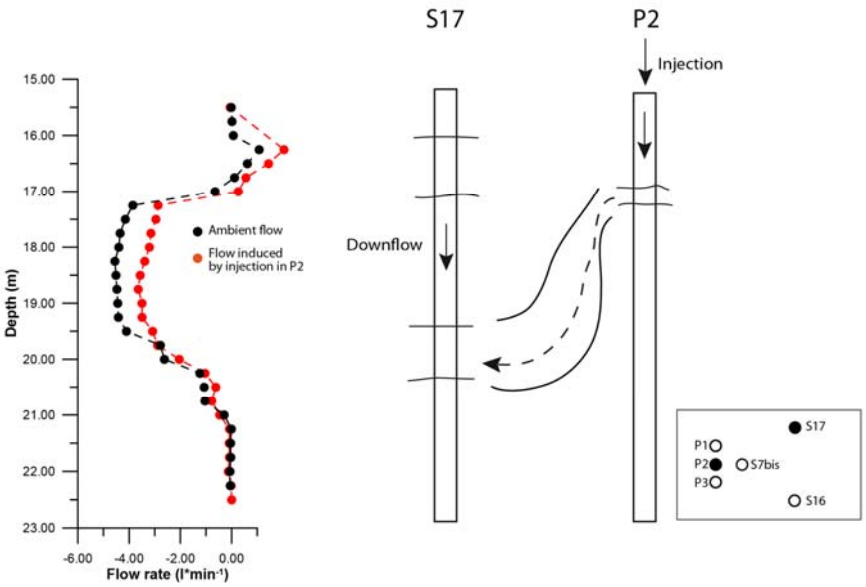

Figure 44: connection between wellbores S17 and P2. Injection flow rate in wellbore P2 is 15 l*min^{-1}.

Interesting relationship are those observed between P1, P2 and P3, three very close boreholes.

Between P2 (the injection borehole) and P1 it is evident that the injected water is distributed through a layer between an upper and a lower high transmissivity zone (Figure 45).

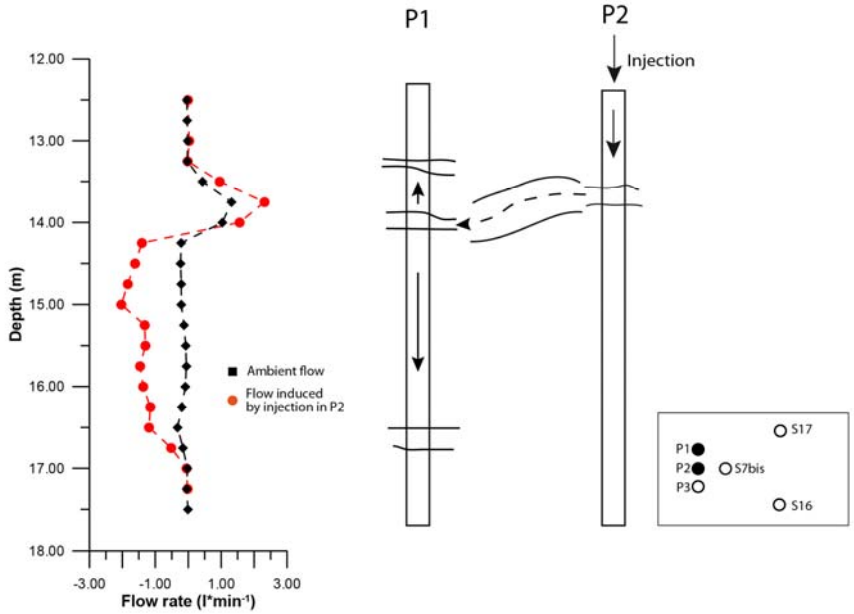

Figure 45: results from cross-hole flowmeter test performed between wellbores P1 and P2. Injection flowrate is 15 l*min^{-1}.

Injection in borehole P2 produces instead, a downward flow in borehole P3 (Figure 46)

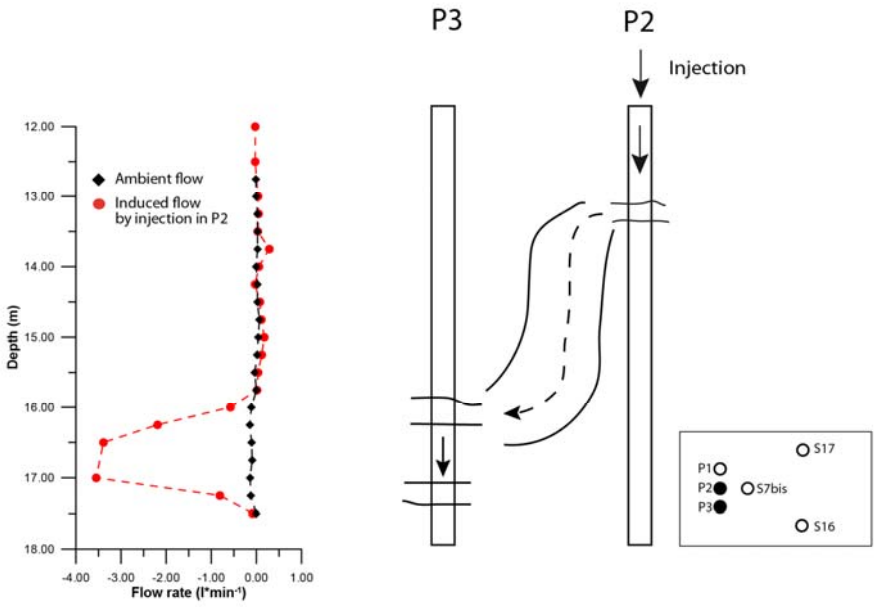

Figure 46: results from cross-hole flowmeter test performed between wellbores P3 and P2. Injection flow rate is 15 l*min^{-1}.

3.3.2 Tracing experiment. Methodology

Tracer tests in fractured rock aquifers have played and still play, a central role in investigations relative to the understanding of retention processes in the field.

Tracer testing is actually regarded as the most reliable and efficient method of gathering surface and subsurface hydraulic information. This is especially true for karstic and fractured-rock aquifers.

Before presenting the tracer tests, it is necessary to define what we mean by a tracer test:

"An investigation where tracer migration within a geological medium is monitored"
(Löfgren et al., 2007).

As concern the distinguishing characteristic of tracer tests, generally the **environment** refers to whether the investigation is carried out in situ or in the laboratory. In the case of in-situ investigations, the tests can be made from boreholes drilled from ground surface or from tunnels. The **flow situation** refers if a tracer test is performing in natural gradient or forced gradient conditions and if the tests involve one or more wells.

In *single well* tests two techniques, injection/withdrawal and point dilution, give values of parameters which are valid at a local scale.

In *inter-well* tracer tests, also called cross-hole tracer tests, investigations are made using two or more boreholes that intersect the same conductive fracture or fracture system. Injection and withdrawal of tracer is performed in different boreholes. If the hydraulic gradient and transmissivity of the structures connecting the injection and pumping locations is too low, only a limited breakthrough may be achieved within a reasonable time period. This may occur if the boreholes are far apart, if the fracture connectivity is poor, if flowpaths are extremely tortuous, or if the fracture apertures are small. Even though experiments with limited breakthrough cannot be used to asses retention properties of the flowpath, the connection between injection and withdrawal points can be confirmed.

Inter-well tests can either be dipolar or radially converging (Figure 47).

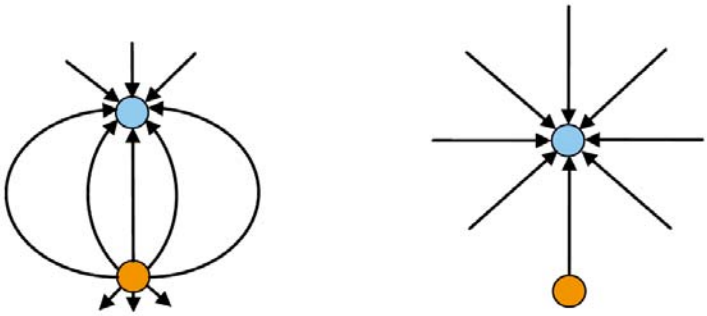

a) b)

Figure 47: radial converging and dipole flow-fields. Orange borehole is the injection well and blue is the withdrawal hole (adapted from Löfgren et al., 2007).

In a *dipolar* experiment, groundwater is injected into the fracture system together with the tracer in the injection borehole. At the same time groundwater is withdrawn by pumping in another borehole.

In a *radially converging* test, the tracer solution is added in an hydraulically conductive structure isolated by packers. Pumping is performed in the withdrawal borehole only, with a radially converging flow field created around the borehole.

In hydraulically conductive fractures, tracer test can be performed from a single borehole. In such tracer test, a borehole section is packed-off around a fracture or fracture zone and the tracer is injected there. After some time, the hydraulic gradient is reversed and the tracer (spiked in groundwater) is withdrawn and analyzed. This particular type of tracer test is often called *Single Well Injection-Withdrawal test* (*SWIW*) (Neretnieks, 2007) or *Push-Pull test* (Snodgrass and Kitandis, 1998).

Measurement device: range and accuracy

The result of a tracer test is closely related to the accuracy in the determination of the tracer concentration in recovered solutions and on the disturbance caused to the hydrologic system.

All the tests described below employed a University of Neuchatel Geomagnetism Group flow-through fluorometer (GGUN-FL) (Schnegg, 2002, Schnegg and Flynn, 2002, Schnegg, 2003).

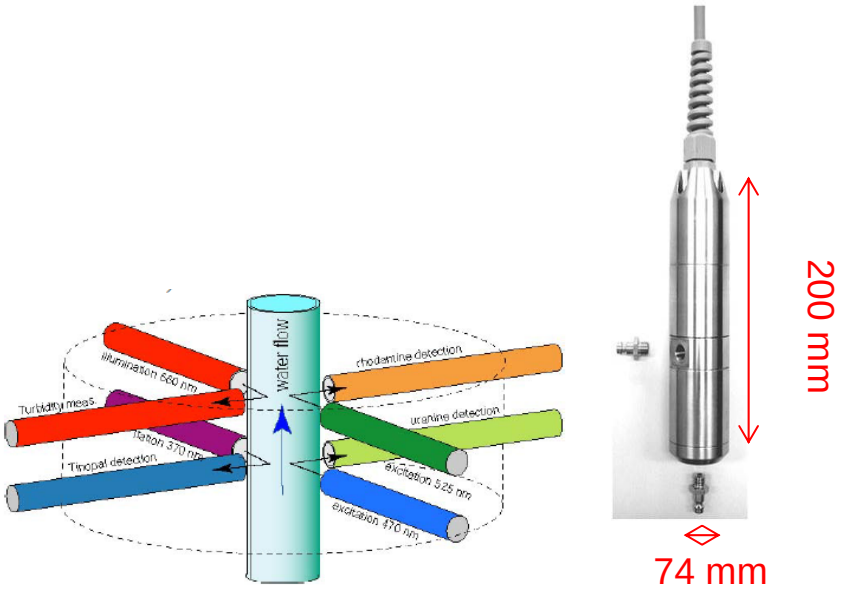

Figure 48: optical scheme with the four sets of light sources and photo-detectors.

An optical cell made of a glass tube placed along the geometrical axis of a metal cylindrical waterproof casing measures the tracer concentration in the water flowing through the flow cell (Figure 48). The optical components used for the measurement of dye concentration are installed along the orthogonal axes of two square crosses in two separate planes. The measurement system consists of:

- an excitation section, comprising a quasi-monochromatic light source, a filter and a condenser lens, and
- a detection section, oriented at 90° to the excitation beam, with a lens, a filter and a photo-detector.

The light sources and the filters are selected according to the absorption-emission spectra of the dyes. This geometry allows the installation of up to four measuring systems. One of the sets is dedicated to the measurements of the water turbidity while the three others are used to measure the dye concentrations.

The sampling frequency can be set to 10 s, 30 s, 1 min, 2 min to 15 min.

Light sources with spectral maxima at 370, 470 and 525 nm are ideally suited for excitation of dyes such as Tynopal CBS-X, Uranine (Na-Fluorescein) and any molecule in the Rhodamine family (amidorhodamine G, sulforhodamine B, rhodamine WT).

The sonde (74 mm in diameter by 200 mm in length) is submersible in a water column to a maximum depth of 100 m.

For non-sorbing dye tracers (e.g. Uranine), the tracer concentration can be analyzed with a

resolution (in clear water) of 0.02 ppb in the range of 0.02–430 ppb. The accuracy is within ± 5% (Schnegg, 2002).

The strength of the borehole fluorometer is its versatility. The GGUN field fluorometer offers an accurate, inexpensive and non-destructive means of automatically monitoring for up to three different tracers while also removing the effects of turbidity. The apparatus has been shown to be well suited to field situations in which installation of permanent monitoring devices is either impractical or infeasible (Schnegg, 2002).

Discussion about QTRACER2

The code QTRACER2, has been developed to facilitate tracer-breakthrough curve (BTC) analysis. It solves the necessary equations from user-generated data input files using robust integration routines (Field, 2002).

Quantitative tracing studies consist of the development of a tracer budget, comparing the amount of tracer injected into the aquifer system with the amount of tracer recovered over time in conjunction with ground-water discharge measurements.

Hydraulic parameters are estimated by the method of moments. The zero-th moment is used to estimate the tracer mass recovery. The first moment is used to estimate the mean residence time and mean flow velocity. The second moment is used to estimate the longitudinal dispersion.

Analysis by the method of moments is nothing more than determining the area under the BTC generated by plotting time versus measured tracer concentrations (Figure 49).

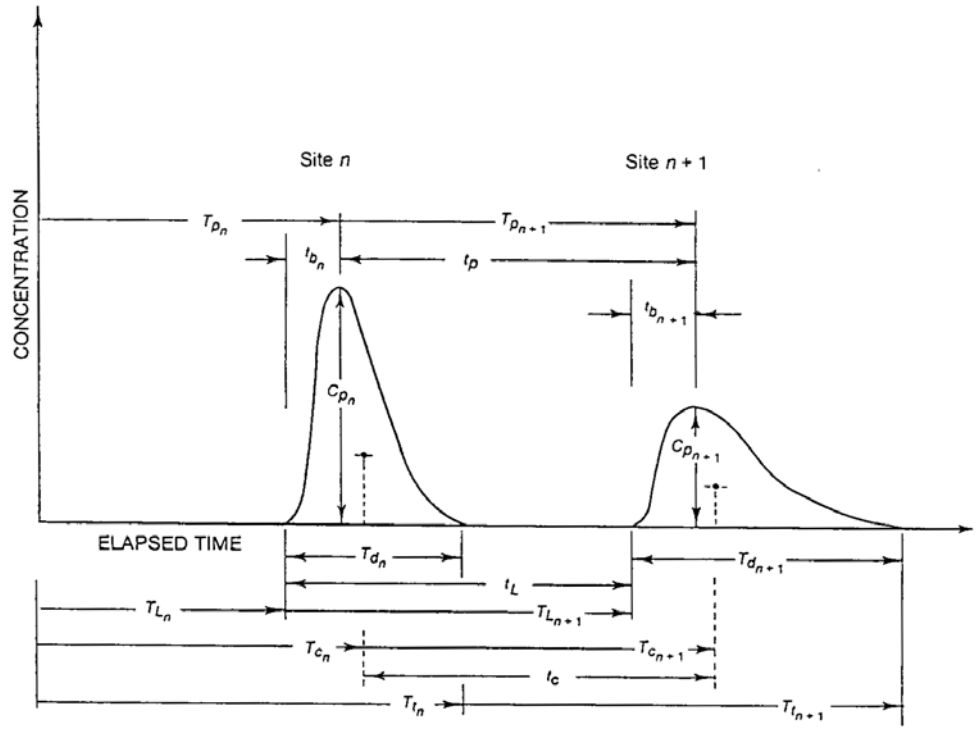

Figure 49: Definition sketch of BTCs along a selected tracer streamline from an instantaneous tracer injection (Kilpatrick and Wilson, 1989).

The following discussion is taken from Kilpatrick and Wilson (1989, p. 3 and 4).

Characteristics pertinent to the BTC analysis are:

- T_L, elapsed time to the arrival of the leading edge of the BTC at a sampling point;
- T_p, elapsed time to the peak concentration Cp of the BTC at a point;
- T_c, elapsed time to the centroid of the BTC at a point; and
- T_t, elapsed time to the trailing edge of the response curve at a point.

The mean travel time for the flow along a streamline is the difference in elapsed time of the centroids of the BTCs defined upstream and downstream on the same streamline given by

$$t_c = T_{cn+1} - T_{cn} \qquad \text{Eq. 11}$$

where n is the number of the sampling site. Similarly, the travel times of the leading edge, peak concentration, and trailing edge along a given streamline are, respectively

$$t_L = T_{Ln+1} - T_{Ln} \qquad \text{Eq. 12}$$

$$t_p = T_{Pn+1} - T_{Pn} \qquad \text{Eq. 13}$$

and

$$t_t = T_{tn+1} - T_{tn} \quad \text{Eq. 14}$$

The time Td necessary for the tracer mass to pass a sampling point in a section is

$$t_d = T_{tn} - T_{Ln} \quad \text{Eq. 15}$$

As shown in Figure 49, a typical tracer cloud may travel faster in the center of the stream than along the flow channel walls, where it may also be elongated. Complete definition of the BTC may involve measurement at more than one point or streamline at several sections (if possible).

The quality of the tracer experiment may be quantified in terms of mass recovered. Usually, the quality of the tracer experiment is given as a percent of mass recovered, but this affords little insight. An accuracy index (A_I) given by Sukhodolov et al. (1997):

$$A_I = \frac{M_{in} - M_T}{M_{in}} \quad \text{Eq. 16}$$

Where M_{in} is tracer mass injected, while M_T is the total mass of tracer recovered.

The Accuracy Index provides more insight into the quality of the tracing experiment. An A_I = 0 indicates a perfect tracing experiment. A positive A_I indicates more mass injected than was recovered, while a negative A_I suggests more mass recovered than was injected. As A_I moves further away from zero, the quality of the tracing experiment gets poorer.

Tracer mass recovery should be quantified to ensure that all relevant locations are properly monitored for ground-water quality. Otherwise, it is likely that important ground-water discharge locations may be missed. A low-percent recovery of a conservative tracer mass may be an indication of significant loss of tracer during the study, often a result of improper determination of downgradient receptors. A high-percent recovery is a probable indication that most, if not all, relevant downgradient receptors were properly monitored for tracer recovery.

Experimental procedure

The tracer tests within the site investigation are generally carried out according to the following procedure. The equipment is lowered to the correct borehole depth where background values of Uranine and supporting parameters, electric conductivity and temperature, are measured and logged. For the forced gradient tracer test, a pump (Grundfos

model MP1) is used to pump groundwater from the test section to the ground surface in order to obtain steady state flow conditions. Then, after pressure stabilization, the tracer diluted with groundwater is injected. Following this procedure, and with the aid of the borehole fluorometer (section 3.2), the concentration is measured without any system disturbance.

3.3.2.1 March 2010 tracer experiment.

To investigate tracer migration in ground water system, in **March 2010** a tracing experiment has been carried out using 10 g of Na-Fluorescein (Uranine) CAS [2321-07-5] diluted in 0.5 l of local groundwater and injected during 30 seconds at borehole S16. The test was a forced gradient tracer test with the wellbore S7bis used as extraction well (*Figure 50*).

Injection point in wellbore S16 was chosen by the qualitative analysis of flowmeter data. So, in correspondence of the outflow zone between 16.00 and 16.50 m a 0.0127 m (½ inch) pipe was used to inject the tracer solution. Due to the very short duration a pulse injection can be assumed.

Tracer dilution was observed in wellbore S17 by two flow-through field fluorometers positioned in correspondence of two transmissive layers detected by flowmeter analysis: one above 18.75 m and another one above 18.00 m. Pumping flow rate in well S7bis was 15 $l*min^{-1}$.

As shown in Figure 50, the electromagnetic borehole flowmeter was installed above the deepest fluorometer to account the flow rate passing through the fluorometer (for the mass balance) from the inflow point between 18.75 and 19.00 m.

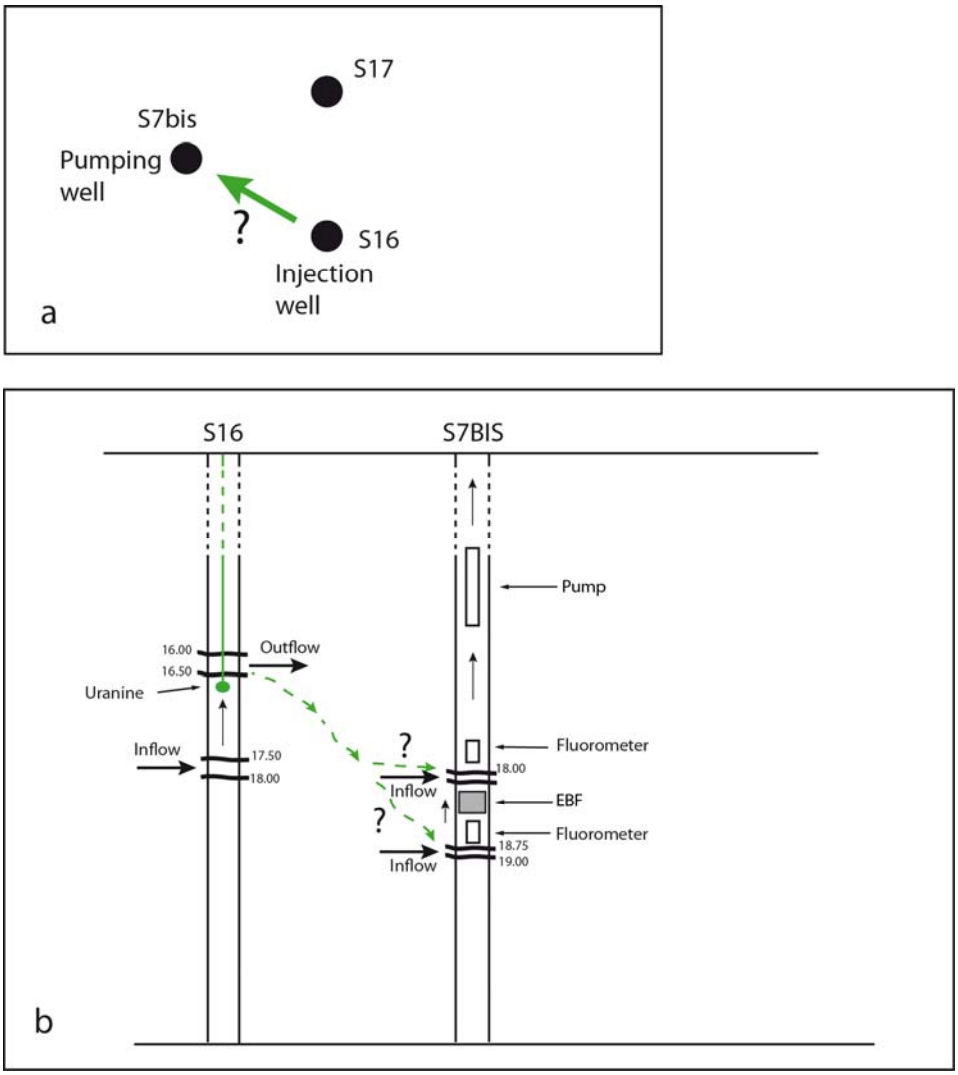

Figure 50: Tracer injection at wellbore S16 (March, 26th 2010) below 16.50 m. It was supposed that the ambient upward flow would lead to exit from S16 to S7bis. a) plain view; b) section view. Drawing not to scale.

Results

As expected, the measured data show a movement of the tracer to S7bis. Unfortunately, as shown in Figure 51, the test was compromised by a too high concentrations of tracer and therefore the instrument has gone off the scale of measurement.

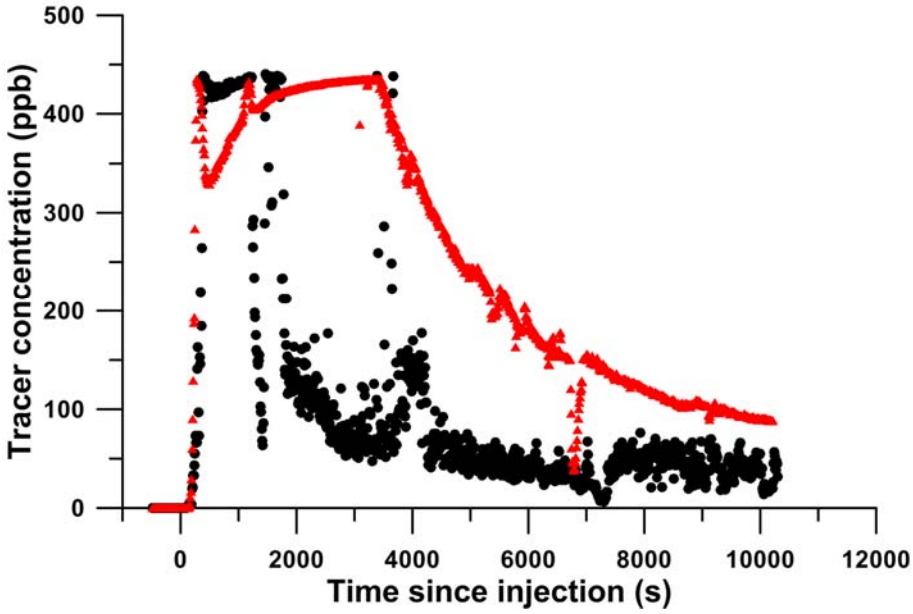

Figure 51: tracer concentration detected by two borehole fluorometers positioned at 18.00 m and at 18.75 m bgs. Red triangles is tracer detected at 18.00 m, black circles is tracer detected at 18.75 m. Sampling interval is 10 seconds.

Borehole fluorometer positioned above 18.00 m remained longer at higher concentrations because it measured tracer that arrived from the two levels.

Despite the test was technically compromised, were analyzed the two tracer-breakthrough curves.

The following *Table 4* summarizes the analytical results of the tracer test:

Fluorometer position (m. BGS)	Quantity of tracer recovered (inj. 10 g) [g]	Percent recovery of tracer injected [%]	Time to leading edge (first arrival) [min]	Time to peak tracer concentration [min]	For a peak tracer concentration [ppb]	Mean tracer transit time [min]	Peclet number	Maximum tracer velocity [m/s]	Accuracy index (0.0 = Perfect Recov.)
18.75	0.279	2.79	3.53	26.31	438.83	55.88	3.58	0.269E-01	0.9720
18.00	0.704	7.00	2.91	63.91	435.59	73.61	4.71	0.327E-01	0.9295

Table 4: results of tracer testing carried out on March 23rd, 2010. All data are affected by high concentration injected. Note that detection threshold for Uranine is around 430 ppb

3.3.2.2 November 2010 tracer experiment.

On November, 26th a new tracer test was performed as shown in the table below (Table 5):

Well name and injection depth (m)	Monitoring well and fluorometer depth (m bgs)	Monitoring well and fluorometer depth (m bgs)	Mass of uranine injected (mg)	Volume of solution injected (l)
S7bis; 18.50	S17; 18.00	S16; 16.50	2.5	0.250

Table 5: tracer tests performed on November 26th, 2010

The mass of uranine injected was considerably reduced compared to the test performed in March, 2010.

The test was a natural gradient tracer test and the objective was to understand how the permeable layers intercepted by the three boreholes S16, S17 and S7bis are connected, particularly to verify if there is a connection between the outflow zone in S7bis (around 18.00 m BGS) and the inflow zone in boreholes S16 and S17 (*Figure 52 a* and *b*).

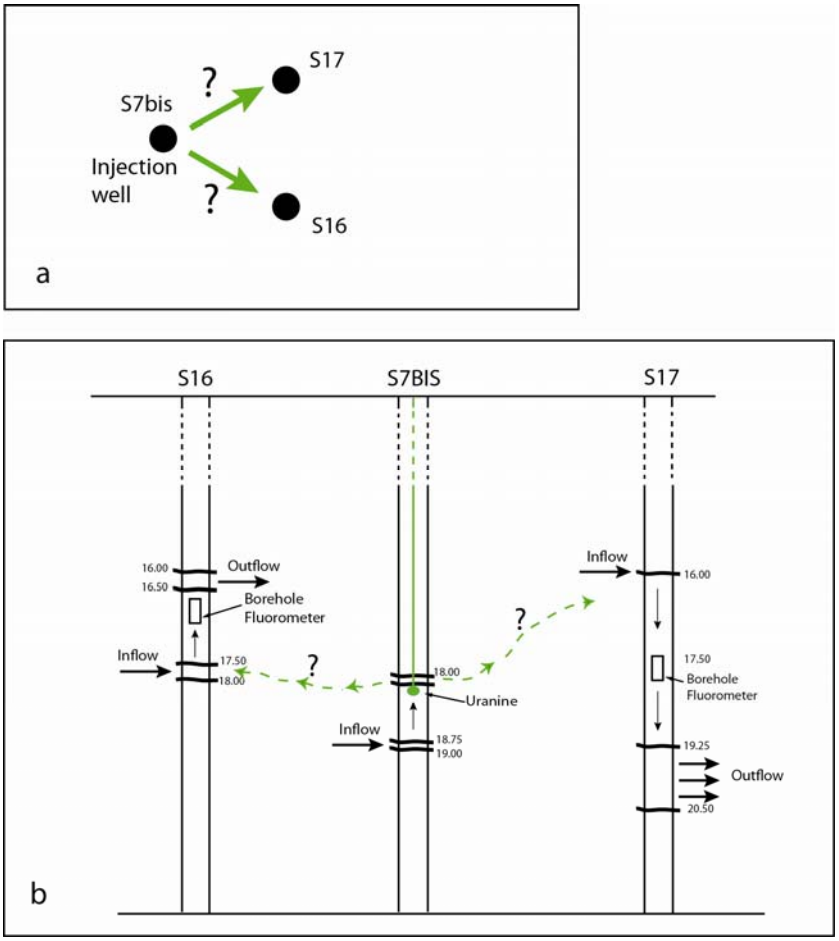

Figure 52: natural gradient tracer test performed on November 26th, 2010. a) plain view; b) section view. Drawing not to scale.

The tracer release was a slug release, with a very short duration (less than 30 seconds),

obtained exploding a balloon containing the tracer solution, just below the outflow zone in the injection borehole (*Figure 52 b* and *Figure 53*).

Figure 53: detail of the tool used to tracer injection

The breakthrough curve detected is show in *Figure 54* for borehole S16 and in *Figure 55* for borehole S17.

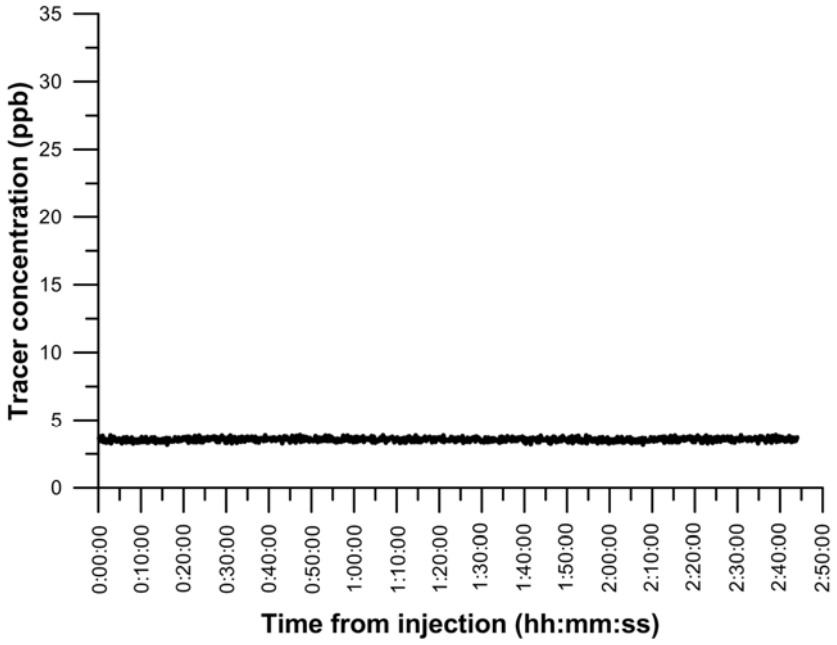

Figure 54: breakthrough curve in borehole S16. Clearly no tracer arrived

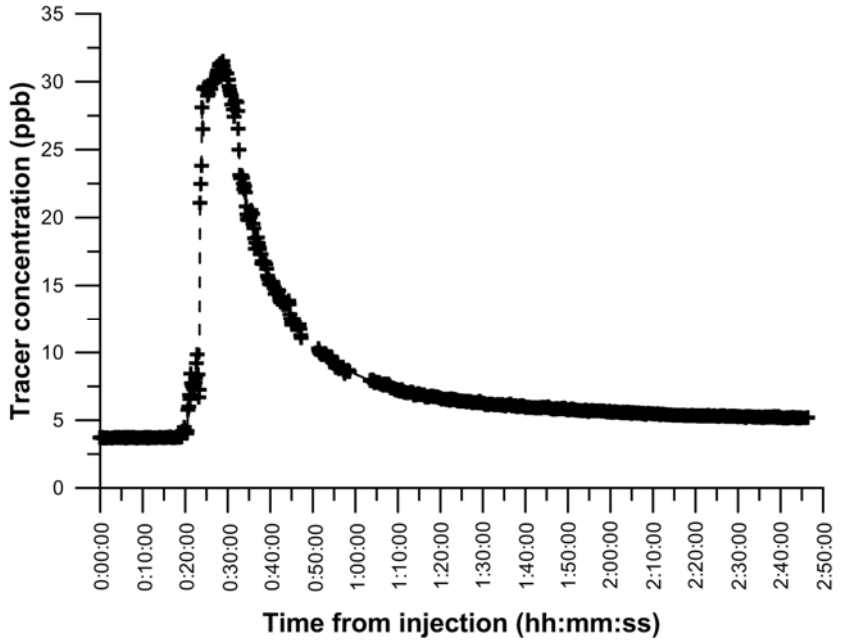

Figure 55: breakthrough curve in borehole S17.

For the borehole S16 it was possible to exclude any connection with borehole S7bis, while it was possible to perform a quantitative analysis of the tracer test for the BTC detected in the borehole S17.

Quantity of tracer recovered [mg]	Percent recovery of tracer injected [%]	Time to leading edge (first arrival) [min]	Time to peak tracer concentration [min]	For a peak tracer concentration [ppb]	Mean tracer transit time [min]	Peclet number	Maximum tracer velocity [m/s]	Accuracy index (0.0 = Perfect Recov.)
1.5572	62.29	18.96	28.77	27.719	57.291min	12.615	0.52E-02	0.3771

The quantitative analysis was performed assuming a flow rate through the fluorometer of 2.10 $l*min^{-1}$. This is the vertical ambient flow rate measured inside the borehole by EBF (Figure 56).

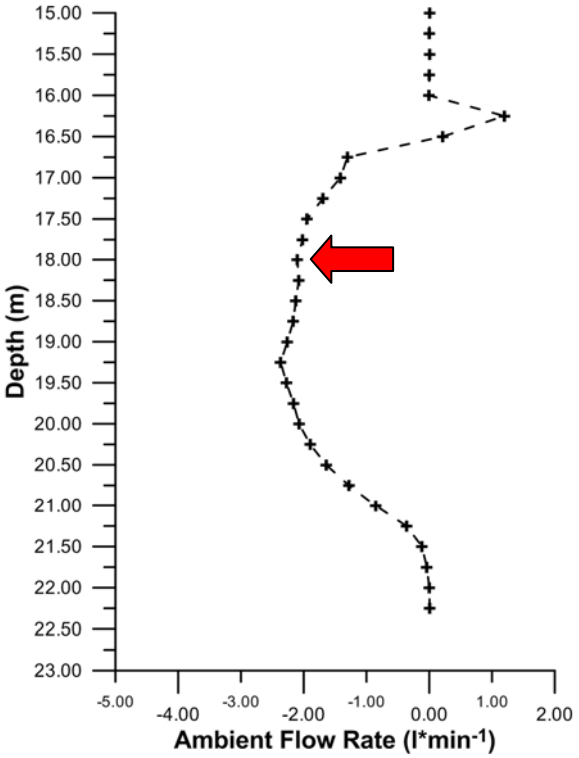

Figure 56: Flowmeter log in borehole S17 under ambient condition. The flow rate measured at 18.00 m BGS was used to estimate the tracer budget.

The accuracy index assumes a value of 0.37, indicating an high quality tracer test.

Discussion and conclusion

Single-hole flowmeter test provides information about the properties of the individual fracture segments surrounding the borehole (shown in chapter 2). Cross-borehole flowmeter test provides information on the properties of the flow zones that connect borehole pairs.

The permeable fracture network is composed of few of the fractures identified in the boreholes that form a connected cluster at site scale.

Data obtained from flowmeter logging demonstrates moreover their applicability and importance in tracer test design and interpretation.

Figure 57 shows the results of the integration between cross borehole flowmeter test and the two tracer tests performed at the study site.

Designing a tracer test without any information on vertical borehole flow can lead to erroneous considerations on tracer arrival and concentration, and thus on calculated hydraulic parameters.

Both tracer tests performed on March and November are examples supporting this

hypothesis.

Borehole S17 was interpreted like a "natural pumping well" because it causes a withdrawal of water from other boreholes. So, the role of borehole S17 is crucial to understand the water circulation in this aquifer section.

It was proposed the idea that borehole S17 should be close. It conduce and accelerates the contaminant transport and migration through the aquifer.

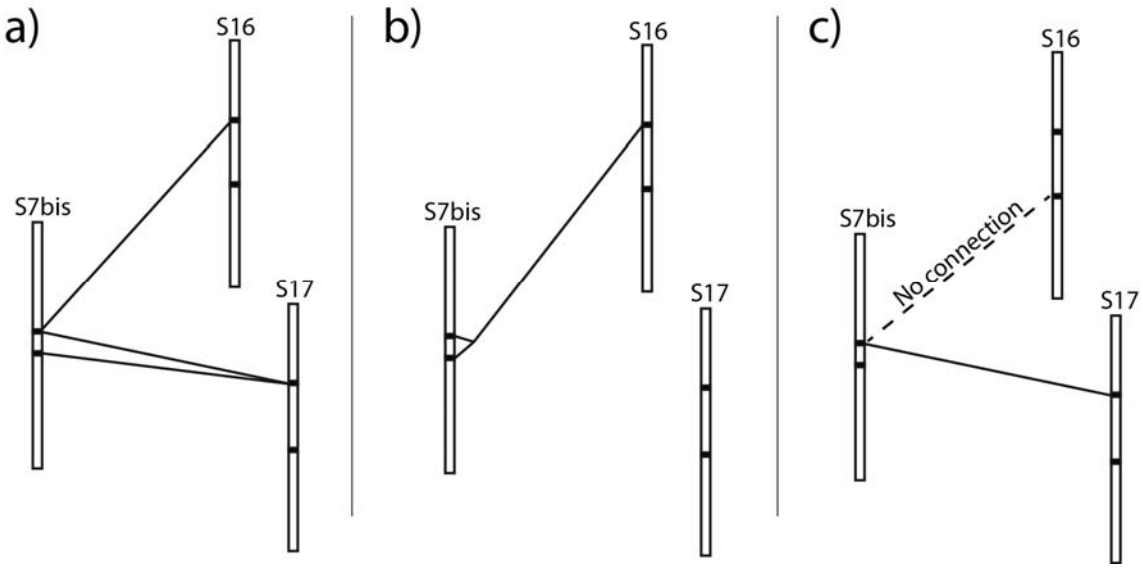

Figure 57: Synthesis of the hydraulic connection inferred from a) cross borehole flowmeter test (a), tracer test performed on March, 2010 (b) and tracer test performed on November, 2010 (b).

3.4 Analysis on the annual variations in ambient flow (Activity Index) – An approach for evaluation of the variation over time in flow measurements.

The study project in the test site involving a set of borehole flow measurement over about a year and a half, as summarized in the following Table 6:

Borehole	January 20th, 2010	February 01st, 2010	May 21st, 2010	September 13th, 2010	November 26th, 2010	August 4th, 2011
S16	A P	A C (pump S7bis)	A	A C (inj P2)	A	A
S17	A P C (pump S16)	A C (pump S7bis)	A	A C (inj P2)	A	A
S7bis	A P	A	A P	A C (inj in P2)	A	A
P1				A	A	A
P2				A	A	A
P3				A	A	A

Table 6: flowmeter log measurements. A = ambient flow; P = pumping flow; C = cross borehole flow

Due to amount of ambient flow data, we looked for the better way to describe the variations in ambient flow observed both over time in each boreholes and the different "activity" - in flow terms - between the boreholes.

In fact we observed that boreholes had, among them, important differences in vertical flow rate, furthermore they present a degree of variability over time that is difficult to express analytically (see Figure 59).

So, we introduce the concept of "Activity Parameter" or AP (Eq. 17), a parameter that could represents boreholes in flow rate terms, useful to describe its temporal evolution.

$$AP = \sum_{i=1}^{n} \left| \frac{\Delta Q_i}{z_{i+1} - z_i} \right| \qquad \text{Eq. 17}$$

Where:

ΔQ_i = differential ambient flow = $Q_{(z_{i+1})} - Q_{z_i}$

Q_{z_i} ambient flow at a depth z

$Q_{(z_{i+1})}$ ambient flow at a depth z+1

$z =$ elevation where flow readings are taken

The steps to compute the AP are the follows: (1) measure the vertical ambient flow (l*min^{-1}) with the appropriate vertical resolution; (2) calculate the Differential Ambient Flow (DAF), that is the difference between an ambient flow measurement at a depth minus the ambient flow measurement at the depth immediately below; (3) compute the ratio between the absolute value of DAF and the length to which the DFA refers; (4) finally the Activity Parameter is the sum of each DAF ratio computed at step (3).

In the following spreadsheet (Table 7) steps (1), (2), (3) and (4) are indicated.

Depth (m BGS)	Ambient Flow (l*min^{-1}) STEP 1	Differential Ambient Flow (l*min^{-1}) STEP 2	Differential Ambient Flow (absolute value) (l*min^{-1}) STEP 3
21.50	-0.006		
21.25	-0.035	-0.029	0.029
21.00	-0.076	-0.041	0.041
20.75	-0.094	-0.018	0.018
20.50	0.014	0.108	0.108
20.25	-0.047	-0.061	0.061
20.00	-0.059	-0.012	0.012
19.75	-0.07	-0.011	0.011
19.50	-0.078	-0.008	0.008
19.25	0.072	0.15	0.15
19.00	-0.023	-0.095	0.095
18.75	-0.002	0.021	0.021
18.50	-0.065	-0.063	0.063
18.25	-0.118	-0.053	0.053
18.00	0.243	0.361	0.361
17.75	1.561	1.318	1.318
17.50	2.481	0.92	0.92
17.25	2.525	0.044	0.044
17.00	2.562	0.037	0.037
16.75	2.59	0.028	0.028
16.50	2.696	0.106	0.106
16.25	2.85	0.154	0.154
16.00	0.302	-2.548	2.548
Sum		**0.308**	**6.186**
		Activity Index (l/min) STEP 4	**1.125**

Table 7: flow data analysis for borehole S16 for the log made on January 20th, 2010. The length of the borehole section investigated is 5.50 m.

Figure 58 shows the AP for a set of measures obtained from January, 2010 to August, 2011.

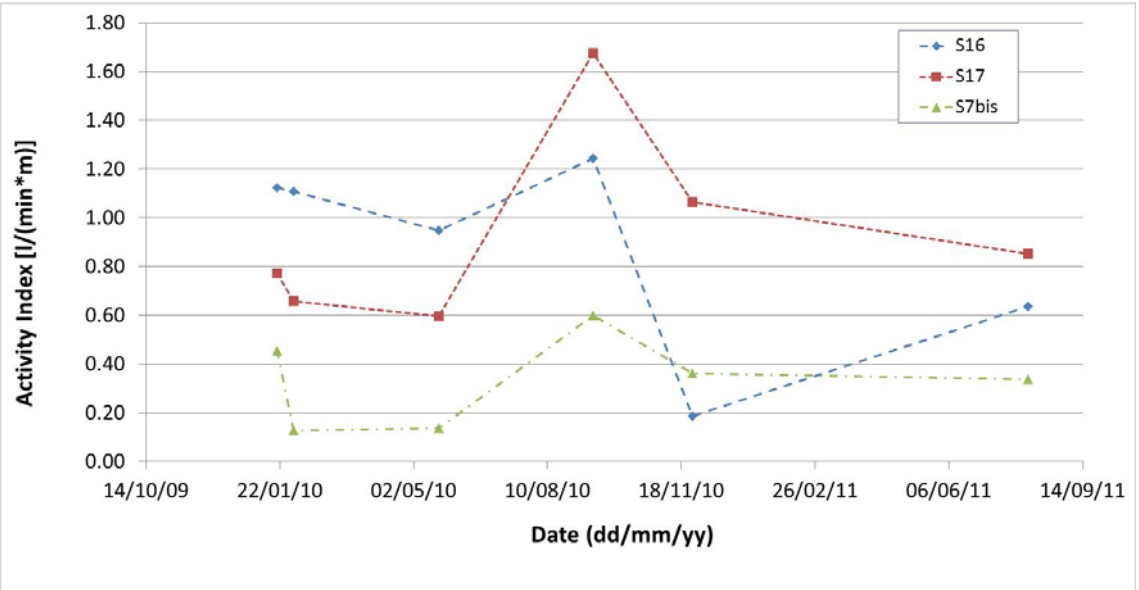

Figure 58: Activity index trend for wellbore S16, S17, S7b, P1, P2 and P3.

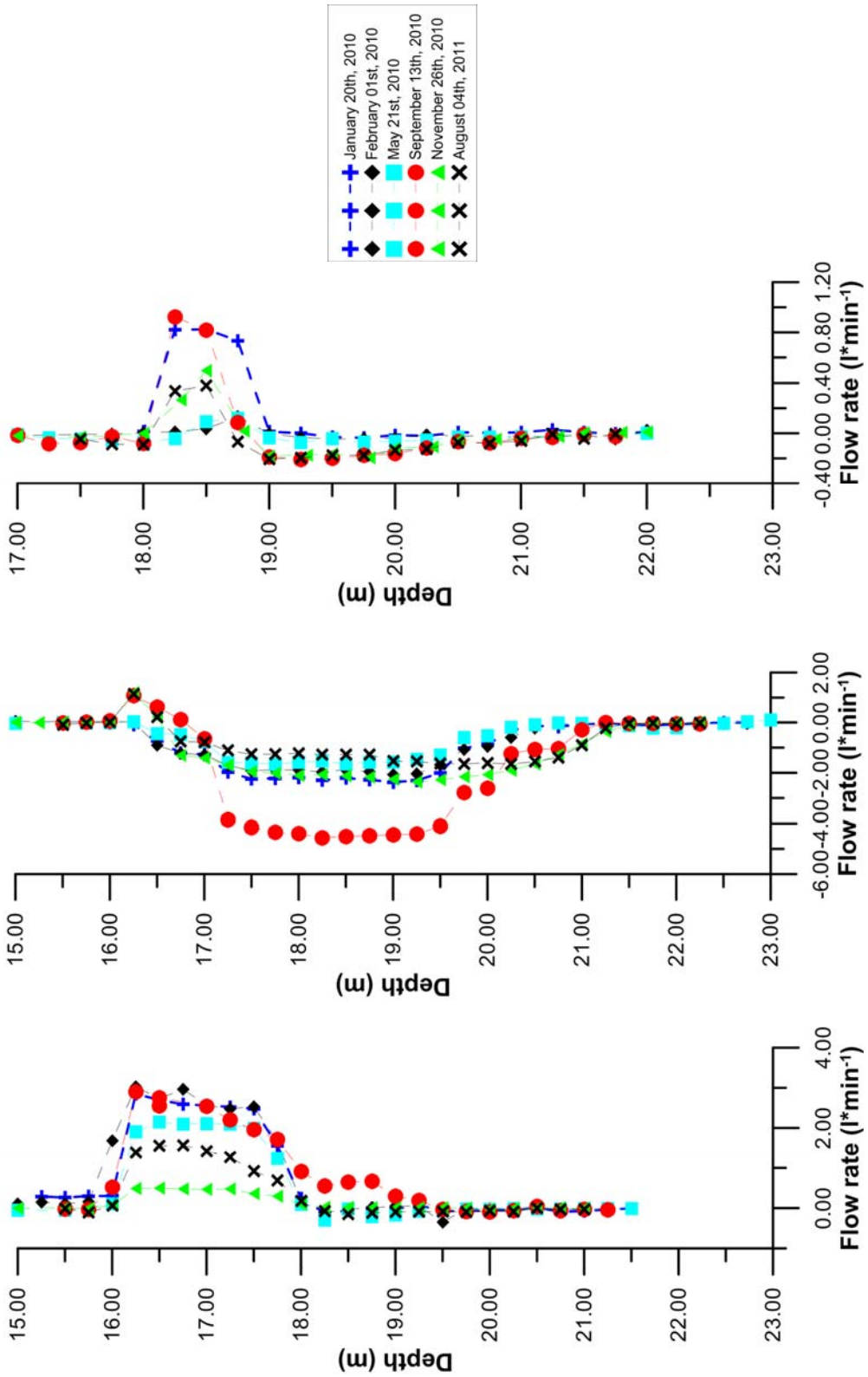

Figure 59: Flow rate seasonality for the well S16, S17 and S7bis (from left to right)

Chapter 4
Integration of flowmeter and GPR data

4.1. Introduction

A large effort for a better understanding of heterogeneous hydrogeologic properties consists in the exploration of the potential of geophysical data to compensate for the lack of in situ hydrological measurements (Rubin et al., 1992). Geophysical data used for hydrogeological characterization often include electrical resistivity (Kelly, 1977), seismic velocity (Rubin et al., 1992) and Ground Penetrating Radar (GPR) velocity (Hubbard et al., 1997).

It has been recognized that the most difficult part of the integration of hydrogeological and geophysical data are the scale and resolution disparity between hydrogeological and geophysical measurements and because of their non-unique relationship due to the uncertainty associated with field data acquisition and interpretation (Urish, 1981).

We have explored the potential use of GPR measurements for hydraulic conductivity estimation and on the potential integration of flowmeter and geophysical data.

Figure 60 schematically presents the resolution and sampled fraction of aquifer volume associated with each geophysical and hydrogeological characterization method (Hubbard et al, 2001). In Figure 60 are also related the scale of geophysical characterization tools to the traditional hydrological tools of core analysis and well tests. This chart illustrates how geophysical data can help to bridge the information gap between conventional hydrogeological core analysis and well testing.

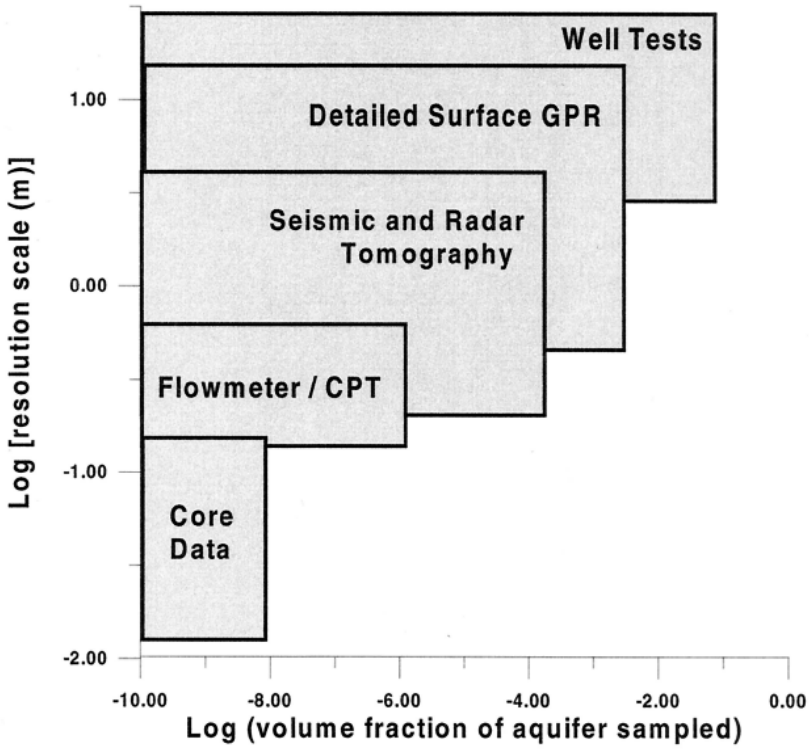

Figure 60: comparison of resolution and fraction of aquifer volume sampled using different characterization tools. Geophysical data help to bridge the information gap in terms of both resolution and fraction of aquifer volume sampled between the more conventional hydrological sampling techniques of core analysis and well tests. (from Hubbard et al., 2001)

4.2 Ground-Penetrating Radar (GPR)

GPR is a geophysical tool that has become increasingly popular between researchers that attempt to better understand near-surface conditions. GPR uses electromagnetic energy at frequencies of 50–1500 MHz to probe the subsurface. At these frequencies, dielectric properties - the separation (polarization) of opposite electric charges within a material subjected to an external electric field - dominate the electrical response (Davis and Annan, 1989).

A GPR system consists of an impulse generator, which repeatedly sends an impulsive signal of fixed voltage and frequency spectrum to a transmitting antenna. The signal propagates from the transmitting antenna through the soil/rock and is reflected, scattered, and attenuated by subsurface dielectric contrasts. The receiving antenna subsequently records the modified signal. Dielectric constants, ε, vary as a function of material saturation, porosity, temperature, and pore fluid composition.

The most common surface GPR acquisition mode is **surface single-offset reflection**, which

involves collecting one trace per surface location from a transmitter-receiver antenna pair as the pair moves along the ground surface, (Figure 61a). Data collected in this mode are typically displayed as wiggle-trace profiles, with distance on the horizontal axis and arrival time (which can be converted to depth using electromagnetic wave velocity information) on the vertical axis. The variations in arrival time, amplitude, and phase of the signals indicate subsurface variations in electromagnetic properties. Surface GPR profiles are useful for investigating changes in physical and hydrological properties, and for inferring the stratigraphy and structural geology along two-dimensional profiles or within a pseudo three-dimensional grid composed of several two-dimensional profiles.

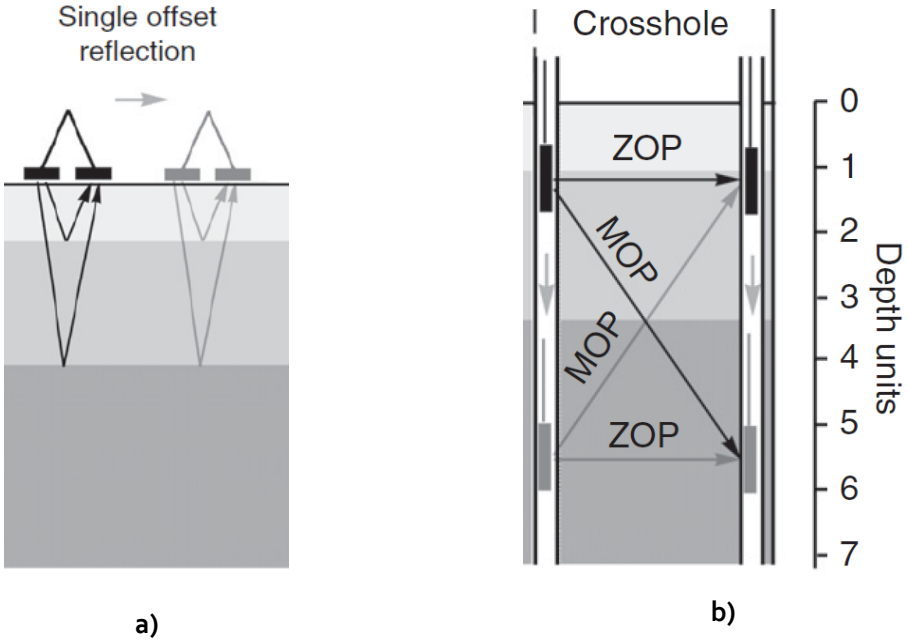

Figure 61: Ground penetrating radar (GPR) surveying techniques for moisture content estimation: (a) single-offset reflection; (b) cross-hole transmission (adapted from Slater and Comas, 2009)

In **cross-hole Ground penetrating radar** surveys (Figure 61b), high frequency electromagnetic waves are propagated from transmitter locations in one borehole to receiver locations in a second borehole. Waveform traces are recorded at receiver locations and quantities such a travel time, energy or amplitude are calculated for each transmitter-receiver raypath. Measurement of the received electromagnetic wave permits determination of the first arrival and hence velocity of the wave (v).

Borehole-to-borehole radar surveys may be conducted in two transmission modes in order to determine dielectric properties at the field scale.

In one mode (MOG or MOP), using a multiple offset gather (Peterson, 2001), the receiver is moved to different locations in one borehole, whilst the transmitter remains fixed. The

transmitter is then moved and the process repeated. Following collection of all data in this mode and determination of the travel time for each wave path-line, it is possible to derive a tomogram of velocity within the plane of the borehole pair. In contrast, a zero offset profile (ZOP) may be determined by keeping transmitter and receiver at equal depth. By systematically lowering or raising the pair of antennas in the two boreholes, it is possible to build a one-dimensional profile of average inter-borehole travel time over the entire borehole length.

In both cases, in low loss materials and at high frequency, the bulk dielectric constant (ε) is derived from:

$$\sqrt{\varepsilon} = \frac{c}{v} \qquad \text{Eq. 18}$$

where c is the radar wave velocity in air (≈0.3 m/ns), (Binley et al., 2002).

As mentioned above, the applications of GPR in water resources characterization is supported by strong petrophysical relations that link measured dielectric permittivity (ε) to moisture content (θ) and porosity (ϕ).

The most commonly applied relationship for estimating θ of soils and rocks is the empirical Topp equation (Topp et al., 1980):

$$\theta = -5.3\times10^{-2} + 2.92\times10^{-2}\varepsilon - 5.5\times10^{-4}\varepsilon^2 + 4.3\times10^{6}\varepsilon^3 \qquad \text{Eq. 19}$$

This equation satisfies measurements performed on mineral soils, although organic rich soils (eg. peat) tend to deviate from this relationship.

4.3 Gorgonzola case study

4.3.1 Introduction

This section presents a combined interpretation of borehole flowmeter, tracer testing, radar and ERT data to accomplish an improved hydrogeological characterization.

In 2005 a project was initiated at the Dipartimento di Scienze Geologiche e Geotecnologie of University of Milan-Bicocca to examine, using geophysical methods, unsaturated flow and transport processes at one purposely developed field site in Gorgonzola (Milan-Italy) (Deiana et al. 2007 and 2008).

In this thesis, in conjunction with prof. Alberto Godio (Dipartimento di Ingegneria del Territorio, dell'Ambiente e delle Geotecnologie of Politecnico di Torino) and with prof. Andrew Binley (Lancaster Environment Centre, Lancaster University - UK), we monitored an infiltration process in the vadose zone. 15000 liter of water marked with 1 g sodium Fluorescein were injected from a 2.5 m long well positioned approximately at the center of 3 boreholes. The aim was to measure, using two borehole fluorometers in two boreholes located downstream, the arrival time of the Fluorescein to the groundwater (about 14 m below ground surface). This time was used as direct data to calibrate Electrical Resistivity Tomography (ERT) and Ground Penetrating Borehole Radar (GPR) survey.

The experiment was performed at the Gorgonzola test site between January 24st, 2011 and February 02nd, 2011 .

4.3.2 Hydrogeologic Setting

The Gorgonzola experimental site is located a few km east of Milan (Italy) in a plain area in the alluvial Quaternary sediments of the Po River plain (Figure 62).

In 2004 four boreholes were drilled at the site (A, B, C and D in Figure 63) to monitor the unsaturated flow dynamics in the local alluvial Quaternary sediments (Deiana et al., 2007). Boreholes are cased with PVC and extend to a depth of about 20 m. The complete technical information are presented in Table 8.

Three boreholes (A, B, C,) are permanently equipped with a set of 24 stainless-steel borehole electrodes for ERT imaging (details in Figure 72), spaced vertically at intervals of 0.8 m, between 2 m and 20 m depth.

Figure 62: Gorgonzola site study in a satellite image of the Po River Plain.

The sediments are characterized by a fairly coarse sandy-gravel grain size. A gravel pack was placed around the slotted section, between 15 and 20 m depth, to ensure that the changing elevation of the water table could be measured all year round.

Deiana et al. (2007) observed that the main features noted by the analysis of a soil core (borehole D in Figure 63) are (a) the presence of a 3-m-thick superficial layer composed of rubble and agricultural soil; (b) a prevalence of Quaternary fluvial sand/gravelly sediments; (c) the existence of a 2-m-thick layer of cemented gravel and sand at roughly 12 m depth.

A Lefranc permeability test was performed at a depth of 6 m. The resulting field-saturated hydraulic conductivity value was 36 m/d (Deiana et al., 2007).

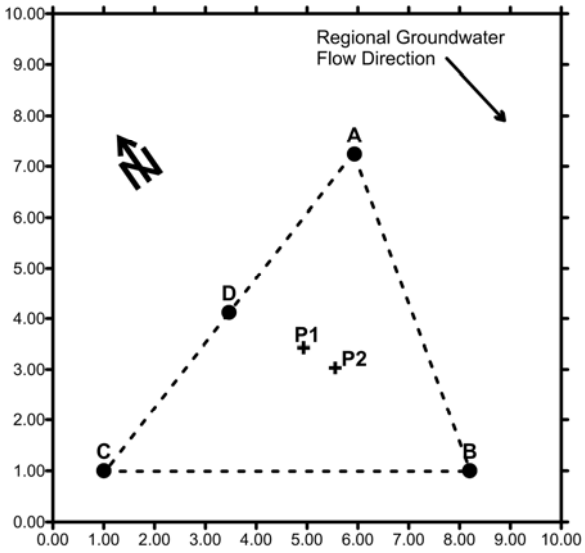

Figure 63: geometry of the study site. Distances are in meters. P1 and P2 are the 2.5 depth injection wells. Boreholes A, B and C are equipped with ERT electrodes.

Well ID	Borehole Diameter (cm)	Casing Diameter (mm)	Top of Casing elevation (m above MSL)	Top of screen (m below TOC)	Bottom of screen (m below TOC)	Static depth to water (m below TOC)
A	152	76.2	137.0	15	20	14.25
B	152	76.2	137.0	15	20	14.25
C	152	76.2	137.0	15	20	14.25
D	152	101.6	137.0	3	20	14.25

Table 8: Well construction information for Gorgonzola Study site. MSL= Mean Sea Level; TOC=Top of Casing. Bottom of the screen matches with borehole depth.

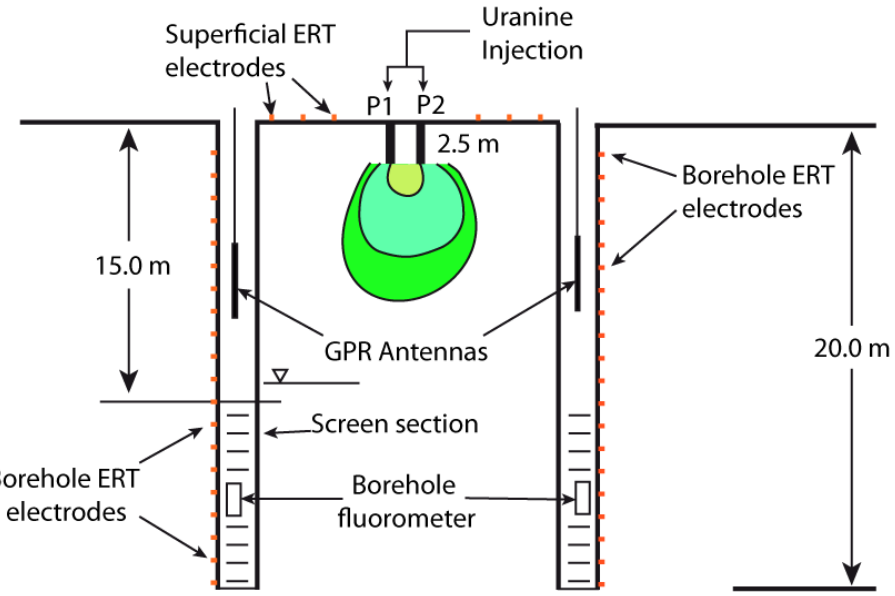

Figure 64: uranine injection and geophysical monitoring scheme (drawing not to scale)

4.3.3 Flowmeter Measurements

The flowmeter test was performed with the EBF system in an effort to characterize ambient vertical flow variations along wellbores screen.

A rubber skirt was used to create a seal between the borehole flowmeter probe and well casing.

Flow measurements were taken at 0.25 m intervals starting from the well. The flowmeter readings in the unscreened section of the wellbore were used as a zero setting.

Figure 65 to 71, illustrate ambient flow rate profiles where upward flows were designated as positive.

As concern borehole A (Figure 65), the ambient vertical flow profile indicates a measurable upward flow between 15.50 m and 18.00 m below TOC with a maximum flow-rate of about 0.64 $l*min^{-1}$ at 17.25 m.

In borehole B, no significant ambient flow was measured (Figure 66).

In borehole C (Figure 67) the ambient vertical flow profile indicates low, but measurable, downward flow between top of screen and 17.25 m, while from this depth to the bottom of the wellbore, there is an increment in downward flow with a maximum (0.96 $l*min^{-1}$) at 18.00 m.

In borehole D (Figure 68) an upward ambient flow was recorded between 15.75 and 17.50 m with a maximum flow-rate of 0.40 $l*min^{-1}$ at 16.50 m.

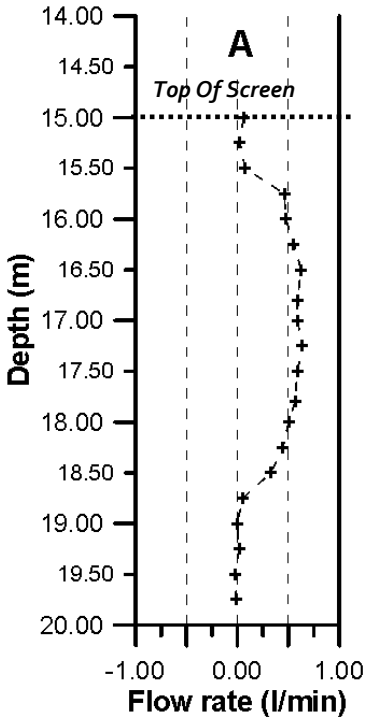

Figure 65: ambient flow rate in borehole A

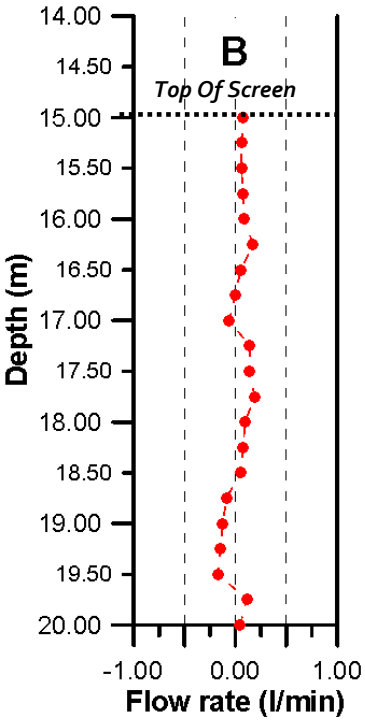

Figure 66: ambient flow rate in borehole B

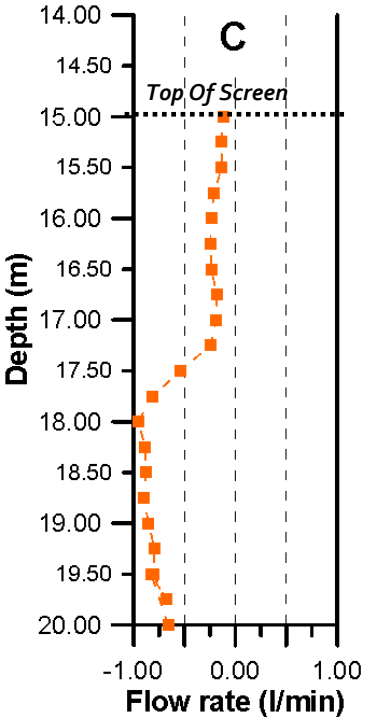

Figure 67: ambient flow rate in borehole C

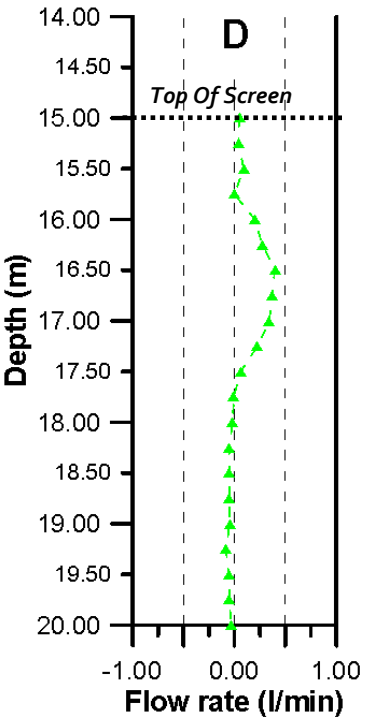

Figure 68: ambient flow rate in borehole D

4.3.4 Tracer Test Setting

A total of 14 m^3 of tap water (from municipal water supply) was injected into two shallow boreholes, P1 and P2, over about 45 hours at a depth of 2 m below TOC. A flow gauge system (Figure 71) allowed to measure the injection flow rate and the volume of injected water keeping the flow rate constant (approximately 320 l/h). At the beginning of the injection, the injected water was marked with a 0.5 l of solution of 1 g of Na-Fluorescein. The tracer injection lasted about 1 minute and can be considered istantaneous.

The evolution of the injected water plume in space and time was monitored by ERT and GPR measurements in time-lapse mode for a total of 216 hours, from January 24 (date of water injection) to February 02, 2011.

Date and Time (hh.mm) of water injection	Date and Time (hh.mm) of the end of injection	Date of the end of the geophysical survey	Duration of the water injection (hh.mm)	Volume of water injected (l)	Average Flow rate Injection ($l*h^{-1}$)
January 24, 2011 12:30	January 26, 2011 08:33	February 02, 2011	43.57	14360	326

Table 9: overview of the experiment performed at Gorgonzola test site

Time-lapse ERT data were acquired both by a superficial electrodes array (Figure 69) and between boreholes A, B and C (Figure 70), using an IRIS Syscal Pro system.

ERT array was formed by 84 electrodes: 15 electrodes on the ground level (superficial) while in boreholes A, B, C, D there are 24, 23, 22 and 1 electrodes respectively (1 electrode was specifically positioned at the bottom of borehole D).

For the background measurement a total of 10584 measurements were taken including direct and reciprocal configurations (interchanging potential with current electrodes, Deiana et al., 2007). The total time required for each acquisition, was about 90 minutes.

After injection, for 23 steps a total of 4203 measurements were taken and the total time required was about 35 minutes for each acquisition. For these cases were taken only the direct measurements.

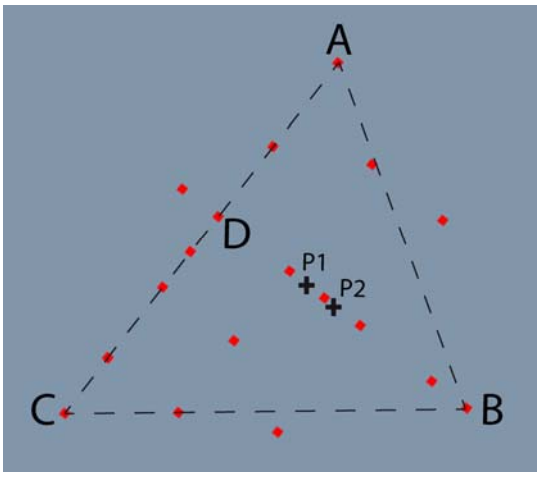

Figure 69: superficial electrodes array for ERT acquisition

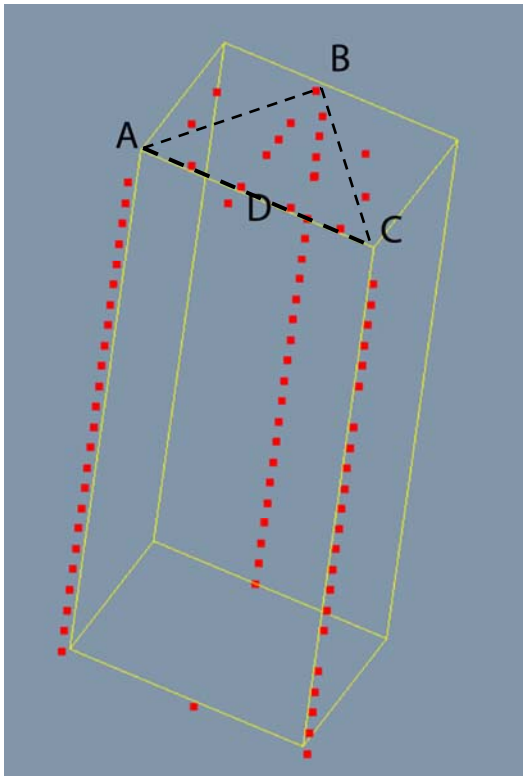

Figure 70: elecrodes array within borehole A, B, C and D

Cross-hole GPR data were acquired for the following panels: AB, AC, BD and BC for a total of 92 GPR profiles (23 steps). As observed by Deiana et al. (2007) in spite of the existence of electrodes and cables in each borehole, it was possible to acquire good quality data.

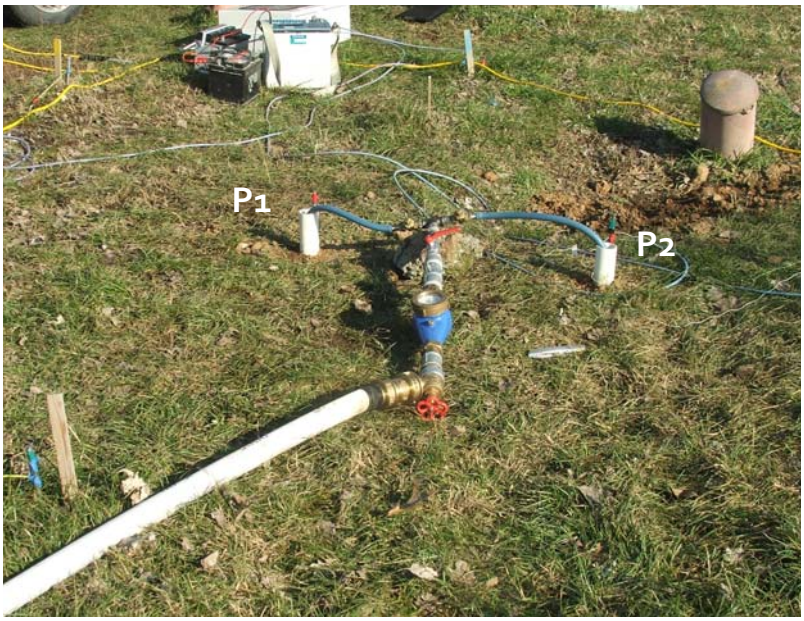

Figure 71: water injection in shallow boreholes P1 and P2

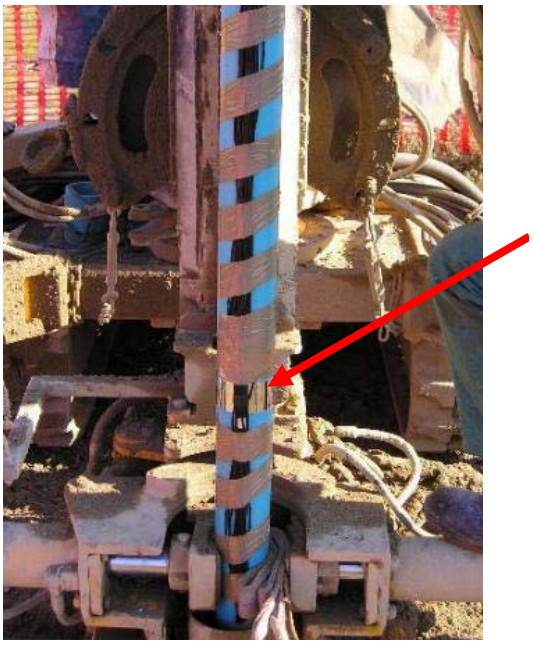

Figure 72: A detail of the stainless-steel borehole electrodes for ERT imaging installed on the PVC casing

At test site, 23 Zero-Offset-Profile (ZOP) surveys were acquired before, during and after water injection. A PulseEkko 100 system was used with 100 MHz borehole antennas, lowered with a 0.25 m vertical spacing.

The GPR measurements acquired before injection in all four panels were used as "background values".

4.3.5 Results of time-lapse GPR monitoring

GPR data analysis was limited to traveltime picking and inversion for velocity distribution. The

moisture content profile was obtained by Topp et al. (1980) equation (Eq. 17). According to Deiana et al. (2007), zero-offset profiles were analyzed under the assumption of straight-ray horizontal propagation.

As above mentioned infiltration was performed at 2 meters below TOC.

The resolution of the GPR measurements is controlled by their spacing along the borehole vertical (0.25 m).

Figures 74-77 show moisture content profiles obtained for twelve time steps. Each moisture content profile is compared with the background value, measured two hours before the water injection.

Due to the geometry of the system, the infiltrating water front was particularly clear in panel BD. After three hours the maximum depth of the perturbed zone was around six meters. The high velocity of the system was outlined by the depth of the water front after 21 hours (step 3 in figure 74-77), when the water table was reached. The maximum infiltration rate calculated in the unsaturated zone was around 13 m/d.

The return to the background moisture content value occurred 123 hours after the end of the injection. The lowering of the water table (from 14.25 to 14.44 m below ground level) is clearly evident in moisture content profiles.

Another particularity of the moisture content profile along panel BD is the evidence of a layer between 12.00 and 14.00 m where the increase in water content occur at to the 2 m thick layer of cemented gravel and sand detected in the drilling core (Deiana et al., 2007).

Changes in moisture content are not so evident in panels AB, AC and BC. Probably because the plume is of limited extension in lateral direction.

Gpr Result Panel BD

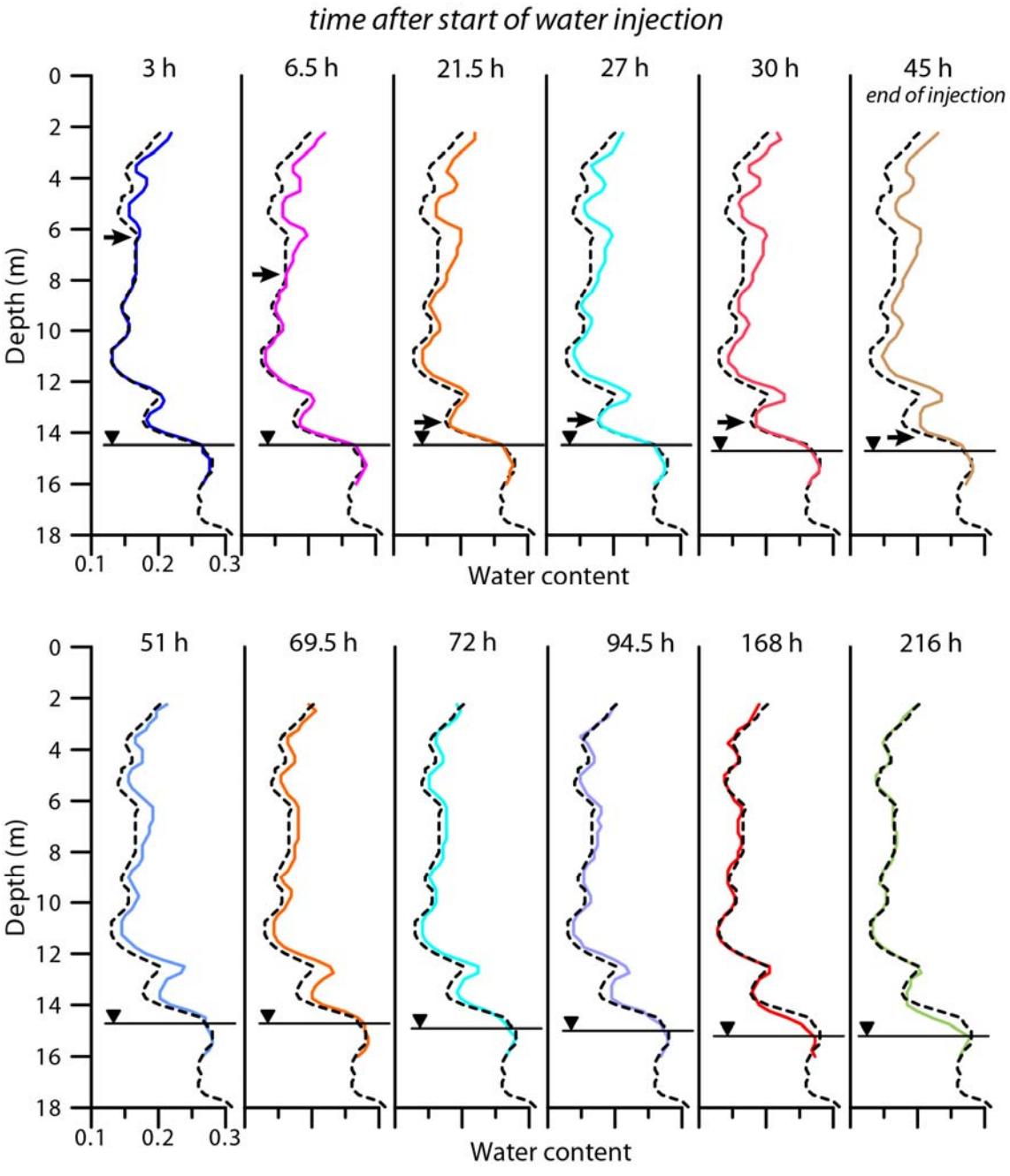

Figure 73: profiles of moisture content as a function of depth, derived from zero offset profile (ZOP) for twelve steps after the start of the water injection for panel BD (see Figure 63). The black arrow indicates the position of the maximum propagation of the infiltration front. The depth to groundwater changes from 14.25 m to 14.44 m below TOC. Dotted line is the background water content.

Gpr Result Panel AB

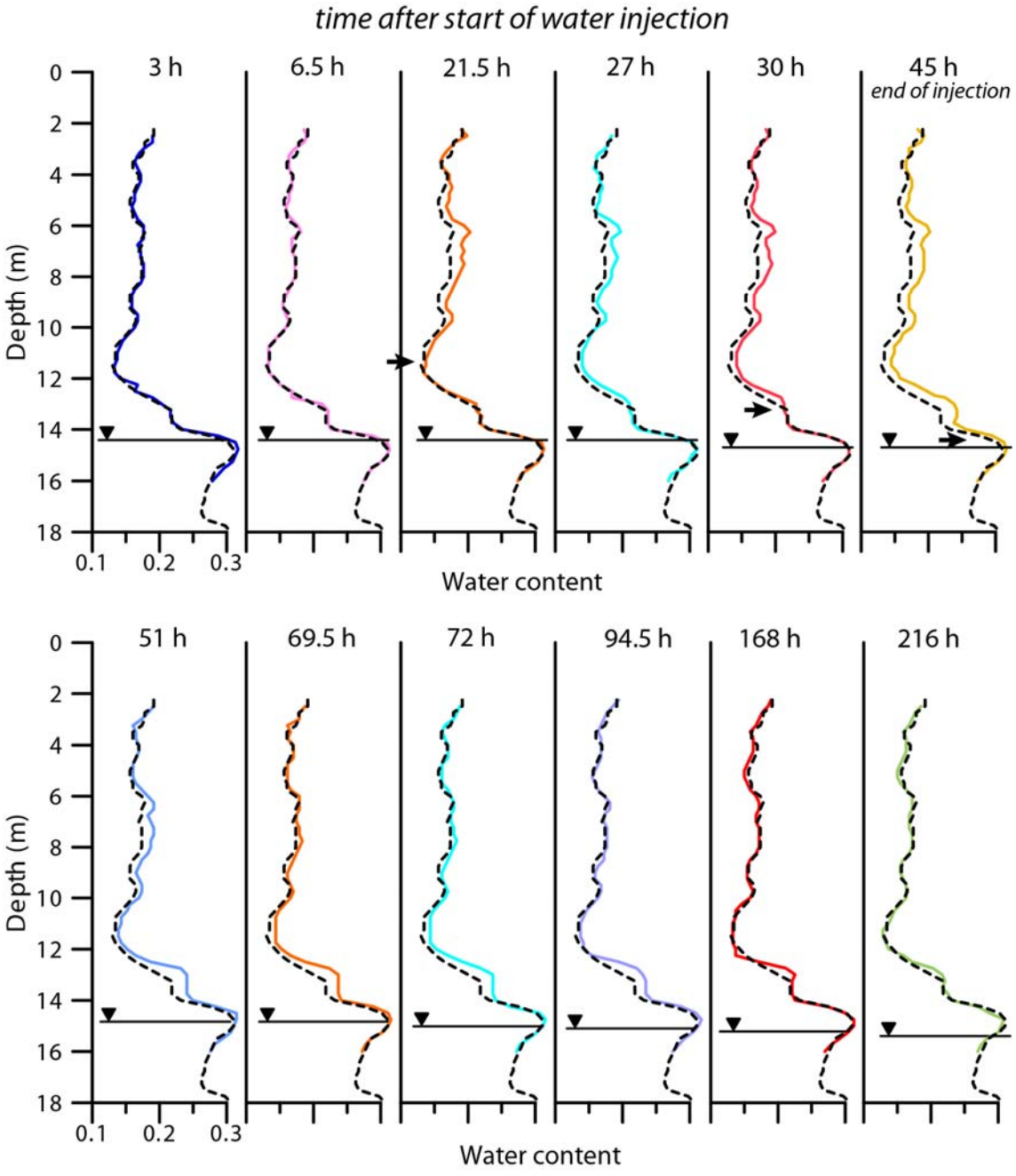

Figure 74: profiles of moisture content as a function of depth, derived from zero offset profile (ZOP) for twelve steps after the start of the water injection for panel AB (see Figure 63). The black arrow indicates the position of the maximum propagation of the infiltration front. The depth to groundwater changes from 14.25 m to 14.44 m below TOC. Dotted line is the background water content.

Gpr Result Panel AC

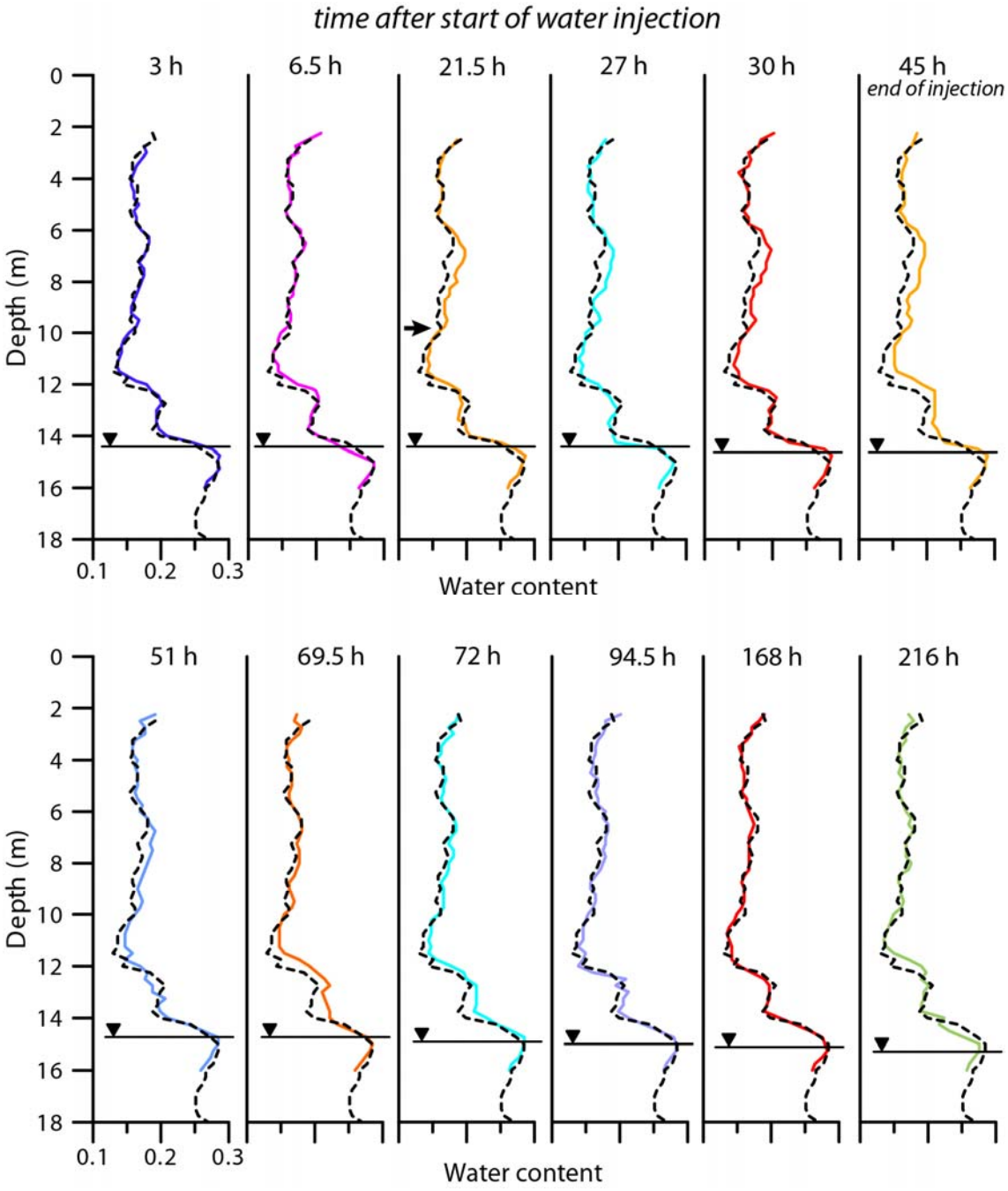

Figure 75: profiles of moisture content as a function of depth, derived from zero offset profile (ZOP) for twelve steps after the start of the water injection for panel AC (see Figure 63). The black arrow indicates the position of the maximum propagation of the infiltration front. The depth to groundwater changes from 14.25 m to 14.44 m below TOC. Dotted line is the background water content.

Gpr Result Panel BC

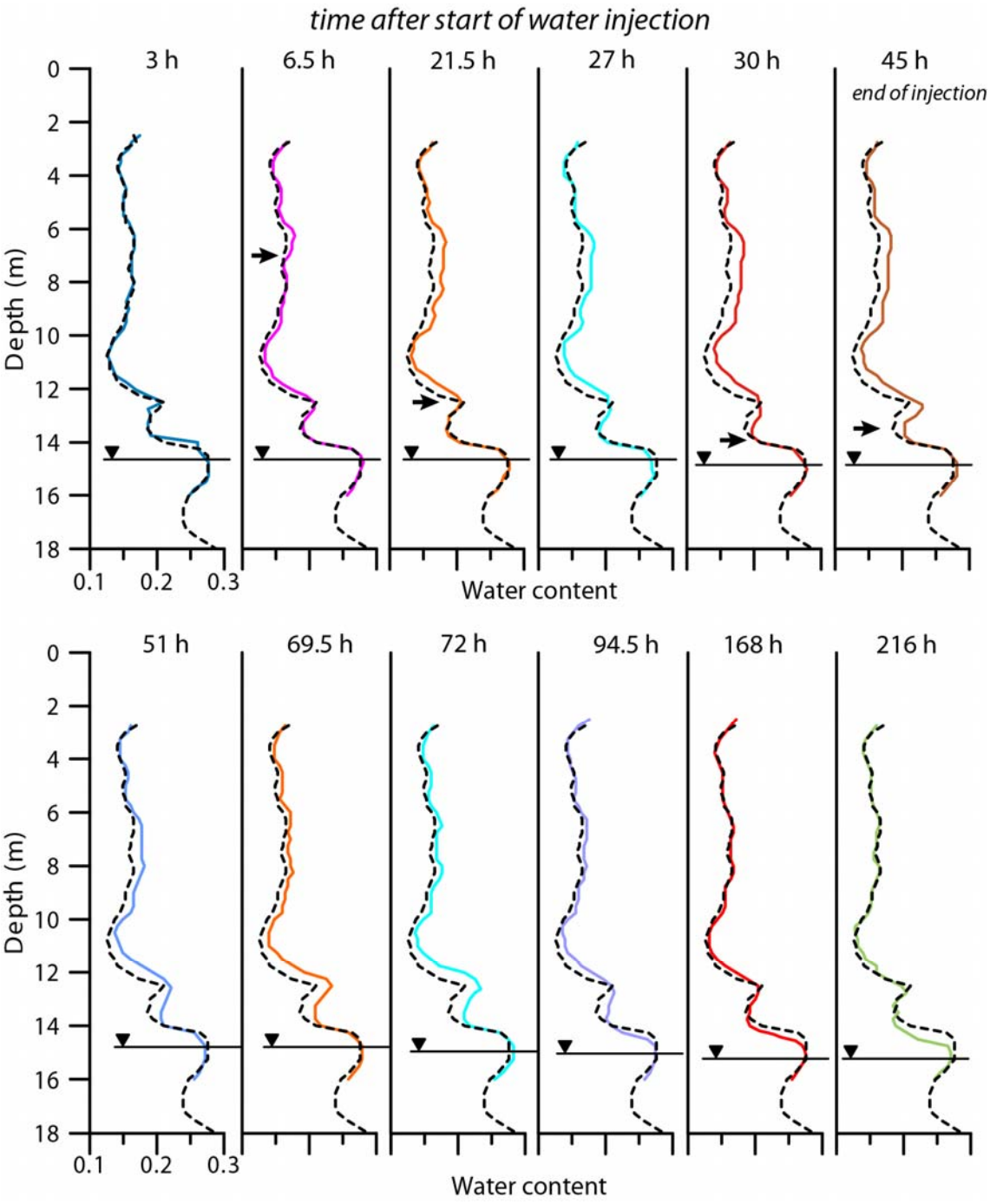

Figure 76: profiles of moisture content as a function of depth, derived from zero offset profile (ZOP) for twelve steps after the start of the water injection for panel BC (see Figure 63). The black arrow indicates the position of the maximum propagation of the infiltration front. The depth to groundwater changes from 14.25 m to 14.44 m below TOC. Dotted line is the background water content.

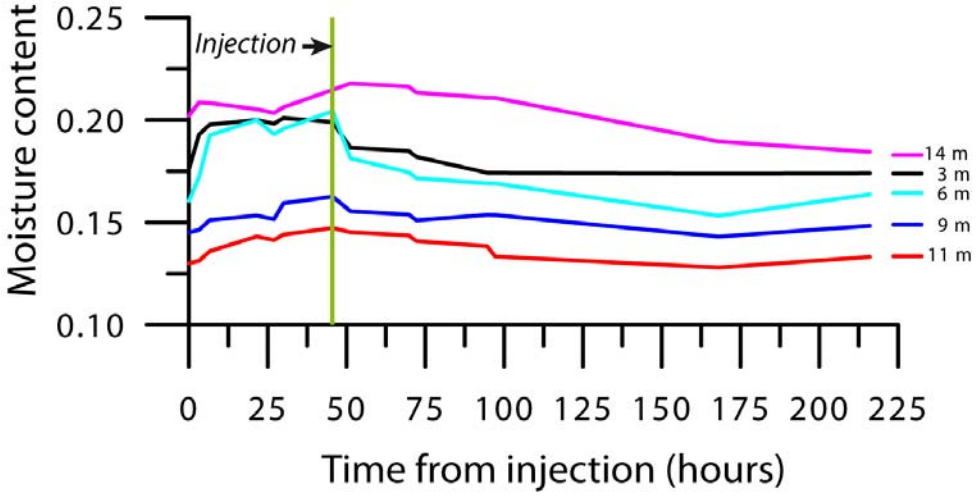

Figure 77: Changes in moisture content at different depth for panel BD.

The infiltration pattern is described in Figure 77 where are showed variation in moisture content at selected depths during and after water injection. Three hours later beginning of water injection, moisture content is changed both at 3 and 6 meter. A significant increase in water content at 11 m was recorded after 21 hours.

The redistribution of infiltrated water started immediately after interruption in injection of water. As expected the water content decreased faster in the upper layers (profile at 3 and 6 m in Figure 77) due to the downward flow of water and resulted in a more slow decline of moisture content at the bottom of the profile. Moisture content at 14 m is so high because this layer is more related to the capillary fringe.

4.3.6 ERT results

The difficulty in solving for the adopted electrodes array requires an opportune numerical code, which it is in progress yet. This analysis is carried out also in collaboration with Prof. A. Binley (Lancaster University).

4.3.7 Tracer Test Results

As showed in Figure 64, two borehole fluorometers were positioned in boreholes B and C to acquire the Uranine breakthrough curves.

To exactly locate the sampling positions, ambient flowrate profiles were recorded. Borehole B (Figure 66) did not show relevant ambient flow, while borehole C (Figure 67) showed a significant downflow below 18.00 m. Therefore we decided to locate the probes at 18.00 m in both wellbores.

Unfortunately, both in boreholes B and C, no tracer was detected during the test. We observed several turbidity peaks and consequent peaks in Uranine concentration due to the insertion of antennas into the well (Figure 78). This is true especially in borehole C. As consequence we need to perform other tracing experiments (e.g. increasing the mass of injected uranine) to understand the reasons of the failure in detection.

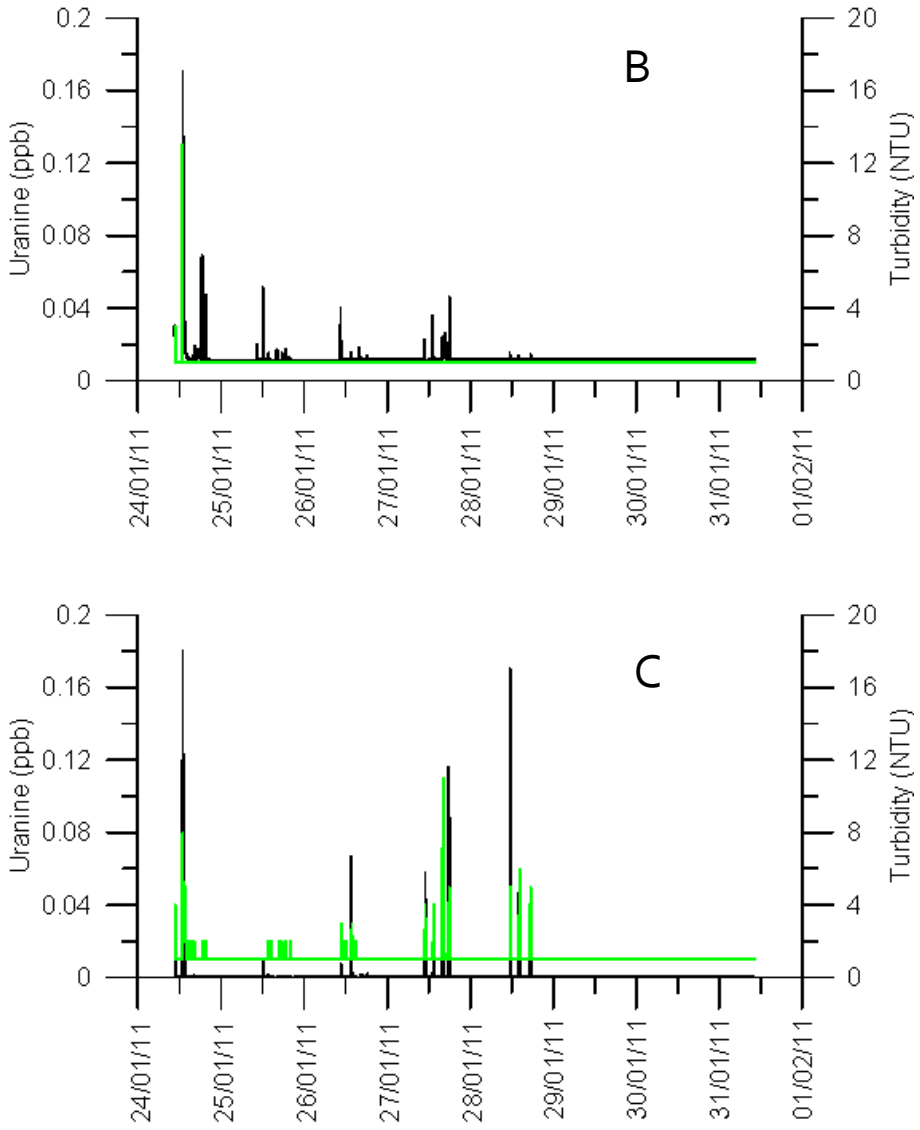

Figure 78: breakthrough curves detected in borehole B (up) and C (down). Green: Uranine; black: Turbidity.

4.3.8 Summary

Cross-borehole radar and resistivity measurements acquired in time lapse mode have been used to characterize changes in moisture content due to controlled injection of water and fluorescent tracer in the unsaturated zone.

Borehole radar moisture content, performed along four panels, showed the vertical migration of the wetting front during the tracer test.

Cross-borehole electrical resistivity tomography was arranged to monitor changes in resistivity over time. It is not possible to present results of ERT tomography due to the need to implement a code to process the acquired data.

When we will be able to combine the resistivity tomograms with cross-borehole radar data it will be possible to estimates changes in pore water concentration in three dimensions over time.

A direct measurement of the travel time through the unsaturated zone was not achieved because the borehole fluorometers positioned downstream did not reveale any tracer arrival. We will try to investigate the possible cause for this failure, increasing the mass of tracer injected and trying to change the fluorometers locations whitin the wellbore.

Conclusion

This study represents an extensive test of the application of the flowmeter technique in conjunction with other geophysical and hydrogeological survey methods.

Sensitive borehole flowmeters, including the electromagnetic flowmeter described in this thesis, demonstrate that they are valuable tools for detailed characterization of hydrogeology. These tools may be used in existing wells to obtain such information as natural ground-water flow patterns within the well, identification of hydraulically active fracture zones in rock, and, potentially, estimates of the relative hydraulic conductivities of materials adjacent to the well screen and evaluate contaminant transport and fate and monitoring network design.

The borehole flowmeter is especially useful at sites where boreholes are intersected by permeable horizontal fractures or bedding planes. Data obtained from flowmeter logging demonstrates moreover their applicability and importance in tracer test design and interpretation.

At one test site (Serravalle Scrivia test site), the most important topic is the relative ease and simplicity of flowmeter measurements that permits reconnaissance of naturally occurring flows. Flowmeter surveys provided a valuable means by which to identify fracture interconnections and solute transport pathways during planning for tracer test design. The simple and direct measurements of vertical flows provided information pertaining to the relative magnitude and vertical extent of naturally occurring hydraulic-head differences in a few hours of measurement.

The experiment carried out at Gorgonzola test site presents a combined interpretation of borehole flowmeter, tracer testing, radar and ERT data to accomplish an improved hydrogeological characterization. Cross-borehole radar and resistivity measurements acquired in time lapse mode have been used to characterize changes in moisture content due to controlled injection of water and fluorescent tracer in the unsaturated zone.

Flowmeter log provided the correct position of the sampling points.

Designing a tracer test without any information on vertical borehole flow can lead to erroneous considerations on tracer arrival and concentration, and thus on calculated hydraulic parameters.

While the studies described in this thesis did not involve directly contaminated ground water, the potential application to contaminant migration problems and monitoring well screen location is obvious.

References

Allen-King, R.M., Divine, D.P., Taylor, K.M., Gaylord, D., Alldredge, R. 2003. Predicting the heterogeneous distribution of aquifer permeability through mapping lithofacies. Abstracts with Programs - Geological Society of America 35 (6), 54.

Anderson, M.P., Woessner, W.W. 1992. Applied Groundwater Modeling: Simulation of Flow and Advective Transport. Academic Press, San Diego, CA. 381 pp.

Arnold, K.B., and F.J Molz. 2000. In-well hydraulics of the electromagnetic borehole flowmeter: further studies. Ground Water Monitoring and Remediation 20, No. 1, pp. 52-55.

Barahona-Palomo, M., M. Riva, X. Sanchez-Vila, E. Vazquez-Sune, A. Guadagnini. 2011. Qualitative comparison of impeller-flowmeter and particle-size-distribution techniques for the characterization of hydraulic conductivity variability. Hydrogeology Journal, Vol. 19, No 3, pp. 603-612.

Bear, J. 1972. Dynamics of Fluids in Porous Media. American Elsevier Publishing Co., New York. 764 pp.

Beliveau, D. 2002. Reservoir heterogeneity, geostatistics, horizontal wells, and black jack poker. AAPG Bulletin 86 (10), 1847– 1848.

Berkowitz, B., Balberg, I. 1993. Percolation theory and its application to groundwater hydrology. Water Resources Research 29 (4), 775–794.

Binley A., G. Cassiani, R. Middleton, P. Winship. 2002. Vadose zone flow model parameterisation using cross-borehole radar and resistivity imaging. Journal of Hydrology, Volume 267, Issues 3-4, Pages 147-159.

Binley A., P. Winship, R. Middleton, M. Pokar and J. West. 2001. High-resolution characterization of vadose zone dynamics using cross-borehole radar. Water Resources Research, **37,** *2639–2652*

Boman, G.K., F.J. Molz, and K.D. Boone. 1997. Borehole flowmeter Application in Fluvial Sediments: Methodology, results and Assessment. Ground Water, Vol. 35, No. 3, pp. 443-450.

Butler A.P., S.A. Mathias, A.J. Gallagher, D.W. Peach and A.T. Williams. 2009. Analysis of Flow Processes in Fractured Chalk Under Pumped and Ambient Conditions (UK). Hydrogeology Journal, 17:1849-1858.

Chatelier M., S. Ruelleu, O. Bour, G. Porel, F. Delay. 2011. Combined fluid temperature and flow logging for the characterization of hydraulic structure in a fractured karst aquifer. Journal of Hydrology, vol. 400, pp. 377-386.

Chen J., S. Hubbard, Y. Rubin. 2001. Estimating the hydraulic conductivity at the South Oyster Site from geophysical tomographic data using Bayesian techniques based on the normal linear regression model. Water Resources Research, vol. 37, no. 6, 1603-1613.

Church P.E. and G.E. Granato. 1996. Bias in ground-water data caused by well-bore flow in long screen

wells. Ground Water, Vol. 34, No. 2, pp. 262-273.

Clapp, R. V., and R.D. *Stibolt. 1991. Useful Measures of Exploration Performance. Journal of Petroleum Technology, pp. 1252-1257.*

Cooper, H.H., and Jacob, C.E. 1946. A generalized graphical method for evaluating formation constants and summarizing well-field history. Transaction of the American Geophysical Union. 27, pp. 526-534.

Davis, J., and A. Annan. 1989. Ground-penetrating radar for high-resolution mapping of soil and rock stratigraphy, Geophys. Prospect. 37, 531–551.

Day-Lewis, F.D., J.W, Lane, S.M., Gorelick. 2006. Combined interpretation of radar, hydraulic, and tracer data from a fractured-rock aquifer near Mirror Lake, New Hampshire, USA. Hydrogeology Journal, 14, pp. 1-14.

Dinwiddie, C.L., N.A. Foley, and F.J. Molz. 1999. In-well hydraulics of the Electromagnetic Borehole Flowmeter. Ground Water, Vol. 37, No. 2, pp. 305-315.

Eaton T.T. 2006. On the importance of geological heterogeneity for flow simulation. Sedimentary Geology, 184 pp 187-201.

Elci A, F.J. Molz, and W.R. Waldrop. 2001. Implications of observed and simulated ambient flow in monitoring wells. Ground Water, Vol. 39, No. 6, pp. 853-862.

Field, M.S. 2002. The QTRACER2 Program for Tracer-Breakthrough Curve Analysis for Tracer Tests in Karstic Aquifers and Other Hydrologic Systems. Report EPA/600/R-02/001.

Foley, N.A. 1997. Pressure distribution around an electromagnetic borehole flowmeter in an artificial well. M.S. thesis, Department of Environmental Systems Engineering, Clemson University.

Fraser, G.S., Davis, J.M. (Eds.). 1998. Hydrogeologic Models of Sedimentary Aquifers, SEPM Concepts in Hydrogeology and Environmental Geology, vol. 1. Society for Sedimentary Geology, Tulsa, OK. 180 pp.

Genereux D., and Guardiario J. 2001. A borehole flowmeter investigation of small-scale hydraulic conductivity variation in the Byscain Aquifer, Florida. Water Resources Research, Vol. 37, No. 5, pp. 1511-1517.

Giddings, T. 1987. What is an adequate screen length for monitoring wells? Opinion 1. Ground Water Monitoring Review, Vol. 7, No. 2, pp. 96-97.

Gierczak R.F., J.F. Devlin , D.L. Rudolph*. 2006.* Combined use of field and laboratory testing to predict preferred flow paths in an heterogeneous aquifer. Journal of Contaminant Hydrology, Vol. 82, Issues 1-2, Pages 75-98.

Hanson R.T., T. Nishikawa. 1996. Combined use of flowmeter and time-drawdown data to estimate hydraulic conductivities in layered aquifer systems. Ground Water, Vol. 34, No. 1.

Hess, A.E. 1982. A heat pulse flowmeter for measuring low velocities in borehole: USGS, Open file Report 82-699.

Hess, A.E. 1986. Identifying hydraulically conductive fractures with a slow-velocity borehole flowmeter. Canadian Geotechnical Journal, 23 pp. 69-78.

Hess, A.E., and Paillet, F.L. 1989. Characterizing flow paths and permeability distribution in fracture rock aquifers using a sensitive thermal borehole flowmeter. Proceedings of the conference on new field technique for quantifying the physical and chemical properties of heterogeneous aquifers. Water Resources research institute, Auburn university, Alabama.

Hsieh, P.A. 1998. Scale effects in fluid flow though fractured geologic media. In: Sposito, G. (Ed.), Scale Dependence and Scale Invariance in Hydrology. Cambridge University Press, New York, pp. 335–353.

Hubbard, S., Y. Rubin, and E. Majer, 1997. Ground penetrating radar assisted saturation and permeability estimation in bimodal systems, Water Resour. Res., 33(5), 971–990.

Huggenberger, P., Aigner, T. 1999. Introduction to the special issue on aquifer–sedimentology: problems, perspectives and modern approaches. Sedimentary Geology 129, 179–186.

Huisman J.A., S.S. Hubbard, J.D. Redman and A.P. Annan. 2003, Measuring soil water content with ground-penetrating radar: a review, Vadose Zone Journal 2 *pp. 476–491.*

Hutchins, S.R. and S.D. Acree. 2000. Ground water sampling bias observed in shallow conventional wells. Ground Water Monitoring & Remediation, Vol. 20, No. 1, pp. 86-93.

Javandel, I. and Witherspoon, P.A. 1969. A method of analyzing transient fluid flow in a multilayered aquifers. Water Resources Research. 5, pp. 856-869.

Kabala, Z.J. 1994. Measuring distribution of hydraulic conductivity and specific storativity by the double flowmeter test. Water Resources Research, vol. 30 (3), pp. 685-690.

Kelly, W. 1977. Geoelectrical sounding for estimating hydraulic conductivity. Ground Water, 15(6), 420–425.

Keys, W.S. 1990. Borehole geophysics applied to water-resources investigations: U.S.Geological Survey Techniques of Water Resources Investigations, book 2, chap. E2, 150 p.

Kilpatrick, F.A. and Wilson, Jr. J.F. 1989. Measurement of time of travel in streams by dye tracing. Techniques of Water-Resources Investigations of the United States Geological Survey, Book 3. Chapter A9. 27 p.

Klepikova, M.V., T. Le Borgne, O. Bour, P. Davy. 2011. A methodology for using borehole temperature-depth profiles under ambient, single and cross-borehole pumping conditions to estimate fracture hydraulic properties. Journal of Hydrology, Vol. 407, pp. 145-152.

Koudina, N., Garcia, R.G., Thovert, J.-F., Adler, P.M. 1998. Permeability of three-dimensional fracture networks. Physical Review E 4 (57), 4466– 4479.

Kuras O., J. Pritchard, P.I. Meldrum, J.E. Chambers, P.B. Wilkinson, R.D. Ogilvy and W.G.P. Wealthall, 2009. Monitoring hydraulic processes with Automated time-Lapse Electrical Resistivity Tomography (ALERT), Comptes Rendus Geosciences 341, 868–885.

Lane J.W., F.D. Day-Lewis and C.C. Casey, 2006. Geophysical monitoring of a field-scale biostimulation pilot project, Ground Water 44 (3), pp. 430–443.

Lane J.W., F.D. Day-Lewis, R.J. Versteeg and C.C. Casey. 2004. Object-based inversion of crosswell radar tomography data to monitor vegetable oil injection experiments. Journal of Environmental & Engineering Geophysics 9 (2), 63–77.

Lapcevic P.A., K.S. Novakowski, F.L. Paillet. 1993. Analysis of flow in an observation well intersecting a single fracture. Journal of Hydrology (151), 229-239.

Le Borgne, T., F.L. Paillet , O. Bour, J.-P. Caudal. 2006b. Cross-borehole flowmeter tests for transient heads in heterogeneous Aquifers. Ground Water, Vol. 44, No. 3, pp. 444-452.

Le Borgne, T., O. Bour, F.L. Paillet, J.-P. Caudal. 2006a. Assesment of preferential flow path connectivity and hydraulic properties at single-borehole and cross-borehole scales in a fractured aquifer. Journal of Hydrology, 328, 347-359.

Le Borgne, T., O. Bour, M.S. Riley, P. Gouze, P.A. Pezard, A. Belghoul, G. Lods, R. Le Provost, R.B. Greswell, P.A. Ellis, E. Isakov. B.J. Last. 2007. Comparison of alternative methodologies for identifying and characterizing preferential flow paths in heterogeneous aquifers. Journal of Hydrology, 345, 134-148.

Le Borgne, T., O. Bour, M.S. Riley, P. Gouze, P.A. Pezard, A. Belghoul, G. Lods, R. Le Provost, R.B. Greswell, P.A. Ellis, E. Isakov, B.J. Last. 2007. Comparison of alternative methodologies for identifying and characterizing preferential flow paths in heterogeneous aquifers. Journal of Hydrology, 345, 134-148.

Long, J.C.S., J.S. Remer, C.R. Wilson, and P.A. Witherspoon. 1982. Porous media equivalents for networks of discontinuous fractures. Water Resources Research, 18: 645-658.

Looms M.C., K.H. Jensen, A. Binley and L. Nielsen. 2008. Monitoring unsaturated flow and transport using cross-borehole geophysical methods. Vadose Zone Journal 7 (1), pp. 227–237.

Löfgren M., J. Crawford, M. Elert. 2007. Tracer tests – Possibilities and limitations. Experience from SKB fieldwork: 1977-2007. SKB Report R-07-39.

Min, K.B., L.R. Jing, O. Stephansson. 2004. Determining the equivalent permeability tensor for fractured rock masses using a stochastic REV approach: method and application to the field data from Sellafield, UK. Hydrogeology Journal 12 (5), 497– 510.

Molz F. J., G. K. Boman, S. C. Young, H. E. Julian, and H. S. Pearson. 1998. Application of the Electromagnetic Borehole Flowmeter. Report EPA/600/R-98/058, U. S. Environmental Protection Agency, Washington, DC 20460.

Molz, F.J. and S.C. Young. 1993. Development and Application of Borehole Flowmeters for Environmental Assessment. The Log Analyst, pp. 13-23, January-February 1993.

Molz, F.J., G.K. Boman, S.C. Young, and W.R. Waldrop. 1994. Borehole Flowmeters: Field Applications and Data Analysis, Journal of Hydrology, 163:347-371.

Molz, F.J., Guven O. and Melville, J.G. 1990. A new approach and methodologies for characterizing the hydrogeologic properties of aquifers. National Technical Information Service, Report 90-167063, Washington, D.C.

Molz, F.J., O. Guven, J.G. Melville, R.D. Crocker and K.T. Matteson. 1986. Performance Analysis, and simulation of a two-well tracer test at the Mobile Site. Water Resources Research, 22(7), pp. 1031-1037.

Molz, F.J., Oktay Guven, and J.G. Melville. 1990. Measurement of Hydraulic Conductivity Distributions - A Manual of Practice, U.S. Environmental Protection Agency Technical Report, EPA/600/8-90/046.

Molz, F.J., R.H. Morin, A.E. Hess, J.G. Melville and O. Guven. 1989. The impeller meter for measuring aquifer permeability variations: Evaluation and comparison with other tests. Water Resources Research, Vol. 25, no. 7, pp. 1677-1683.

Morin, R.H., Hess, A.E., and Paillet, F.L. 1988. Determining the distribution of hydraulic conductivity in a fractured limestone aquifer by simultaneous injection and geophysical logging. Ground Water, 26, pp. 387-595.

Neretnieks, I. 2007. Single Well Injection Withdrawal Tests (SWIW) in Fractured Rock – Some Aspects on Interpretation, Report R-07-54, Department of Chemical Engineering and Technology, Royal Institute of Technology, Stockholm, Sweden.

Neuman, S.P. 2003. Multifaceted nature of hydrogeologic scaling and its interpretation. Reviews of Geophysics 41 (3), 4.1– 4.31.

Newhouse M.W., J.A. Izbicki, and G.A. Smith. 2005. Comparison of Velocity-Log Data Collected Using Impeller and Electromagnetic Flowmeters. *Ground Water****, Vol. 43, No. 3, May pages 434–438.***

Paillet F.L. 1998. Flow modeling and permeability estimation using borehole flow logs in heterogeneous fractured formations. Water Resources Research, Vol. 34, No. 5, pp. 997-1010.

Paillet F.L., A.E. Hess, C.H. Cheng and E. Hardin. 1987. Characterization of fracture permeability with High-resolution vertical Flow measurements during borehole pumping. Ground Water, Vol. 25. No. 1.

Paillet, F.L. 2004. Borehole flowmeter applications in irregular and large-diameter boreholes. Journal of

Applied Geophysics, Vol. 55, pp. 39-59.

Paillet, F.L. 1993. Using Borehole geophysics and cross-borehole flow testing to define hydraulic connections between fracture zones in bedrock aquifers. Journal of Applied Geophysics, 30 pp. 261-279.

Paillet, F.L., R.S. Reese. 2000. Integrating Borehole Logs and Aquifer Tests in Aquifer Characterization, Ground Water, Vol. 38, No 5, pp. 713-725.

Parker, A.H., L.J. West, N.E. Odling, and R.T. Bown. 2010. A forward modeling approach for interpreting impeller flow logs. Ground Water, Vol. 48 No. 1, pp. 79-91.

Pirson S.J. 1953. Performance of fractured oil reservoirs. Bull. Amer. Assoc. Petrol. Geologists, v.37, 1953, pp. 232-244.

Rehfeldt K.R., P. Hutschmied, L.W. Gelhar, M.E. Schaefer. 1989. Measuring Hydraulic Conductivity with the Borehole Flowmeter. Electric Power Research Institute. Report EN 6511.

Reilly, T.E., O.L. Franke, and G.D. Bennet. 1989. Bias in groundwater samples caused by wellbore flow. ASCE, Journal of Hydraulic Engineering, Vol. 115, pp. 270-276.

Rubin, Y., G. Mavko, and J. Harris. 1992. Mapping permeability in heterogeneous aquifers using hydrologic and seismic data, Water Resour. Res., 28(7), 1809–1816.

Rucker D.F. and Ferré T.P.A. 2003. Near-surface water content estimation with borehole ground penetrating radar using critically refracted waves. Vadose Zone Journal 2 *247–252.*

Rucker D.F. and Ferré T.P.A. 2004. Correcting water content measurement associated with critically refracted first arrivals on zero offset profiling borehole ground penetrating radar profiles, Vadose Zone Journal 3 *pp. 278–287.*

Schnegg P.A. and Flynn, R. M. 2002. Online field fluorometers for hydrogeological tracer tests. In: Isotope und Tracer in der Wasserforschung, Technische Universität Bergakademie Freiberg, Wissenschaftliche Mitteilungen, Institut für Geologie, 19, pp 29-36.

Schnegg P.A. 2002. An inexpensive field fluorometer for hydrological tracer tests with three tracers and turbidity measurement. XXXII IAH & ALHSUD Congress Groundwater and Human Development. Balkema, Mar del Plata, Argentina, pp. 1484-1488.

Schnegg P.A. 2003, A new field fluorometer for multitracer tests and turbidity measurement applied to hydrogeological problems, 8° Congresso Internacional da Sociedade Brasileira de Geofísica, Rio de Janeiro, RJ, Brasil, CDROM, resumo SBGF167.

Schulze-Makuch D., D.S. Cherkauer. 1998. Variations in hydraulic conductivity with scale of measurement during aquifer tests in heterogeneous, porous carbonate rocks. Hydrogeology Journal 6 (2), 204– 215.

Slater L. and X. Comas. 2009. The contribution of Ground Penetrating Radar to Water Resource Research.

In Ground Penetrating Radar: Theory and Applications. Elsevier Science.

Slater L., A.M. Binley, W. Daily and R. Johnson. 2000. Cross-hole electrical imaging of a controlled saline tracer injection, Journal of Applied Geophysics 44, 85–102.

Snodgrass M.F., P.K. Kitandis. 1998. A method to infer in situ reaction rates from push-pull experiments. Ground Water 36, no. 4. pp. 645–650.

Sudicky, E.A., 1986. A natural gradient experiment on solute transport in a sand aquifer: spatial variability of hydraulic conductivity and its role in the dispersion process. Water Resources Research 22 (13), 2069– 2082.

Sukhodolov, A.N., V.I. Nikora, P.M.Rowi´nski, and W. Czernuszenko. 1997. A case study of longitudinal dispersion in small lowland rivers. Water Environ. Resour. 97, pp. 1246–1253.

Topp G.C., J.L. Davis and A.P. Annan. 1980. Electromagnetic determination of soil water content: measurements in coaxial transmission lines, Water Resources Research 16, *pp. 574–582.*

Truss S., M. Grasmueck, S. Vega and D.A. Viggiano. 2007. Imaging rainfall drainage within the Miami oolitic limestone using high-resolution time-lapse ground-penetrating radar. Water Resources Research 43 *p. W03405 10.1029/2005WR004395.*

Urish, D. W. 1981. Electrical resistivity-hydraulic conductivity relationships in glacial outwash aquifers. Water Resour. Res. 17(5), 1401–1408.

Wilkinson P.B., P.I. Meldrum, O. Kuras, J.E. Chambers, S.J. Holyoake and R.D. Ogilvy. 2009. High-resolution electrical resistivity tomography monitoring of a tracer test in a confined aquifer. Journal of Applied Geophysics 70, 268–276.

Williams, J.H., and F.L. Paillet. 2002. Using flowmeter pulse tests to define hydraulic connections in the subsurface: a fractured shale example. Journal of Hydrology, v. 265, pp. 100-117.

Young, S.C. and H.S. Pearson, 1991. Characterization of a three-dimensional hydraulic conductivity field with an electromagnetic borehole flowmeter. Tennessee Valley Authority Report.

Young, S.C. and W.R. Waldrop, 1989. An electromagnetic Borehole Flowmeter for Measuring Hydraulic Conductivity Variability. Conference Proceedings for New Field Techniques for quantifying the Physical and Chemical Properties of Heterogeneous Aquifers. Water Well Journal Publishing Company, Dallas, TX, pp. 463-474.

Young, S.C. 1995. Characterization of high-K Pathways by borehole Flowmeter and Tracer Tests. Ground Water, vol.33, No.2, 311-318.

Young, S.C. 1998. Impacts of positive skin effects on borehole flowmeter tests in an heterogeneous granular aquifer. Ground Water, Vol. 36, No. 1, pp. 67-75.

Young, S.C., H.E. Julian, H.S. Pearson, F.J. Molz and G.K. Boman. 1998. Application of the Electromagnetic Borehole Flowmeter, U.S. Environmental Protection Agency Research Report EPA/600/R-98/058, August 1998.

Zlotnik V.A., B.R. Zurbuchen. 2003. Estimation of hydraulic conductivity from borehole flowmeter tests considering head losses. Journal of Hydrology, 281, pp. 115-128.